Hydrothermal Liquefaction of Microalgae and Other Microorganisms: Developing a Kinetic Model

by

Peter Joseph Valdez

A dissertation submitted in partial fulfillment
of the requirements for the degree of
Doctor of Philosophy
(Chemical Engineering)
in the University of Michigan
2013

Doctoral Committee:

Professor Phillip E. Savage, Chair
Professor Hugh Scott Fogler
Professor Adam J. Matzger
Assistant Professor Charles W. Monroe

Biocrude from *Nannochloropsis* sp.

To my wife, Jana

Acknowledgements

I would like to thank my advisor Phillip Savage for his support during my time at the University of Michigan. I appreciated his patience, guidance, and assistance throughout my graduate school career. He has played an important role in helping me to start my career as an engineer. I would like to thank the members of my dissertation committee, Scott Fogler, Adam Matzger, and Charles Monroe for their thoughtful input along the way.

I am especially grateful to my wife Jana who provided me with the love, support, encouragement, and care that I needed to get through graduate school. She married a student bum, but is now married to a doctor finally. I am also grateful to her for bringing Jacob into our lives and for taking care of him while I finished my dissertation. I thank Jacob for being a relatively easy baby to handle for his novice parents. I would like to express gratitude to my family and my in-laws who also supported me along the way.

I thank the past and present members of the Savage Group: Tanawan Pinnarat, Tylisha Brown, Peigao Duan, Jie Fu (Jackie), Zheng Li, Yang Guo, Qingqing Guan, Chad Huelsman, Allison Wilson Franck, Na Mo (Tiffany), Le Yang (Claire). It was a pleasure to get to know them all and to work with them in the lab.

I would especially like to thank Natalie Rebacz who taught me how to disassemble a GC and reassemble it again, Bobby Levine for introducing me to the lab and lab procedures, and Shujauddin Changi for his advice and help in the office we shared together.

I am especially grateful for Jake Dickinson and the thoughtful conversations we had in the office about research, religion, politics, Michigan, travel, and hockey. I thank Thomas Yeh, for general tomfoolery, shooting outings, and cycling advice. Thomas was the first person I met when I arrived at Michigan for Summer Institute, he showed me where to get my ID. I thank

Mike Nelson for being a great collaborator, our partnership resulted in improving the quality of our publications. I thank Julia Faeth for all of the collaborative projects we worked on together and for taking over for me as Chemical Hygiene Officer. I am grateful for the order she helps bring to the lab.

I thank Johanness Schwank, Galen Fisher, and Susan Montgomery for the helpful conversations along the way. I appreciated the help of Claire O'Connor, Shelley Fellers, Susan Hamlin, Kelly Raickovich, Pam Bogdanski, Laurel Neff, and Sandy Swisher for the administrative support over the last few years.

I am grateful to Chirapon 'Pete' Wangwongwiroj, Hao Chen, Ryan Hockstad, and Yiyi Zhao who helped me to collect the experimental data presented in this work. I am especially grateful to Nick Garza and VJ Tocco for spending their summers working with me. Their diligence in the lab allowed me to collect a large portion of the data presented in this dissertation.

I am grateful to my good friends Leo, Michelle, Richmond, and Lillian for the time spent together not doing research. I am grateful to the members of the Ann Arbor 2nd Ward and the Ann Arbor Stake who provided my family with a strong feeling of community.

I thank the National Science Foundation (Grant EFRI-0937992), the Rackham Graduate School and the College of Engineering for their financial support. Portions of this work were made possible by EPA fellowship number FP-917507. Its contents are solely the responsibility of the fellow and do not necessarily represent the official views of the EPA. Further, the EPA does not endorse the purchase of any commercial products or services mentioned in the publication.

Table of Contents

List of Figures

List of Tables

Abstract

We present the results from the systematic investigation of the experimental parameters that affect the product fractions from the hydrothermal liquefaction (HTL) of microalgae and other single-cell microorganisms. From the systematic study, we elucidated reaction pathways and derived a global kinetic model of HTL, enabling predictions of the yields of product fractions based on the feedstock composition, residence time, and reaction temperature.

We investigated HTL of *Nannochloropsis* sp. at different temperatures (250 - 400 °C), times (10 - 90 min), water densities (0.3 - 0.5 g/mL), biomass loadings (5 - 35 wt %), headspace compositions (He, air), initial headspace pressures (0 - 90 psig), and recovery solvents. HTL of the alga produced a biocrude with light and heavy fractions, along with gaseous, aqueous, and solid by-product fractions. The yields of light and heavy biocrude depend on reaction time and temperature, but their combined yield depends primarily on temperature. Regardless of reaction time and temperature, the yield of products distributed to the aqueous phase is 51 ± 5 wt %. The gravimetric yields of the product fractions are independent of water density at 400 °C. Increasing the biomass loading increases the biocrude yield from 36 to 46 wt %. By varying the headspace composition and initial pressure in the reactor we found that the yield of biocrude is similar for both He and air reaction atmospheres. The yield of biocrude is also independent of increasing pressure of the reactor headspace at 0, 30, 60 and 90 psig. We used both non-polar solvents (hexadecane, decane, hexane, cyclohexane) and polar solvents (methoxycyclopentane, dichloromethane, and chloroform) to recover the biocrude. Hexadecane and decane provided the

highest gravimetric yields of biocrude (39 ± 3 wt % and 39 ± 1 wt % respectively), but biocrude had a lower carbon content (69 wt % for decane) than did those recovered with polar solvents such as chloroform (74 wt %) and dichloromethane (76 wt %).

We isolated the solids, aqueous-phase, and biocrude product fractions from the HTL of *Nannochloropsis* sp. and then further reacted each individually. These results permitted construction of a detailed reaction network for HTL that comprises the pathways for consumption and formation of each product fraction. We used the reaction network to develop a quantitative kinetic model and estimated its parameters using experimental results for the HTL of *Nannochloropsis* sp. at different temperatures and times. The model accurately predicted previously published biocrude and gas yields for the hydrothermal treatment of *Nannochloropsis* sp. The model predicts that the yields of light and heavy biocrudes are highest at temperatures above 300 °C and reaction times below 20 min. We investigated the liquefaction of *Chlorella protothecoides* and *Scenedesmus* sp. and measured the biochemical content of each alga. We incorporated the biochemical content into the reaction network and kinetic model to provide a means to correlate the initial concentration of proteins, lipids, and carbohydrates in the biomass to the yields of the different product fractions.

We hydrothermally treated *Escherichia coli*, *Pseudomonas putida*, *Bacillus subtilis*, and *Saccharomyces cerevisiae* at isothermal (350 °C for 60 min) and at fast (rapid heating for 1 min) HTL conditions. Fast HTL of *P. putida* and *S. cerevisiae* produced the highest biocrude yields of 47 ± 13 wt % and 48 ± 9 wt %, respectively. Up to 62 ± 9 % of the chemical energy in the biomass could be recovered in the biocrude product fraction. These results demonstrate the feasibility of producing biocrude from bacteria and yeast.

Chapter 1

Introduction

"The fuel of the future is going to come from fruit like that sumac out by the road, or from apples, weeds, sawdust—almost anything."

-Henry Ford

1.1. The Case for Biofuels

Biofuels are fuels derived from biological materials such as plant matter. Biofuels are becoming increasingly important as a replacement for our fossil energy resources and as a way to reduce the environmental impact of our energy consumption. By 2040, the U.S. Energy Information Administration estimates that 6% of our supply of liquid transportation fuels will come from biofuels [1]. Transitioning to the use of biofuels creates an opportunity to reduce the amount of CO_2 released into the atmosphere, rather than continuing to release carbon from previously sequestered sources [2]. Other potential benefits of developing sustainable biofuels are stability in the domestic supply and price of the fuel and reduced trade deficit and increased global competitiveness in the fuel market. Presently, before a transition to a new energy source can occur, any new technology must demonstrate at least of some the following traits: a renewable supply, reduced cost, improved performance, and environmentally driven policy support [3]. Additional research is needed to permit biofuels to achieve those milestones so society can successfully transition to this new energy carrier [4].

1.2. Algal Feedstock for Biofuels

Microalgae are single-celled, photosynthetic microorganisms that are a feedstock candidate for biofuels because of their fast growth rate, high lipid content, and high areal yield [5,6]. Algae do not compete for arable land [5,7], they are capable of capturing carbon dioxide emissions [6,8] and they can remove pollutants from wastewater streams [8-10]. Research has shown that growth rates of microalgae improved with additional carbon dioxide [8]. Other experiments demonstrate that algae can treat livestock manure and remove 50 – 90% of nitrogen and phosphorus compounds, preventing their release into the environment [10]. The use of microalgae as a biofuel feedstock provides an opportunity for waste-to-energy conversion.

Certain algae have been selected for their advantageous biological properties. For example, *Botryococcus braunii* is a natural producer of long chain hydrocarbons known as botryococcenes (C30 – C37) [11]. *Dunaliella tertiolecta* is halotolerant and is already produced commercially for β-carotene [11]. Other microalgae such as *Nannochloropsis* sp., *Schizochytrium* sp., and *Chlorella* sp. have been used for biodiesel production because of their higher concentration of lipids [5].

1.3. Hydrothermal Liquefaction of Algae

To advance the development of biofuels derived from microalgae, many recent studies focus on processes such as transesterification [5], pyrolysis [12], carbonization [13], gasification [14], and hydrothermal liquefaction (HTL) [11,15-23]. HTL can convert wet algal biomass (> 80% water) at elevated temperatures (> 250°C) and pressures (> 40 bar) into an energy-dense biocrude (> 30 MJ/kg) without the need of energy- and resource-intensive steps of drying the biomass or extracting the lipids. Hydrothermal treatment is advantageous because the whole

biomass is processed in its natural state and the biomacromolecules are fragmented via hydrolysis. HTL of algae also produces gases, solids, and water-soluble products. To derive the full benefits of the HTL of microalgae requires a comprehensive investigation of the processing parameters and feedstock selection.

The biocrude from the HTL of microalgae is a complex mixture of compounds varying in chemical structure and molecular weight [16,23,24]. The diversity of compounds in the biocrude makes it a reasonable replacement for petroleum crude instead of a replacement for or supplement of petroleum products such as gasoline, diesel, or jet fuel. HTL of microalgae creates an opportunity to isolate high-value lipids in the algae [25]. A review of hydrothermal liquefaction processes demonstrates a positive net energy value from the production of algae biocrude when compared to biocrudes from other feedstocks [11]. Overall, these traits call attention to the feasibility of microalgae as a feedstock for HTL when compared to other biomass materials.

1.4. Research Scope and Proposed Work

Although the field of hydrothermal treatment of biomass continues to expand, there is still a significant lack of understanding of how feedstock composition of algae and processing conditions affect the yield and composition of the various liquefaction products. The need to understand the kinetics and reaction pathways of microalgae liquefaction will be important as the field progresses towards the development of large-scale biocrude production. Understanding the reaction capabilities and pathways will also permit the prediction and control of liquefaction products based on feedstock characteristics and reaction conditions. Researchers have attempted to correlate the biochemical content of the feedstock to the characteristics of the liquefaction

products [15,26,27], but recent studies have been limited in their approach and depth. The variety of microalgal feedstocks makes microalgae a suitable model system that will provide insight into the liquefaction of other biomass materials with similar biochemical composition.

The objective of this research is to enable the engineering of microalgal biocrude by studying the reaction kinetics to model the outcome of HTL based on the biochemical content of a feedstock and the reaction conditions. The specific objectives discussed in this dissertation are the systematic study of the processing conditions related to the HTL of microalgae, the elucidation of reaction pathways, and the development of a kinetic model of the HTL of microalgae. This research improves the understanding of how feedstock characteristics and processing conditions affect product yields, elemental and molecular composition, and heating value of the liquefaction products. Figure 1.1 summarizes the experimental approach and research objectives.

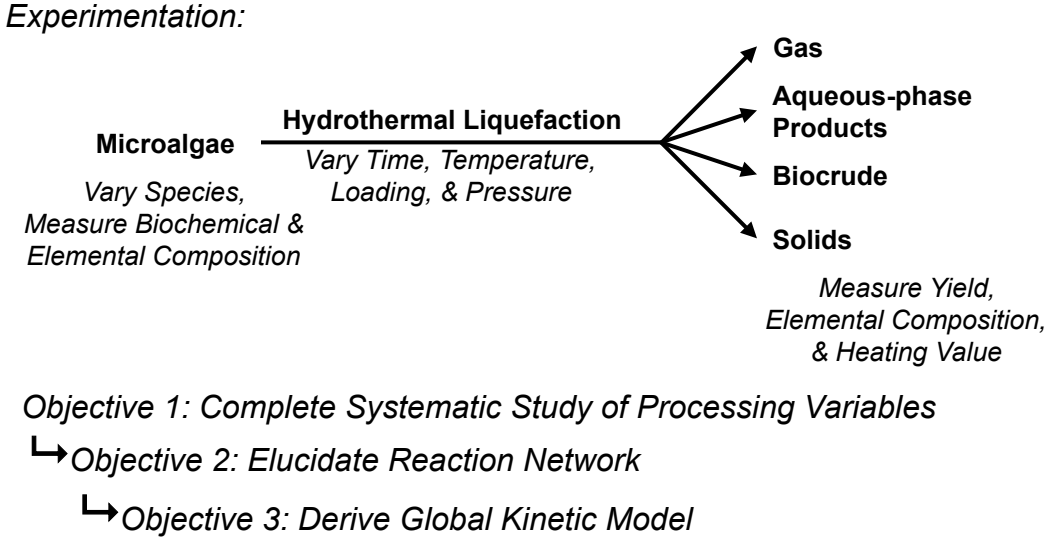

Figure 1.1. Experimental summary and research objectives

The subsequent chapters provide additional background information about the hydrothermal liquefaction of microalgae and other biomass as well as results and analysis of the each of the research accomplishments. Chapter 2 discusses the available literature pertaining to the hydrothermal liquefaction of microbial biomass. Chapter 3 outlines the experimental methods used to complete the dissertation research. Chapter 4 shows results of experimentation examining several parameters of HTL. Chapter 5 discusses the development and study of the reaction pathways and network for liquefaction of microalgae. Chapter 6 summarizes the kinetic model and its use to predict the yields of the liquefaction products from *Nannochloropsis* sp. Chapter 7 summarizes HTL experiments with *C. protothecoides* and *Scenedesmus* sp. as feedstocks and discusses the incorporation of biochemical content into the model. Chapter 8 summarizes experiments of the HTL of bacteria and yeast, and compares the results to those from algae liquefaction. The last chapter discusses the impact of this research, key conclusions, and some directions for future research.

References

[1] U.S. Energy Information Administration, *Annual Energy Outlook 2013 with Projections to 2040*, (2013)

[2] U.S. Department of Energy, *Report on the First Quadrennial Technology Review*, Report on the First Quadrennial Technology Review (2011)

[3] PA O'Connor, *Energy Transitions*, The Pardee Papers 12 (2010) 1-43.

[4] SK Hoekman, *Biofuels in the U.S. - Challenges and Opportunities*, Renewable Energy 34 (2009) 14-22.

[5] Y Chisti, *Biodiesel from microalgae*, Biotechnol Adv 25 (2007) 294-306.

[6] S Sawayama, T Minowa, S-Y Yokoyama, *Possibility of renewable energy production and CO2 mitigation by thermochemical liquefaction of microalgae*, Biomass Bioenergy 17 (1999) 33-39.

[7] AF Clarens, EP Resurreccion, MA White, LM Colosi, *Environmental life cycle comparison of algae to other bioenergy feedstocks*, Environ Sci Technol 44 (2010) 1813-1819.

[8] M Packer, *Algal capture of carbon dioxide; biomass generation as a tool for greenhouse gas mitigation with reference to New Zealand energy strategy and policy*, Energy Policy 37 (2009) 3428-3437.

[9] WJ Catallo, JL Comeaux, *Reductive hydrothermal treatment of sewage sludge*, Waste Manag 28 (2008) 2213-2219.

[10] W Mulbry, S Kondrad, C Pizarro, E Kebede-Westhead, *Treatment of dairy manure effluent using freshwater algae: algal productivity and recovery of manure nutrients using pilot-scale algal turf scrubbers*, Bioresour Technol 99 (2008) 8137-8142.

[11] S Inoue, Y Dote, S Sawayama, T Minowa, T Ogi, S-Y Yokoyama, *Analysis of oil derived from liquefaction of Botryococcus braunii*, Biomass Bioenergy 6 (1994) 269-274.

[12] AA Peterson, F Vogel, RP Lachance, M Fröling, MJ Antal Jr, JW Tester, *Thermochemical biofuel production in hydrothermal media: A review of sub-and supercritical water technologies*, Energy Environ Sci 1 (2008) 32-65.

[13] SM Heilmann, HT Davis, LR Jader, PA Lefebvre, MJ Sadowsky, FJ Schendel *et al.*, *Hydrothermal carbonization of microalgae*, Biomass Bioenergy 34 (2010) 875-882.

[14] Y Matsumura, T Minowa, B Potic, S Kersten, W Prins, W van Swaaij *et al.*, *Biomass gasification in near- and super-critical water: Status and prospects*, Biomass Bioenergy 29 (2005) 269-292.

[15] P Biller, AB Ross, *Potential yields and properties of oil from the hydrothermal liquefaction of microalgae with different biochemical content*, Bioresour Technol 102 (2011) 215-225.

[16] TM Brown, P Duan, PE Savage, *Hydrothermal Liquefaction and Gasification of Nannochloropsis sp*, Energy Fuels 24 (2010) 3639-3646.

[17] Y Dote, S Sawayama, S Inoue, T Minowa, S-Y Yokoyama, *Recovery of liquid fuel from hydrocarbon-rich microalgae by thermochemical liquefaction*, Fuel 73 (1994) 1855-1857.

[18] P Duan, PE Savage, *Hydrothermal Liquefaction of a Microalga with Heterogeneous Catalysts*, Ind Eng Chem Res 50 (2011) 52-61.

[19] JL Faeth, PJ Valdez, PE Savage, *Fast Hydrothermal Liquefaction of Nannochloropsis sp. To Produce Biocrude*, Energy Fuels 27 (2013) 1391-1398.

[20] L Garcia Alba, C Torri, C Samori, J van der Spek, D Fabbri, SRA Kersten *et al.*, *I - Hydrothermal Treatment (HTT) of Microalgae: Evaluation of the Process As Conversion Method in an Algae Biorefinery Concept*, Energy Fuels 26 (2012) 642-657.

[21] AB Ross, P Biller, ML Kubacki, H Li, A Lea-Langton, JM Jones, *Hydrothermal processing of microalgae using alkali and organic acids*, Fuel 89 (2010) 2234-2243.
[22] PJ Valdez, MC Nelson, HY Wang, XN Lin, PE Savage, *Hydrothermal liquefaction of Nannochloropsis sp.: Systematic study of process variables and analysis of the product fractions*, Biomass Bioenergy 46 (2012) 317-331.
[23] DR Vardon, BK Sharma, J Scott, G Yu, Z Wang, L Schideman *et al.*, *Chemical properties of biocrude oil from the hydrothermal liquefaction of Spirulina algae, swine manure, and digested anaerobic sludge*, Bioresour Technol 102 (2011) 8295-8303.
[24] PJ Valdez, JG Dickinson, PE Savage, *Characterization of Product Fractions from Hydrothermal Liquefaction of Nannochloropsis sp. and the Influence of Solvents*, Energy Fuels 25 (2011) 3235-3243.
[25] C Ratledge, Z Cohen, *Microbial and algal oils: Do they have a future for biodiesel or as commodity oils?*, Lipid Technology 20 (2008) 155-160.
[26] Y Dote, S Inoue, T Ogi, S-Y Yokoyama, *Studies on the direct liquefaction of protein-contained biomass: the distribution of nitrogen in the products*, Biomass Bioenergy 11 (1996) 491-498.
[27] Y Dote, S Inoue, T Ogi, S-Y Yokoyama, *Distribution of nitrogen to oil products from liquefaction of amino acids*, Bioresour Technol 64 (1998) 157-160.

Chapter 2

Background

This chapter summarizes the research related to the hydrothermal liquefaction (HTL) of biomass. The first sections outline the different parameters and approaches that have been studied to further the field with an emphasis on the HTL of microalgae. The last section provides a critical analysis of the presented literature. The background information in this chapter represents a snapshot of the research related to the HTL of microalgae through 2011, while the research presented in this dissertation expands upon the knowledge in the field since then. More recent publications will be presented alongside the results in later chapters as the field progressed concurrently with the research presented herein.

HTL experiments with various types of microalgae demonstrate that the feedstock, temperature, pressure, residence time, and catalyst can affect the biocrude yield. Table 2.1 summarizes some of the experimental variables and the biocrude yield from previous research related to the liquefaction of microalgae. Biocrude yield is calculated as the mass of biocrude recovered per mass of microalgae used (with or without ash). Most research is dedicated to the variation and testing of a single reaction parameter (e.g. catalyst, temperature, etc.). To date, no attempts have been made to complete a systematic and exhaustive study of these parameters and how they relate to one another. Additional research is needed to develop a kinetic model for HTL of microalgae.

Table 2.1. Summary of liquefaction experiments using microalgae

Ref.	Feedstock	Temperature (°C)	Pressure[a] (MPa)	Residence Time (minutes)	Catalyst	Biocrude Yield (wt %)
[1]	*Botryococcus braunii*	200-340	2	60	Na_2CO_3	57-64[b]
[2]	*Microcystis viridis*	300, 340	3	30, 60	Na_2CO_3	33[b]
[3]	*Dunaliella tertiolecta*	250-340	3	5, 60	Na_2CO_3	31-44[b]
[4]	*Nannochloropsis* sp.	200-500	0.069	60	none	16-43
[5]	*Nannochloropsis* sp.	350	0.101	60	none	30-39
[6]	*Nannochloropsis* sp.	350	7,35	60	Pd/C, Pt/C, Ru/C, Ni/SiO_2-Al_2O_3, $CoMo/Al_2O_3$, Zeolite	35-57
[7]	*Chlorella vulgaris*, *Nannochloropsis occulata*, *Porphyridium cruentum*, *Spirulina*	350	0.101	60	Na_2CO_3, HCOOH	~25-40[b]
[8]	*Chlorella vulgaris, Spirulina*	300, 350	0.101	60	Na_2CO_3, KOH, CH_3COOH, HCOOH	11.6-27.3[b]
[9]	*Spirulina platensis*	200-380	2	0-120	none	~30-60
[10]	*Desmodesmus* sp.	175-450	0.101	5-60	none	8.6-49.4

[a]Initial headspace pressure of the reaction vessel at room temperature
[b]Yield calculated as mass biocrude per mass dry and ash free alga

The literature presented in Table 2.1 highlights the key contributions from other researchers who have used HTL of microalgae to produce biocrude. Since there are still gaps in the literature examining how some processing conditions can affect the hydrothermal treatment of microalgae, examples from the hydrothermal liquefaction other types of biomass (e.g. cellulose, manures, etc.) are presented to provide additional background information about possible effects.

2.1. Selecting a Feedstock

Past studies have focused on liquefaction feedstocks such as industrial waste [11,12], animal waste [13-15], sewage sludge [16,17], and lignocellulosic materials [18-20]. Table 2.2 summarizes several studies examining the liquefaction of biomass to produce biocrude.

Table 2.2. Summary of liquefaction experiments of biomass

Ref.	Feedstock	Temperature (°C)	Pressure[a] (MPa)	Residence Time (minutes)	Catalyst	Bio-oil Yield (%)
[21]	Swine Manure	275-350	0-9	5-180	none	64[b] [14]
[15]	Cattle Manure	270-350	0-0.7	0-40	NaOH	28.0-48.8[b]
[22]	Sewage Sludge	250-340	0-9	0[c]	Na_2CO_3	25.3-51.8[b]
[16]	Sewage Sludge	400	0.101	240	none	4-11[b]
[11]	Cornstarch Sludge	225-340	3	60[c]	Na_2CO_3	25.6-30.4[d]
[12]	Pulp/Paper Sludge	250-380	2	15-120	K_2CO_3, $Ca(OH)_2$, $Ba(OH)_2$	45-60[d]
[19]	Eucalyptus lignin	200-300	4-11.5	30[b]	HCOONa	18.3-44.8
[18]	Cellulose	200-350	3	0-60[c]	Na_2CO_3, Ni	22

[a]Initial headspace pressure of the reaction vessel at room temperature
[b]Yield calculated as mass bio-oil per mass volatile solids content
[c]Hold time after reaction vessel raised to given temperature at a rate of 7°C/min.
[d]Yield calculated as mass biocrude per mass dry and ash free alga
[e]15g loaded into flow system at 25MPa, 410°C, and water flow of 3mL/min.

Presently, microalgae are investigated as a feedstock for hydrothermal conversion because of their rapid growth rate, high yield, positive net energy ratio, and potential for waste treatment [23]. Algae have a faster growth rate and better per-acre yield (~10×) compared to other biomass such as corn, soy, or other lignocellulosic materials [24], and can be grown using either fresh or

salt water. While water usage is a concern, the use of closed-system photobioreactors can reduce evaporative losses [24]. Additionally, the use of wastewater streams for algae cultivation has significantly lower environmental impact than fresh-water use [25]. Other experiments demonstrate that algae can treat livestock manure and remove 50-90% of nitrogen and phosphorus compounds, preventing their release into the environment [26]. Also, microalgae can be used to capture carbon emissions because its growth improves with increasing carbon dioxide partial pressure [27]. Therefore, algae cultivation provides both an energy source and a method of treatment for waste materials.

Bacteria and yeasts are widely used in industrial biochemical processes that convert feedstock substrates into finished products such as specialty chemicals [28], food products [29], and biofuels [30-33]. Although there is significant value in the aforementioned products, the microbial biomass itself is usually discarded as a waste. Biochemical processes are also used in wastewater treatment, where they create a secondary, microorganism-rich sludge that is often collected and discarded [34]. HTL of bacteria and yeasts may create an opportunity to produce a renewable biofuel from low-value materials. The HTL of microbial communities in sludge is not new: HTL of sludge from biologically treated cornstarch and pulp/paper waste resulted in biocrude yields of 15 - 30 wt % and 42 - 65 wt %, respectively [11,12]; HTL of anaerobically digested sludge from municipal sources has been less successful, producing biocrude yields of ≤ 10 wt % [16,17].

There is an opportunity to utilize the by-products from the liquefaction of microalgae and the cultivation and HTL of bacterial biomass. Although a majority of the algal biomass is converted into biocrude, the aqueous co-product also contains some organic carbon along with nutrients such as nitrogen- and phosphorus-containing substrates. This aqueous co-product can be utilized

for cultivating additional biomass. Using it to grow more algae can be difficult as several studies have shown that it can be toxic or nutrient-limited [35-38]. Moreover, recycling this water, which contains organic carbon, to an open pond for algae growth may substantially increase the risk of invasion of contaminating heterotrophs into the algae culture. However, Nelson et al. have recently demonstrated the feasibility of cultivating *Escherichia coli* and *Pseudomonas putida* monocultures utilizing this aqueous-phase with minimal dilution and nutrient supplementation [39]. Adding a microbial cultivation step in an algae liquefaction biorefinery to utilize the organic carbon in the aqueous phase can enhance ease of its recycling to an open pond and provide additional biomass for HTL. To the best of our knowledge, the HTL of microbial monocultures, such as bacteria and yeast, has not been examined.

2.2. Product Recovery

This section summarizes procedures used to recover and to quantify the products from the hydrothermal liquefaction of biomass.

2.2.1. Selecting a Recovery Solvent

Liquefaction of microalgae produces a biocrude, along with gaseous products, solids, and an aqueous byproduct phase. As shown in Figure 2.1, the typical laboratory practice after releasing the gaseous products is to add an organic solvent to the liquefaction product mixture, to dissolve the biocrude and form an organic liquid phase that is easily separated from the aqueous and solid phases by decanting. After phase separation, the biocrude is recovered by evaporating the solvent. Likewise, removing the water from the aqueous byproduct phase permits recovery of the dissolved aqueous solids. In both cases, removal of the solvent is probably also accompanied by some loss of volatile products. The portion of Figure 2.1 pertaining to biocrude recovery has

been used in nearly all previous HTL studies, but with several different organic solvents (e.g., dichloromethane [1,4,6,8], chloroform [2], hexane [40], cyclohexane [20]).

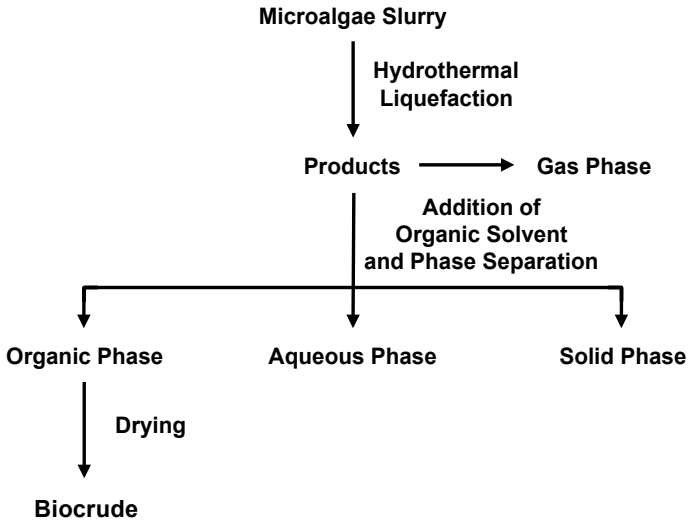

Figure 2.1. Common post-reaction procedure for isolating product fractions from algae liquefaction.

2.2.2. Closing the Mass Balance

Previous work has demonstrated the difficulty in directly determining a gravimetric yield for all of the products from liquefaction. The difficulty in closing the mass balance arises from the direct measurement of a gravimetric yield of the liquefaction products that partition into the aqueous phase. Most researchers have simply assumed closure of the mass balance and determined the yield of the aqueous-phase products as the difference between the total biomass loaded into the reactor and the total mass collected from the biocrude, gas, and solid products [7,8,10,37]. Directly accounting for all of the mass initially from the algae in the HTL products is another important step for improving the field.

2.3. Effect of Processing Conditions

This section summarizes how temperature, pressure and headspace composition, catalysts, water density, biomass loading, and batch holding time affect the liquefaction products.

2.3.1 Temperature

High temperature water is used as a reaction medium for the HTL of algae. At low temperatures (< 250 °C), biomass is carbonized to produce solid carbon residues, similar to coal, that can be used as an energy carrier [41]. At high temperatures (> 400 °C), gasification decomposes the biocrude and the other biomass materials to carbon residues (char), carbon dioxide, hydrogen, and methane [42]. Previous liquefaction experiments, carried out between 250 - 400 °C, demonstrate that the biocrude yield reaches a maximum around 300 - 350 °C [4,11,12,15]. Other experiments with swine manure suggest that increasing temperature will decrease the viscosity, reduce the oxygen content, and increase the heating value of the biocrude [14]. More recent studies show that more of the nitrogen in the biomass is distributed to the aqueous phase at higher temperatures (> 200 °C), reducing the nitrogen content of the biocrude [7,43,44]. Other results demonstrate that the carbon content of the biocrude increases as temperature increases [4,9].

2.3.2. Pressure and Headspace Composition

Reaction vessels are usually pressurized to ensure that the water at elevated temperatures will remain in the liquid phase, or they are filled sufficiently to ensure that the water will remain liquid as it expands with increasing temperature. The effect of the headspace pressure is unclear because increased pressure has shown both positive and negative effects on biocrude yields from

the HTL of cattle manure [15]. Varying the headspace pressure during HTL has not been studied using microalgae as a feedstock; however, the reaction atmosphere composition can have a more significant effect on the products formed during liquefaction. The biocrude yield from non-catalytic liquefaction of *Nannochloropsis* sp. improved in a high-pressure (3.5 MPa) hydrogen atmosphere [6]. The effect of varying the headspace composition and pressure during the HTL of microalgae is not well understood.

2.3.3. Catalysts

The use of catalysts is beyond the scope of this work, but is mentioned here to call attention to the issues surrounding their use and integration into the HTL of biomass. The use of catalysts has been shown to both increase and decrease biocrude yield [1,2,6,8,11,22]. Alkali and alkaline metal catalysts marginally improve biocrude yields [2,3,22,45]. On the other hand, Dote et al. showed no catalytic effect from sodium carbonate for microalgae liquefaction [1]. Duan and Savage's investigation of microalgae liquefaction using precious-metal catalysts showed improved yields, but marginal decrease in the oxygen, nitrogen, and sulfur concentration of the biocrude [6]. Catalysts such as nickel and ruthenium can also improve the physical properties of biocrude from a given feedstock, for example, decreasing its viscosity and increasing its heating value [3].

2.3.4. Water Density

To date, the effect of water density at supercritical conditions on the product fractions from the HTL of microalgae has not been investigated in detail. Brown et al., Jena et al., and Garcia Alba et al. studied liquefaction of microalgae at supercritical conditions (221 bar, 374°C) but did

not examine the effect of water density at a fixed temperature [4,9,10]. Varying the water density during the hydrothermal gasification of lignin can affect the yield and composition of the products [46]. The extent of this effect on the products from the hydrothermal liquefaction of microalgae at supercritical conditions is still unexplored.

2.3.5. Biomass Loading

The effect of biomass loading has not been thoroughly addressed. Jena et al. examined biomass concentrations of 10 - 50 wt % of *Spirulina* slurry. Although they found a minimal effect of the loading on the biocrude yield, it is not clear if their results can be extrapolated to other species of microalgae. The biomass to water ratio for liquefaction reactions can have a significant impact on the economics of this process and merits further examination [42,47].

2.3.6. Batch Holding Time

There is a discrepancy in reports of biocrude yields when the residence time is varied. Some results show that there is a decrease in biocrude yield as the reaction time is increased [2,12,15], while increased residence times, greater than an hour, did not affect the biocrude yield of *Chlorella vulgaris* and *Spirulina* sp. [8]. Yang et al. postulated that the biomass materials decompose as the reaction progresses for longer times > 60 min [2]. The increase in residence time decreased the viscosity of algal biocrude as the product decomposed into smaller molecules [3]. The majority of time-dependence studies only focus on two residence times [2,3,8,12,15,22].

To date, there have only been a few studies that examined how residence time affects the yields and elemental composition of the liquefaction products [3,9,10]. Jena et al. examined four holding times, but only for a single temperature (350 °C) and in an autoclave reactor (1.8 L) [9].

Similar experiments were conducted in large autoclave reactors (>100 mL) at holding times of 5, 30 and 60 min and at nominal temperatures of 250, 300, and 340 °C [2,3]. Garcia Alba et al. used a smaller batch reactor (45 mL) to achieve heat-up times of 6 - 7 min. They examined holding times of 5, 15, 30, 60 min, but for only 2 temperatures (200, 300 °C) [10]. It is not clear that the data from these studies can be treated as being from isothermal reactions because of the large reactor volumes and correspondingly large thermal mass and slow heat-up times. Thus their use in kinetic modeling is limited.

2.4. Understanding Reaction Pathways

Analyses of HTL feedstocks and products have allowed researchers to deduce some of the reactions that take place during hydrothermal liquefaction [4,7]. Many of the compounds are hydrolyzed in the hydrothermal media [4,7,45,48]. For example, the lipids (phospholipids and triglycerides) in the biomass are hydrolyzed to form free fatty acids. Free fatty acids are one of the primary products from liquefaction of microalgae [4,5]. Other research has demonstrated that proteins will decompose to amino acid monomers and then further decompose to ammonia during HTL [7,43,44]. From these reactions, some researchers have attempted to construct reaction pathways and networks. An example of a generalized reaction network depicting manure liquefaction is illustrated in Figure 2.2a [15]. A simpler reaction network in Figure 2.2b shows how the amino acids are decomposed in high temperature water [49]. There is no research available about how to unify similar studies into a single reaction network that models hydrothermal liquefaction.

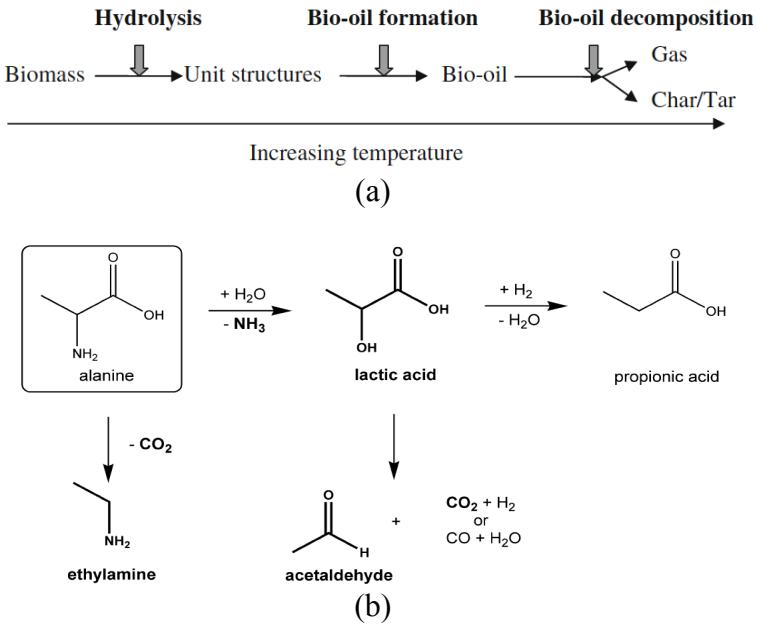

Figure 2.2. Examples of reaction networks: a) proposed network for cattle manure liquefaction [15], b) decomposition of amino acids [49]

Though no validated reaction network is available, the literature does provide insights suggesting the existence of certain pathways for hydrothermal liquefaction. For example, Torri et al. showed that proteins and carbohydrates from algal cells interact to form diketopiperazines, melanoidins, asphaltenes, and water-soluble compounds [50]. They describe how the proteins and carbohydrates react to form products that are classified as biocrude. Changi et al. showed that a model algal phospholipid, 1,2-dioleoyl-sn-glycero-3-phosphocholine (DOPC) [51], decomposed in near critical water to produce both water-soluble and organic solvent-soluble products. Reactions with phenylalanine [52], a water-soluble molecule, resulted in the formation of both significant amounts of CO_2 gas and hydrocarbons (e.g. styrene). Thus pathways from water-soluble products to both gas and biocrude could be operative during HTL.

This brief survey shows that the literature provides some qualitative glimpses into portions of the HTL reaction network, but a comprehensive picture is lacking. There is no quantitative

description available and there has been no prior work wherein isolated products from HTL have been reacted individually to elucidate their individual reaction pathways.

2.5. Literature Analysis

In the field of hydrothermal liquefaction, a broad range of biomass materials, including algae, have been tested for feasibility as liquefaction feedstocks. Reaction parameters such as temperature, time, and reaction atmosphere have been studied. The results of those experiments reveal that shorter reaction times (≤ 60 minutes) produce a maximum biocrude yield at temperatures between 300 - 350°C in a reducing gas atmosphere. Also, it is common practice to use elevated initial headspace pressure to ensure that the water remains liquid during processing. The available literature also demonstrates that the combination of techniques to determine heating value, viscosity, and composition provide satisfactory information to evaluate the biocrude's characteristics.

There are several gaps that stand out in the reviewed literature that provide opportunities for research. Even though algal biomass stands out as a feasible feedstock material, there has been no clear selection of a preferred alga for liquefaction that will result in a biocrude with high yield, carbon content, and heating value, with a low viscosity. Some researchers select species because of desirable ancillary characteristics such as the abundance of natural hydrocarbons (e.g. triterpenes) within a species [1], but presently they offer no comparisons with liquefaction experiments of other algae species. The need for comparative studies is especially important because species will vary with respect to biochemical content and regional availability [53].

The different solvents used in the procedures for product recovery make it difficult to compare results from the literature, even with the same feedstock. It is unclear how or whether

the different solvents affect the yields and compositions of the biocrude, and by extension, the dissolved aqueous solids and insoluble solid residue. It is likely that some of the HTL products partition differently among the solid, aqueous, and organic phases when different solvents are used to recover the biocrude. Thus, the solvent might have an effect on the yield and composition of the biocrude and other fractions produced from hydrothermal liquefaction. To our knowledge, this potential effect has not been the subject of any previously published research.

Presently, reports of thorough analyses of the water-soluble products and solid residues are limited in the literature and improvement is needed to provide analysis of these products. There are very few analyses available of the water-soluble products formed after liquefaction [2,19,20,54], although researchers have qualitatively examined the composition and molecular structure of some compounds [2,7,8,11,54]. Elucidation of the aqueous-phase composition will help researchers to understand how to utilize this by-product stream, as a nutrient recycle for algae growth or for other uses [37]. Additionally, there are few reports about the solid residues. It is possible to perform elemental analysis and determine heating value measurements [2], but there is no research available about the structures of functional groups in or molecular compositions of the solid residues.

There are still several processing conditions that have not been examined thoroughly. Although some catalysts have been reported to be effective for increasing algae biocrude yields [2,6,8], it is unclear why. It is also unclear why some biocrude yields improve with the addition of catalyst [2,8] while others show no improvement [1,3]. Additionally, the effect of the reaction atmosphere has not been fully studied with respect to algae liquefaction [6]. Another gap is the lack of investigation of the high-molecular-weight compounds that are present in the biocrude

[2]. The yield and composition of the high-molecular-weight compounds (> 300 amu) has not been determined. The biomass-to-water ratio is an important parameter that has not been fully studied except for a few cases using cattle manure, paper sludge and microalgae [9,12,15]. This is an important factor to consider because of the energy and cost associated with the dewatering of microalgae [41].

The HTL of other types of biomass cultivated in water-rich environments, such as bacteria and yeast, has not been studied. As mentioned previously, there are opportunities to mass-cultivate bacteria or yeast using effluents from other processes. The feasibility of hydrothermally treating bacteria or yeast cultures has yet to be demonstrated.

Presently, there is a significant gap with respect to kinetic studies of microalgal liquefaction. Most authors only focus on testing one or two residence times without measuring how certain products are formed with respect to time to evaluate the kinetics of algae liquefaction [2,3]. Additionally, there has not been a systematic study of how algae composition and reaction parameters affect biocrude composition. Independently, several of the reaction parameters have been studied [1-10], but no research has been accomplished to unify and correlate these studies. Overall, there are no clear correlations between residence time and reaction temperature with respect to the product yield, composition, viscosity, and heating value. While one review gives insight of some of the pathways that occur, it does not address how the multiple components of the algal cell interact with one another [42]. Reaction network design for the liquefaction of biomass is limited, if available at all. While some researchers have focused on reaction pathways that lead to biocrude formation, they have given limited attention to the formation of gas, water-soluble products, and solids [48]. Some work has included the study of protein and carbohydrate mixtures, but most studies focus on the use of model compounds [49]. The use of model

compounds will help to understand some of the underlying mechanisms, but ultimately may not be able to represent the complexity of an actual biomass system.

References

[1] Y Dote, S Sawayama, S Inoue, T Minowa, S-Y Yokoyama, *Recovery of liquid fuel from hydrocarbon-rich microalgae by thermochemical liquefaction*, Fuel 73 (1994) 1855-1857.

[2] YF Yang, CP Feng, Y Inamori, T Maekawa, *Analysis of energy conversion characteristics in liquefaction of algae*, Resour Conserv Recycl 43 (2004) 21-33.

[3] T Minowa, S-Y Yokoyama, M Kishimoto, T Okakura, *Oil production from algal cells of Dunaliella tertiolecta by direct thermochemical liquefaction*, Fuel 74 (1995) 1735-1738.

[4] TM Brown, P Duan, PE Savage, *Hydrothermal Liquefaction and Gasification of Nannochloropsis sp*, Energy Fuels 24 (2010) 3639-3646.

[5] PJ Valdez, JG Dickinson, PE Savage, *Characterization of Product Fractions from Hydrothermal Liquefaction of Nannochloropsis sp. and the Influence of Solvents*, Energy Fuels 25 (2011) 3235-3243.

[6] P Duan, PE Savage, *Hydrothermal Liquefaction of a Microalga with Heterogeneous Catalysts*, Ind Eng Chem Res 50 (2011) 52-61.

[7] P Biller, AB Ross, *Potential yields and properties of oil from the hydrothermal liquefaction of microalgae with different biochemical content*, Bioresour Technol 102 (2011) 215-225.

[8] AB Ross, P Biller, ML Kubacki, H Li, A Lea-Langton, JM Jones, *Hydrothermal processing of microalgae using alkali and organic acids*, Fuel 89 (2010) 2234-2243.

[9] U Jena, KC Das, JR Kastner, *Effect of operating conditions of thermochemical liquefaction on biocrude production from Spirulina platensis*, Bioresour Technol 102 (2011) 6221-6229.

[10] L Garcia Alba, C Torri, C Samori, J van der Spek, D Fabbri, SRA Kersten *et al.*, *I - Hydrothermal Treatment (HTT) of Microalgae: Evaluation of the Process As Conversion Method in an Algae Biorefinery Concept*, Energy Fuels 26 (2012) 642-657.

[11] M Murakami, S-Y Yokoyama, T Ogi, K Koguchi, *Direct liquefaction of activated sludge from aerobic treatment of effluents from the cornstarch industry*, Biomass 23 (1990) 215-228.

[12] C Xu, J Lancaster, *Conversion of secondary pulp/paper sludge powder to liquid oil products for energy recovery by direct liquefaction in hot-compressed water*, Water Res 42 (2008) 1571-1582.

[13] KB Cantrell, T Ducey, KS Ro, PG Hunt, *Livestock waste-to-bioenergy generation opportunities*, Bioresour Technol 99 (2008) 7941-7953.

[14] BJ He, Y Zhang, Y Yin, TL Funk, GL Riskowski, *Preliminary characterization of raw oil products from the thermochemical conversion of swine manure*, Trans ASABE 42 (2001) 1865-1871.

[15] S Yin, R Dolan, M Harris, Z Tan, *Subcritical hydrothermal liquefaction of cattle manure to bio-oil: Effects of conversion parameters on bio-oil yield and characterization of bio-oil*, Bioresour Technol 101 (2010) 3657-3664.

[16] WJ Catallo, JL Comeaux, *Reductive hydrothermal treatment of sewage sludge*, Waste Manag 28 (2008) 2213-2219.

[17] DR Vardon, BK Sharma, J Scott, G Yu, Z Wang, L Schideman *et al.*, *Chemical properties of biocrude oil from the hydrothermal liquefaction of Spirulina algae, swine manure, and digested anaerobic sludge*, Bioresour Technol 102 (2011) 8295-8303.

[18] T Minowa, F Zhen, T Ogi, *Cellulose decomposition in hot-compressed water with alkali or nickel catalyst*, J of Supercrit Fluids 13 (1998) 253-259.

[19] U Schuchardt, JAR Rodrigues, AR Cotrim, JLM Costa, *Liquefaction of hydrolytic eucalyptus lignin with formate in water, using batch and continuous-flow reactors*, Bioresour Technol 44 (1993) 123-129.
[20] C Song, H Hu, S Zhu, G Wang, G Chen, *Nonisothermal catalytic liquefaction of corn stalk in subcritical and supercritical water*, Energy Fuels 18 (2004) 90-96.
[21] BJ He, Y Zhang, Y Yin, TL Funk, GL Riskowski, *Operating temperature and retention time effects on the thermochemical conversion process of swine manure*, Trans ASABE 43 (2000) 1821-1825.
[22] S-Y Yokoyama, A Suzuki, M Murakami, T Ogi, K Koguchi, E Nakamura, *Liquid fuel production from sewage sludge by catalytic conversion using sodium carbonate*, Fuel 66 (1989) 1150-1151.
[23] S Sawayama, T Minowa, S-Y Yokoyama, *Possibility of renewable energy production and CO2 mitigation by thermochemical liquefaction of microalgae*, Biomass Bioenergy 17 (1999) 33-39.
[24] Y Chisti, *Biodiesel from microalgae*, Biotechnol Adv 25 (2007) 294-306.
[25] AF Clarens, EP Resurreccion, MA White, LM Colosi, *Environmental life cycle comparison of algae to other bioenergy feedstocks*, Environ Sci Technol 44 (2010) 1813-1819.
[26] W Mulbry, S Kondrad, C Pizarro, E Kebede-Westhead, *Treatment of dairy manure effluent using freshwater algae: algal productivity and recovery of manure nutrients using pilot-scale algal turf scrubbers*, Bioresour Technol 99 (2008) 8137-8142.
[27] M Packer, *Algal capture of carbon dioxide; biomass generation as a tool for greenhouse gas mitigation with reference to New Zealand energy strategy and policy*, Energy Policy 37 (2009) 3428-3437.
[28] M Gavrilescu, Y Chisti, *Biotechnology-a sustainable alternative for chemical industry*, Biotechnol Adv 23 (2005) 471-499.
[29] F Leroy, V De, Luc, *Lactic acid bacteria as functional starter cultures for the food fermentation industry*, Trends Food Sci Technol 15 (2004) 67-78.
[30] C Angerbauer, M Siebenhofer, M Mittelbach, GM Guebitz, *Conversion of sewage sludge into lipids by Lipomyces starkeyi for biodiesel production*, Bioresour Technol 99 (2008) 3051-3056.
[31] S Huffer, CM Roche, HW Blanch, DS Clark, *Escherichia coli for biofuel production: bridging the gap from promise to practice*, Trends Biotechnol 30 (2012) 538-545.
[32] C Ratledge, Z Cohen, *Microbial and algal oils: Do they have a future for biodiesel or as commodity oils?*, Lipid Technology 20 (2008) 155-160.
[33] BD Wahlen, MR Morgan, AT McCurdy, RM Willis, MD Morgan, DJ Dye *et al.*, *Biodiesel from Microalgae, Yeast, and Bacteria: Engine Performance and Exhaust Emissions*, Energy Fuels 27 (2013) 220-228.
[34] NJ Horan, *Biological wastewater treatment systems: theory and operation*, Wiley: Chichester: 1990; 52
[35] P Biller, AB Ross, SC Skill, A Lea-Langton, B Balasundaram, C Hall *et al.*, *Nutrient recycling of aqueous phase for microalgae cultivation from the hydrothermal liquefaction process*, Algal Research 1 (2012) 70-76.
[36] L Garcia Alba, C Torri, D Fabbri, SRA Kersten, B (Wim), Derk W.F., *Microalgae growth on the aqueous phase from Hydrothermal Liquefaction of the same microalgae*, Chem Eng J 228 (2013) 214-223.

[37] U Jena, N Vaidyanathan, S Chinnasamy, KC Das, *Evaluation of microalgae cultivation using recovered aqueous co-product from thermochemical liquefaction of algal biomass*, Bioresour Technol 102 (2011) 3380-3387.
[38] M Pham, L Schideman, J Scott, N Rajagopalan, MJ Plewa, *Chemical and biological characterization of wastewater generated from hydrothermal liquefaction of Spirulina*, Environ Sci Technol 47 (2013) 2131-2138.
[39] M Nelson, L Zhu, A Thiel, Y Wu, M Guan, J Minty *et al.*, *Microbial utilization of aqueous co-products from hydrothermal liquefaction of microalgae Nannochloropsis oculata*, Bioresour Technol 136 (2013) 522-528.
[40] T Matsui, A Nishihara, C Ueda, M Ohtsuki, N Ikenaga, T Suzuki, *Liquefaction of micro-algae with iron catalyst*, Fuel 76 (1997) 1043-1048.
[41] SM Heilmann, HT Davis, LR Jader, PA Lefebvre, MJ Sadowsky, FJ Schendel *et al.*, *Hydrothermal carbonization of microalgae*, Biomass Bioenergy 34 (2010) 875-882.
[42] AA Peterson, F Vogel, RP Lachance, M Fröling, MJ Antal Jr, JW Tester, *Thermochemical biofuel production in hydrothermal media: A review of sub-and supercritical water technologies*, Energy Environ Sci 1 (2008) 32-65.
[43] Y Dote, S Inoue, T Ogi, S-Y Yokoyama, *Studies on the direct liquefaction of protein-contained biomass: the distribution of nitrogen in the products*, Biomass Bioenergy 11 (1996) 491-498.
[44] Y Dote, S Inoue, T Ogi, S-Y Yokoyama, *Distribution of nitrogen to oil products from liquefaction of amino acids*, Bioresour Technol 64 (1998) 157-160.
[45] AV Bridgewater, *Catalysis in thermal biomass conversion*, Appl Catal, A 116 (1994) 5-47.
[46] FLP Resende, SA Fraley, MJ Berger, PE Savage, *Noncatalytic Gasification of Lignin in Supercritical Water*, Energy Fuels 22 (2008) 1328-1334.
[47] CF Murphy, DT Allen, *Energy-water nexus for mass cultivation of algae*, Environ Sci Technol 45 (2011) 5861-5868.
[48] A Kruse, A Gawlik, *Biomass conversion in water at 330-410 C and 30-50 MPa. Identification of key compounds for indicating different chemical reaction pathways*, Ind Eng Chem Res 42 (2003) 267-279.
[49] D Klingler, J Berg, H Vogel, *Hydrothermal reactions of alanine and glycine in sub- and supercritical water*, J of Supercrit Fluids 43 (2007) 112-119.
[50] C Torri, L Garcia Alba, C Samori, D Fabbri, DWFW Brilman, *I - Hydrothermal Treatment (HTT) of Microalgae: Detailed Molecular Characterization of HTT Oil in View of HTT Mechanism Elucidation*, Energy Fuels 26 (2012) 658-671.
[51] S Changi, AJ Matzger, PE Savage, *Kinetics and pathways for an algal phospholipid (1,2-dioleoyl-sn-glycero-3-phosphocholine) in high-temperature (175-350 °C) water*, Green Chem. 14 (2012) 2856.
[52] S Changi, M Zhu, PE Savage, *Hydrothermal reaction kinetics and pathways of phenylalanine alone and in binary mixtures*, ChemSusChem 5 (2012) 1743-1757.
[53] EW Becker, *Micro-algae as a source of protein*, Biotechnol Adv 25 (2007) 207-210.
[54] D Zhou, L Zhang, S Zhang, H Fu, J Chen, *Hydrothermal liquefaction of macroalgae Enteromorpha prolifera to bio-oil*, Energy Fuels (2010)

Chapter 3

Experimental Methods

This chapter outlines the procedures used to gather experimental data for the hydrothermal liquefaction (HTL) of the various types of biomass and intermediate products. The first section lists all of the materials used for the experiments, including chemicals and biomass. The second section outlines the methods to analyze the biomass feedstock. The third section explains how we hydrothermally treated the reagents, including an explanation of the reactor design. The fourth and fifth sections describe all of the experimental techniques used to recover the product fractions, quantify the yields, and analyze the elemental composition and molecular properties of the products. The final section outlines the experimental variables that we studied. When necessary, specific modifications to the general procedure are provided later.

HTL presents several challenges because of the multiple phases that are present that need to be collected and quantified (i.e. biocrude, aqueous-phase products, gas, solids). We developed several methods to analyze the feedstocks and liquefaction products based on the techniques used by the Savage group and other laboratories [1-3]. In most cases we measured replicate samples, we report averages, with one standard deviation being the reported uncertainty.

3.1. Materials

This section describes the chemicals and different biomass feedstocks used for experimentation.

3.1.1. Chemicals

We obtained all solvents and chemical reagents from Sigma-Aldrich in high purity (≥ 99%), except for hexane (> 95%), and used them as received. We purchased air (< 1ppm hydrocarbons) and ≥ 99.998% pure N_2, He, H_2, and Ar from Metro Welding Supply Corp. (Detroit, MI) for use in experiments and gas chromatographic analyses. We used deionized water from an in-house source.

3.1.2. Biomass and Intermediate Products

We purchased *Nannochloropsis* sp. slurries, 20 and 35 wt % algal solids, from Reed Mariculture Inc. (San Jose, CA). The 20 wt % slurry, referred to as Nanno3600, was reported to be 52 wt % proteins, 28 wt % lipids, and 12 wt % carbohydrates. This slurry also included a proprietary mixture of preservative compounds that increased the ash content of the algal biomass [4]. The 35 wt % slurry of *Nannochloropsis* sp. was measured by the supplier to be 59 wt % proteins, 14 wt % lipids, and 20 wt % carbohydrates. Any extracellular material in the 35 wt % slurry was from the cultivation medium only. Water-free *Scenedesmus* sp. was donated from the University of Kentucky and was measured to be 50 wt % proteins, 8 wt % lipids, and 31 wt % carbohydrates. We cultivated *Chlorella protothecoides* (UTEX #255) in the laboratory with assistance from Bobby Levine [5] and concentrated it to a 25 wt % slurry in an Eppendorf 5810 centrifuge. We measured the *C. protothecoides*, using the procedure described in section

3.2.2, to be 11 wt % proteins, 53 wt % lipids, and 29 wt % carbohydrates. As needed, the microalgae was diluted with deionized water for experimentation to a specific slurry concentration.

We collaborated with Mike Nelson who cultivated and prepared several different bacteria cultures. We cultivated various microorganisms to study the differences in biochemical content and cellular structure. We grew *Escherichia coli* K12 MG1655*, Pseudomonas putida* KT2440, *Bacillus subtilis* SB491, and *Saccharomyces cerevisiae* S288C in various "rich" media containing high concentrations of complex biologically derived materials such as yeast extract and peptone to maximize biomass yield per volume of culture. We also grew *E. coli* in a "minimal" medium, which contained only chemically defined substrates and nutrients. For the rich media we used Luria-Bertani medium (10 g/L tryptone, 5 g/L yeast extract, 10 g/L NaCl) for *P. putida*, Terrific Broth medium (12 g/L tryptone, 24 g/L yeast extract, 4 mL/L glycerol, 2.3 g/L KH_2PO_4, 12.5 g/L K_2HPO_4) for *E. coli* and *B. subtilis*, and Yeast Peptone Dextrose medium (10 g/L yeast extract, 20 g/L peptone, 20 g/L dextrose) for *S. cerevisiae*. For the *E. coli* minimal medium we used M9 medium (20 g/L glucose, 1 g/L NH_4Cl, 6 g/L Na_2HPO_4, 3 g/L KH_2PO_4, 0.5 g/L NaCl, 120 mg/L Mg_2SO_4, 11 mg/L $CaCl_2$). Both seed cultures and final cultures were grown in the same media. *E. coli* grown in Terrific Broth and M9 minimal medium will be referred to as *E. coli* TB and *E. coli* MM, respectively. We harvested and washed the samples with deionized water to remove any extracellular media, since they were highly concentrated in carbon containing compounds that could possibly affect the products. We harvested the biomass and concentrated it using a centrifuge to at least a 12 wt % slurry.

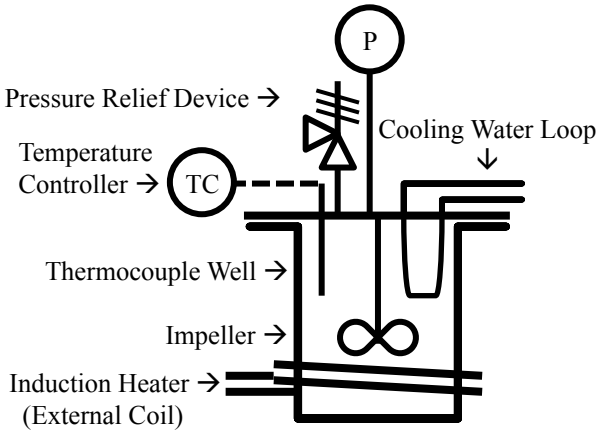

Figure 3.1. Induction-heated reaction vessel

We produced intermediate liquefaction products from microalgae by stopping a liquefaction reaction after a given time and isolating the products to be reacted again separately. To create the intermediate products, we loaded 155 g of 15 wt % microalgal slurry of *Nannochloropsis* sp. into a 283 mL Parr pressure vessel to generate the solids (insoluble in dichloromethane and water), aqueous-phase products (soluble in water), light biocrude (soluble in hexane and dichloromethane), and heavy biocrude (insoluble in hexane, soluble in dichloromethane) used in subsequent experiments. The vessel, depicted in Figure 3.1, was heated from room temperature to 350 °C using an induction heater from LC Miller Co. (Monterey Park, CA). The contents of the reactor were mixed with an impeller at 800 rpm. The reactor reached the reaction temperature in approximately 10 min and remained there for another 30 min. To stop the reaction and cool the vessel we turned off the induction heater, submerged the vessel in room-temperature water, and immediately began to flow cold water through the cooling loop inside the reactor. The reactor cooled to < 50 °C in approximately 10 min. We opened the reactor and poured the contents into a 1 L beaker. We then used 500 mL of dichloromethane in smaller aliquots to rinse the reactor and recover any product residues. The dichloromethane rinse was added to the

contents poured from the reactor. We stirred the beaker contents and then poured them into a separatory funnel. We shook and vented the separatory funnel several times and then allowed the contents to phase separate overnight. We collected the dichloromethane, aqueous, and solid phases from the separatory funnel. The aqueous-phase collected here was retained as-is for use in the subsequent experiments. We dried the solids by flowing N_2 over them for 6 h. This material provides the solid product fraction used for subsequent experiments. We poured the dichloromethane phase into a round-bottom flask and removed the dichloromethane with a Buchi R-114 rotary evaporator until the product appeared visually to be solvent-free. Any residual dichloromethane was evaporated by flowing N_2 over the dichloromethane-soluble products for an additional 6 h. After removal of the dichloromethane, 180 mL of n-hexane was added to the round-bottom flask, which was then stirred for approximately 20 min. After stirring, the insoluble material was allowed to settle to the bottom and the hexane was decanted into another round-bottom flask and this process was repeated twice. The amount of solvent used in the product recovery is similar in proportion to the methodology described for algae liquefaction in section 3.4 [6]. The hexane was then removed under vacuum using a rotary evaporator. Both round-bottom flasks, one with the hexane-insolubles and the other with the hexane-solubles were dried for 24 h under N_2 to remove any residues of solvent. These materials comprise the heavy (hexane-insoluble) and light (hexane-soluble) biocrude product fractions used for subsequent experiments.

3.2. Feedstock Analysis

This section describes the methods to analyze the different biomass feedstocks. The first part outlines the methods for defining the solids concentration in the biomass slurry and the elemental

and ash content of the dried biomass. The second part describes the methods used to determine the biochemical content of the biomass, that is, the concentrations of lipids, proteins, and carbohydrates.

3.2.1. Solids, Ash, and Elemental Content

We transferred biomass slurries to a glass test tube or an aluminum weigh boat to determine the solids or water-free contents. We placed the slurry sample in a 70 °C oven for 48 - 72 h to remove all of the water and then weighed the sample. The methodology for ash content is in accord with guidelines found in ASTM E 1755, standard test method for ash in biomass [7]. For ash content, we measured 50 mg of the dried biomass material into a pre-weighed aluminum weigh boat. A Ney Vulcan 3-130 muffle furnace heated the sample to 250 °C from room temperature at a rate of 10 °C/min to prevent flare-up. After a 30 min holding period, the temperature was increased at a rate of 20 °C/min to 450 or 550 °C and then held for 3 - 30 h. For microalgae samples, the temperature was held at 450 °C for 3 h and for bacteria and yeast samples the final temperature was held at 550 °C for up to 30 h. The lower holding temperature prevents the loss of some salts that are common for microalgae cultivation [8]. After removing the samples from the furnace, we cooled them in a desiccator to room temperature and then recorded the mass of ash. We sent dried samples of the biomass feedstock to Atlantic Microlabs, Inc. (Norcross, GA) for analysis of C, H, N, and S content. We sent selected samples to Midwest Microlab (Indianapolis, IN) for P analysis. We estimated O content of the biomass as the difference between 100 wt % and the combined content of C, H, N, S, P, and ash.

We identified trace metals in the biomass by dissolving 15 mg of dry biomass into 3 mL concentrated nitric acid for 24 h. We then diluted the sample with 12 mL of deionized water, and

injected a sample into a Varian 710ES inductively coupled plasma optical emission spectrometer. We scanned the results for wavelengths between 300 - 800 nm. We report the trace metals that were positively identified by the emission results.

3.2.2. Biochemical Content

We developed a lipid analysis method by combining practices from Levine et al. and Lewis et al. [5,9]. We measured approximately 20 mg of dried biomass into a glass test tube. To each test tube, we added 2 mL of a 5 v/v % solution of acetyl chloride in methanol and a magnetic stir bar. We vigorously stirred the reaction mixture (> 100 rpm) for 90 minutes at 100 °C using a magnetic stir plate and temperature-controlled heating block. After the holding period, we quenched the reaction by adding 1 mL of room-temperature deionized water. After cooling for 10 min, we added 4 mL of n-heptane and agitated each test tube for 10 min on a vortexer set to 1000 rpm. We centrifuged the mixture for 3 min at 1500 rcf to separate and then collect the heptane layer for gas chromatographic analysis. We injected 1 μL of sample, with a 2:1 split ratio, into an Agilent 7890 gas chromatograph. We used an Agilent DB-FFAP column (30 m × 320 μm × 0.25 μm) with a column flow of 1 mL/min and helium as the carrier gas. The injector temperature was 250 °C. The oven temperature was maintained at 60 °C until the injection and then increased to 200 °C at a rate of 20 °C/min and then to 240 °C at a rate of 5 °C/min. The final temperature was held for 3 min. We generated calibration curves using a RESTEK Marine Oil mixture of 20 fatty acid methyl esters as an external standard.

We estimated protein content (wt %) of the biomass using a multiplying factor of 6.25 times the N content (wt %) of the biomass [10,11]. We estimated the carbohydrate content (wt %) as the difference between 100 wt % and the summation of the lipid, protein, and ash content.

3.3. Hydrothermal Liquefaction

This section describes the design of the liquefaction reactors and how we carried out the liquefaction reactions.

3.3.1. Reactors

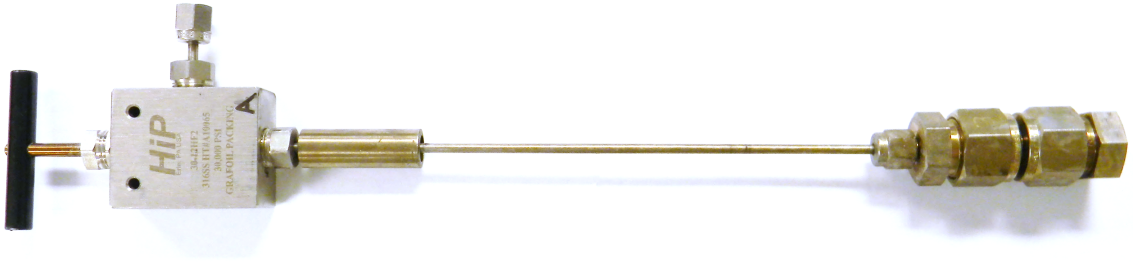

Figure 3.2. 4.1mL Swagelok® batch reactor with gas sampling valve

For the hydrothermal treatment of the various feedstocks we used several different reactors constructed from Swagelok® (Farmington Hills, MI) parts made from 316 stainless steel. We assembled 1.7 and 4.1 mL mini-batch reactors using 3/8 and 1/2 in. Swagelok® port connectors, respectively. We also assembled 31 mL reactors consisting of an 8 in. length of 316 stainless steel tubing (¾ in. OD, 0.065 in. wall thickness). We capped one end of each reactor and fitted a High Pressure Equipment Co. (Erie, PA) high-pressure (15,000 or 30,000 psi) valve to the other end of the reactor via 8.5 in. of 1/8 in. OD stainless steel tubing (0.028 in. wall thickness). The total volume added to the reactor by the valve assembly was 0.5 mL. To vary the composition of the reactor headspace we repeatedly evacuated (1.5 psia) and pressurized (> 10 psig) the reactor using the desired gas. For reactions in which the valve was not needed to analyze gas products or to inject a specific gas into the reactor headspace, the reactor was simply capped. Experimentation (see section 4.3) and stoichiometric calculations showed that oxygen in the reactor headspace does not significantly affect the product yields. To pressure test and condition

the reactors, we loaded them with deionized water and heated them to 350 °C for 60 min prior to use. After cooling, we thoroughly cleaned the reactors with detergent, rinsed with them deionized water and acetone and air-dried them.

3.3.2. Reactions

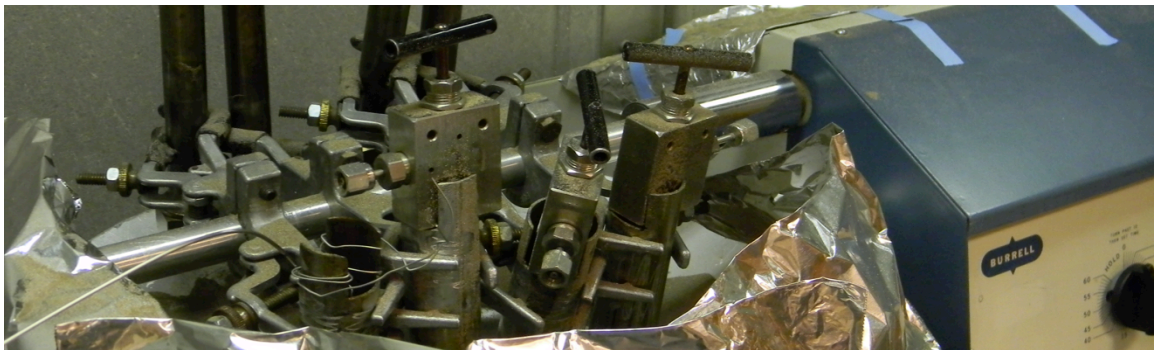

Figure 3.3. Reactors in the shaker setup

We loaded the reactors with enough slurry so that the liquid water would expand to fill 95% of the reactor volume at the subcritical reaction temperatures (T < 374 °C), while maintaining consistent slurry content for a given set of experiments. At supercritical water conditions (T > 374 °C), we loaded enough water to correspond to a set water density for the reaction conditions. We sealed the reactors, keeping ambient air in the reactor headspace unless otherwise noted. We sealed the reactors with a torque wrench set to 45 ft-lbs. We then placed the reactors in a Techne SBL-2 fluidized sandbath. When gas valves were not used, we placed the reactors into a wire basket that was then suspended in the sandbath. For the 1.7 and 4.1 mL reactors with gas valves, we agitated them using a Burrell Wrist-Action® shaker. Figure 3.3 shows reactors with valves placed in the shaker setup. The shaking angle was approximately 2° and the shaking speed was approximately 385 oscillations per minute, as stated by the manufacturer.

A Techne TC-8D temperature controller maintained the sandbath temperature to within ± 2 °C of the reaction temperature. After the desired reaction time, we removed the reactors from the sandbath, quenched them in a room-temperature water bath for > 5 min and allowed them to equilibrate to room temperature for at least 30 min before collecting and analyzing the product fractions.

3.4. Recovery and Separation of the Product Fractions

This section discusses each of the experimental methods used to recover the products from the 1.7 and 4.1 mL reactors and isolating each product for analysis. A different procedure for the larger 31 mL reactors will be described later (section 4.1.1.). The experimental procedure is based on methods developed by myself and other members of the Savage research group [1] and was implemented to collect the data to complete each of the research objectives unless otherwise noted.

3.4.1. Product Recovery and Separation for 1.7 and 4.1 mL Reactors

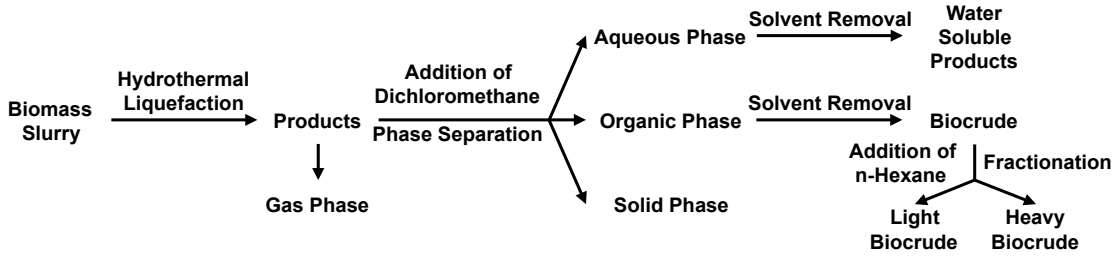

Figure 3.4. Product work-up procedure

Figure 3.4 illustrates the procedure used to collect the various product fractions after reaction. As needed, we first analyzed the gas in the reactor headspace using the method outlined by Brown et al. [1], which will be explained later in section 3.5.3. We opened the reactors by removing the valve assembly and we then poured the contents into a glass conical test-tube. In instances when the gas valve was not used we simply uncapped the reactor slowly to allow gases to escape. In most cases, the products separated naturally in the conical tube into a biocrude phase, an aqueous phase, and a solid phase. We then rinsed the reactors with 9 mL dichloromethane to ensure complete collection of all of their contents. We added the dichloromethane to the reactor in small aliquots ($\leq$ 3 mL), agitated it, and poured the contents into the conical tube. We verified that this procedure left behind < 1 wt % of the original mass loaded into the reactors. After collecting the reactor contents and dichloromethane rinses, we vortexed the conical tube at 3000 rpm for 1 min and then centrifuged the tube in an Eppendorf 5810 centrifuge at 500 relative centrifugal force (rcf) for 1 min. After centrifugation, the solid products accumulated at the interface between the aqueous (top layer) and organic (bottom layer) phases. We transferred the organic phase via pipet to another tube and centrifuged the conical tube again at 1500 rcf for 3 min to remove suspended solids from the aqueous phase. A control experiment verified the absence of additional solids in the organic or aqueous phase after centrifuging both phases at a higher speed for longer time. We transferred the aqueous phase to another tube via pipet. We then dried the remaining material in the conical tube in a 70 °C oven for 72 h to drive off residual dichloromethane and water. The dried solids were weighed and later analyzed.

We removed the dichloromethane from the organic phase by flowing N_2 over the organic phase tubes for approximately 6 h. The dichloromethane-soluble product that remained is

classified as the biocrude. After removing the dichloromethane, we scraped the biocrude from the walls of the tube with a metal spatula, added 8 mL of n-hexane to the tube and agitated it with a vortexer at 1000 rpm for 60 min. We centrifuged the tube for 3 min at 1500 rcf and decanted the hexane phase to another tube. We removed the hexane by flowing N_2 over the hexane phase tubes for 6 h. We classify the hexane-soluble biocrude as light biocrude, while the hexane-insoluble but dichloromethane-soluble fraction is the heavy biocrude. We weighed and analyzed the light and heavy biocrude products.

We transferred at least a 500 μL aliquot of the aqueous phase to a pre-weighed 1 dram vial and removed the water by flowing N_2 over the vial for 6 h. The dried material is classified as the 'water-soluble products' for which we always determined the gravimetric yield and elemental composition.

We calculated the yield of each product fraction as follows:

$$\text{Yield (wt \%)} = (\text{Mass of Product Fraction} / \text{Mass of Biomass}) \times 100\%$$

There is a fundamental difference between the water-soluble products and the aqueous-phase products. The water-soluble products were dried and the yield measured directly, whereas the aqueous-phase products were never dried and the yield is calculated by difference:

$$\text{Yield of Aqueous-phase Products (wt \%)} = 100 \text{ wt \%} - \sum \text{Yield of Solids, Gas, Light and Heavy Biocrude}$$

The yield of aqueous-phase products always exceeded the yield of water-soluble products since some compounds in the aqueous phase were lost as the water was removed to recover the water-soluble products [6].

3.4.2. Zero-minute Products

We modified the work-up procedure to determine the yields of the various solubility-based product fractions originally present in the biomass feedstock. We loaded the same amount of algae slurry into a glass test tube that we would have added to the reactors and then dried the tube in an oven at 70 °C for 72 h to remove the water. After adding 9 mL of dichloromethane to the tube and agitating the tube on a vortexer at 1000 rpm for 1 h, we added the amount of water that would be present in the reaction system and agitated the algae, solvent, and water for 1 h at 1000 rpm on a vortexer. After this step, the phases were easily separated using the aforementioned procedure.

3.4.3. Control Experiments

As a control experiment, we loaded and sealed reactors as described, but omitted immersion in the sandbath. Instead the reactors were agitated with a vortexer at 1000 rpm for 40 - 60 min. We followed the work-up procedure described above to verify the recovery of all of the biomass from the reactor.

3.5. Analysis of the Product Fractions

This section outlines each of the analytical methods used to measure gravimetric yields and elemental and molecular composition of the products. Table 3.1 summarizes the analytical

metrics used to characterize each of the product fractions. The analytical procedures provide a thorough examination of the characteristics of the liquefaction products.

Table 3.1. Summary of the metrics for each product fraction

Product	Characterization Metric
Gas	Yield, Gas Composition via GC-TCD (H_2, N_2, O_2, CO, CO_2, CH_4, C_2H_4, C_2H_6)
Aqueous Phase - Water-soluble products	Yield of Water-soluble Products, Yield of Aqueous-phase Products by difference, Ash Content, Total Carbon (Organic, Inorganic), Total Nitrogen (Ammonia), Total Phosphorus (Phosphate), Elemental Content of dried water-soluble products
Residual Solids	Yield, Ash Content, Elemental Content (C,H,N,O,S)
Biocrude - Light Fraction - Heavy Fraction	Yield, Ash Content, Elemental Content (C,H,N,O,S), Molecular Composition via GC-MSD, GC-FID, EI-MS
Biomass Feedstock	Ash Content, Elemental Content (C,H,N,O,S,P), Trace Metal Content via ICP, Lipid, Protein, & Carbohydrate Content

3.5.1 Elemental Analysis of the Biocrude and Solids

We sent solvent-free samples of the biocrude and solid product fractions to Atlantic Microlab Inc. for elemental analysis of C, H, N, and S. O content of these product fractions was calculated by difference. The elemental content is reported as the weight percent of the element in the total sample. To measure the total amount of inorganic content in these products we removed all of the organic material by dry ashing, as described previously, and reporting the total ash content.

3.5.2. Analysis of the Aqueous Phase

We sent the dried water-soluble products to Atlantic Microlab Inc. for elemental analysis. We also analyzed the aqueous phase for ammonia, total nitrogen, total carbon, inorganic carbon (carbonate and bicarbonate), total phosphorus and free phosphate (orthophosphate) before removing the water. We developed the methodologies to analyze the aqueous phase with Mike Nelson. For spectrophotometric measurements of the absorbance of the analyte solutions we used a Thermo Scientific Genesys20 or Molecular Devices Spectramax M5 spectrophotometer.

We measured total carbon and inorganic carbon using a Shimadzu TOC-VCSH total organic carbon analyzer, and calculated total organic carbon (TOC) by the difference. We prepared 9 mL of a 1:600 dilution of the aqueous phase so the C content was < 50 g C/L. We injected 3 mL of the sample into the analyzer at room temperature. We used potassium hydrogen phthalate as an external calibration standard.

We used Hach® Nitrogen-ammonia reagent (< 50 mg NH_3/L) test kits to measure ammonia and an established persulfate method [12] to measure total N. We used glycine as an external standard to prepare calibration curves for both assays. For the measurement of ammonia, we followed the prescribed procedure that came with the kit, adding 100 μL of a 1:200 diluted sample of aqueous phase to the test kit. Following the directions, we waited 20 min for the reaction to occur at room temperature. We then measured the absorbance of the analyte solution at 655 nm and compared the measured absorbance to the calibration curve.

We used a common oxidation procedure to prepare samples of the aqueous phase for measurement of total N and P. We diluted the samples to 1:4000 and 1:70 for N and P analyses, respectively. For each 2 mL aliquot of analyte solution we added 534 μL of oxidizing reagent (0.18M $K_2S_2O_8$, 0.49M H_3BO_3, and 0.35M NaOH) [12]. We heated the samples to 130 °C for 45

min using an aluminum heating block. After the reaction we allowed the solutions to cool to room temperature before measuring the absorbance of the analyte solution. For total N measurement of the treated solution, we measured the absorbance of nitrate at 220 nm and the absorbance of any interfering organics at 275 nm. We reported the corrected absorbance as follows to remove the interference of organic compounds:

$$\text{Corrected Absorbance} = \text{Absorbance}(220\text{ nm}) - 2[\text{Absorbance}(275\text{ nm})]$$

To measure free phosphate (orthophosphate) in the analyte solution, we reacted a 1:70 dilution of the sample with a vanadomolybdophosphoric acid reagent [13] to obtain an absorbance measurement at 400 nm. To measure total P, we first treated the diluted analyte solution following the oxidation procedure noted above to convert all the P in the analyte to phosphate. We then added the vanadomolybdophosphoric acid reagent and measured the absorbance at 400 nm. We used sodium phosphate as an external standard for both P and orthophosphate assays.

To determine non-cellular aqueous nitrogen and phosphorus in the unreacted algae slurry, we centrifuged a 2.5 wt % slurry at 18,500 rcf, filtered the supernatant through a 0.22 μm acetate filter to remove all of the microalgae cells, and measured the N and P content of the filtrate. We subtracted these background values from the aqueous phase measurements for N and P to ensure reported values were only from cellular N and P, and not from algae growth medium. We assume that the NH_3 and PO_4^{3-} present in the growth medium is insignificant when compared to the N and P in the biomass.

3.5.3. Analysis of the Gas Products

We quantitatively measured the gas in the reactor headspace via gas chromatography with a thermal conductivity detector (GC-TCD). GC-TCD analysis with a Carboxen-1000, (a carbon-sieve) packed-column permitted the measurement of hydrogen, carbon dioxide, carbon monoxide, methane, ethane, ethene, and nitrogen gases. The nitrogen gas present in the reactor headspace from residual air served as an internal standard and was used to determine molar and gravimetric yields of gas products. In instances in which the air in the reactor headspace was replaced with helium, the helium served as an internal standard. Other researchers have confirmed the presence of HCN, N_2O, NO_x, and NH_3 in the reactor headspace as well, but these gases are difficult to quantify with GC methods and are of relatively low concentration (< 220 ppm) [3].

3.5.4. Molecular Composition of the Biocrude

We identified specific biocrude compounds by analyzing the organic phase, prior to evaporating the solvent, on an Agilent Technologies 6890N GC with an autosampler, autoinjector, mass spectrometric detector (GC-MSD), and an Agilent HP-5MS non-polar capillary column (50 m × 200 μm × 0.33 μm). Analyzing the biocrude prior to the evaporation of the solvent allowed us to identify and quantify volatile compounds. We injected 2 μL of organic phase into a 300 °C inlet with a 10:1 split ratio. The column was initially held at 35 °C for 5 min, then ramped at 1 °C/min to 50 °C, 3 °C/min to 300 °C, and finally held isothermally for 15 min. Helium (0.9 mL/min) served as the carrier gas. We also modified the method, injecting 1 μL of organic phase into a 300 °C inlet with a 2:1 split ratio. The column was initially at 100 °C then ramped at 5 °C/min to 300 °C and we used helium as the carrier gas (1 mL/min).

Quantification of biocrude compounds was carried out on an Agilent Technologies 7890 GC with a flame ionization detector (GC-FID). For all compounds except free fatty acids, the quantification was performed with an Agilent HP-5 non-polar capillary column (50 m × 200 μm × 0.33 μm) using the same conditions as the GC-MSD, except the split ratio was increased to 15:1 and the column flow was increased to 1 mL/min. Quantification of free fatty acids proved inconsistent on the HP-5 column, so we used a Supelco Nukol® or Agilent DB-FFAP capillary column (30 m × 320 μm × 0.25 μm) and a cool on-column inlet. Both columns were lined with polyethylene glycol as the stationary phase. A 0.5 μL sample of organic phase was injected onto the column at 100 °C. The temperature was then ramped at 10 °C/min to 220 °C and held for 18 min. Analyzing solvent blanks with the GC-FID, we verified that the solvents contained no detectable impurities that interfered with the quantification of compounds in the biocrude.

We produced calibration curves by analyzing standards containing authentic compounds in known concentrations on GC-FID. It was not practical to generate calibration curves for all of the compounds identified by GC-MSD because of their great number and cost. Thus, some compounds were quantified using the calibration determined experimentally for a different component with a similar chemical structure.

We analyzed the solvent-free biocrude samples with a VG 70-250-S magnetic sector mass spectrometer (MS), using both electron impact ionization (EI) and chemical ionization (CI) techniques. For EI, the ionization source was set at 70 eV. For CI, methane was used with a source accelerating voltage of 8 kV. In both cases, the source temperature was set at 240 ºC and a direct probe, heated from room temperature to 300 ºC under vacuum, volatilized the samples. Jim Windak from the Chemistry department's analytical laboratory assisted with these analyses.

3.5.5. Elemental Distribution

We report the distribution of the elements contained in the original biomass among the various product fractions.

$$\text{Elemental Distribution (\%)} = (\text{Mass of Element in Product Fraction} / \text{Mass of Element in Biomass}) \times 100\%$$

3.5.6. Energy Distribution

We calculated the heating value of the products using the Boie formula and the C, H, O, N, and S weight percentages on a dry basis. Although there are several methods available for calculating the heating value of the biomass and biocrude from elemental composition Boie's formula incorporates the higher N content in the biomass [16].

$$\text{HHV(MJ/kg)} = 0.3516 \cdot C + 1.16225 \cdot H + 0.0628 \cdot N + 0.10465 \cdot S - 0.1109 \cdot O$$

We calculated the chemical energy distributed from the original biomass to the various product fractions based on the estimation of HHV.

$$\text{Energy Distribution (\%)} = (\text{Energy in Product} / \text{Energy in Biomass}) \times 100\%$$

3.6. Experimental Parameters and Conditions

This section describes the different variables that we studied in this work, which are summarized in Table 3.2.

Table 3.2. Experimental design space

Independent Variable	Values Explored		
Recovery Solvent	Hexadecane, decane, cyclohexane, hexane, dichloromethane, chloroform, methoxycyclopentane		
Headspace Composition	Air, He		
Headspace Pressure	0, 30, 60, 90 psig		
Preservation Method	As-is, Oven-dried, Freeze-dried		
Slurry Concentration	5, 10, 15, 20, 35 wt %		
Batch-holding Time (including heat-up)	0, 1, 10, 20, 30, 40, 60, 90 min		
Sandbath Temperature	250, 275, 300, 325, 350, 400, 600 °C		
Microorganism	Microalgae *Nannochloropsis* sp. *Scenedesmus* sp. *Chlorella protothecoides*	Bacteria *Escherichia coli* *Pseudomonas putida* *Bacillus subtilis*	Yeast *Saccharomyces cerevisiae*
Intermediate Products	Solid, Aqueous-phase Products, Light Biocrude, Heavy Biocrude		

We studied how the use of different solvents to recover the liquefaction products from the reactors affected the yields and product distributions. Using the 31 mL reactors, we reacted a 20 - 25 wt % slurry of Nanno3600 at 350 °C for 60 min. We used solvents listed in Table 3.2 to recover the products from the reactor. The results are discussed in section 4.1.

We studied how drying techniques affected the results of algae liquefaction. We used a 20 wt% slurry of Nanno3600 and removed the water from the slurry by oven-drying and freeze-drying. We re-hydrated the alga with deionized water and loaded the slurries into 1.7 mL

reactors without the gas-sampling valve. We reacted each at 350 °C for 60 min and determined the effect on the biocrude yield. Results are shown in section 4.2.

We varied the headspace composition and pressure to determine its effect on the biocrude yield. We loaded 4.1 mL reactors with a 20 wt % slurry of Nanno3600 Before the reaction, we used the gas-sampling valve to add dry-grade air or helium to the reactor at pressures of 30, 60, and 90 psig. To add He to the reactors, the air within the reactor was replaced by three repeated cycles of evacuation (1.5 psia) and pressurization (10 psig) with helium before being increased to the desired pressure (section 3.3.1). As a control we prepared one reactor with ambient air in the headspace. We placed each reactor in the sandbath for 60 min at 350 °C. After the reaction we only measured the biocrude yields to determine the effect of headspace composition.

To study the effect of biomass loading on the product yields we examined slurries with 5, 10, 15, 20, and 35 wt % *Nannochloropsis* sp. We used 4.1 mL reactors without the gas sampling valve and reacted each slurry at 350 °C for 60 min. We examined the effect on the yields of all of the product fractions and report the results in section 4.4.

We liquefied 15 wt % slurries of *Nannochloropsis* sp., *Scenedesmus* sp. and *Chorella protothecoides* in 4.1 mL reactors with gas-sampling valves. The reaction time was varied at 10, 20, 30, 40, 60, and 90 min and the reaction temperature was varied at 250, 275, 300, 350, and 400 °C. At 400 °C we examined water densities of 0.3, 0.4, and 0.5 g/mL. We obtained the different water densities at supercritical conditions (400 °C) by loading the appropriate amount of water into the reactor. We quantified yield, elemental composition, and elemental recovery of each of the product fractions. The data from these experiments was used to determine the parameters of the kinetic model and are reported in chapters 4, 5, 6 and 7.

We isolated the solids, aqueous phase, and light and heavy biocrudes collected from a large-scale reaction of *Nannochloropsis* sp. at 350 °C for 40 min. The isolated product fractions were reacted separately in 4.1 mL reactors at 350 °C for an additional 10, 20, 30, and 40 minutes to understand how each product fraction changed with respect to time. The data from these experiments were used to determine the pathways in the reaction network for the liquefaction of microalgae and are reported in section 5.3.

We liquefied different microorganisms to study several different variables. We cultivated *E. coli*, *P. putida*, *B. subtilis*, and *S. cerevisiae*. We grew *E. coli* using a 'rich' and minimal medium to study how the growth medium affects liquefaction yields. We liquefied each microorganism at two liquefaction conditions. Conventional liquefaction conditions were for 60 min at 350 °C and fast conditions were for 1 min in a 600 °C sandbath. We examined the differences between bacteria and yeast and the differences between Gram-positive and Gram-negative organisms and how they affect the product yield and composition. We report the results in Chapter 8.

References

[1] TM Brown, P Duan, PE Savage, *Hydrothermal Liquefaction and Gasification of Nannochloropsis sp*, Energy Fuels 24 (2010) 3639-3646.

[2] Y Dote, S Sawayama, S Inoue, T Minowa, S-Y Yokoyama, *Recovery of liquid fuel from hydrocarbon-rich microalgae by thermochemical liquefaction*, Fuel 73 (1994) 1855-1857.

[3] AB Ross, P Biller, ML Kubacki, H Li, A Lea-Langton, JM Jones, *Hydrothermal processing of microalgae using alkali and organic acids*, Fuel 89 (2010) 2234-2243.

[4] PJ Valdez, JG Dickinson, PE Savage, *Characterization of product fractions from hydrothermal liquefaction of Nannochloropsis sp. and the influence of solvents*, Energy Fuels 25 (2011) 3235-3243.

[5] RB Levine, AA Bollas, MD Durham, PE Savage, *Triflate-catalyzed (trans)esterification of lipids within carbonized algal biomass*, Bioresour Technol 111 (2012) 222-229.

[6] PJ Valdez, MC Nelson, HY Wang, X Lin, PE Savage, *Hydrothermal Liquefaction of Nannochloropsis sp.: Systematic study of process variables and the analysis of product fractions*, Biomass Bioenergy 46 (2012) 317-331.

[7] ASTM E 1755, *Standard Test for Ash in Biomass*, American Society for Testing and Materials 2007

[8] LS Clescerl, AE Greenberg, AD Eaton, *Standard Methods for the Examination of Water and Wastewater*, 4; Amer Public Health Assn: Alexandria, VA: 1999; 138-145

[9] T Lewis, PD Nichols, TA McMeekin, *Evaluation of extraction methods for recovery of fatty acids from lipid-producing microheterotrophs*, J Microbiol Methods 43 (2000) 107-116.

[10] M Piorreck, K-H Baasch, P Pohl, *Biomass Production, Total Protein, Chlorophylls, Lipids, and Fatty Acids of Freshwater Green and Blue-Green Algae Under Different Nitrogen Regimes*, Phytochemistry 23 (1984) 207-216.

[11] AM Pistorius, WJ DeGrip, TA Egorova-Zachernyuk, *Monitoring of biomass composition from microbiological sources by means of FT-IR spectroscopy*, Biotechnol Bioeng 103 (2009) 123-129.

[12] JC Valderrama, *The simultaneous analysis of total nitrogen and total phosphorus in natural waters*, Mar Chem 10 (1981) 109-122.

[13] GE Pacey, S Stieg, BR Fisher, DC Hillman, OB Mathre, JW O'Dell *et al.*, in *Inorganic Nonmetallic Constituents*, LS Clesceri, AE Greenberg, AD Eaton, Eds. (Amer Public Health Assn, Washington DC, 1999), pp. 139-145.

[14] JM Vargas-Moreno, AJ Callejon-Ferre, J Perez-Alonso, B Velazquez-Marti, *A review of the mathematical models for predicting the heating value of biomass materials*, Renewable Sustainable Energy Rev 16 (2012) 3065-3083.

[15] TJ Buckley, *Calculation of higher heating values of biomass materials and waste components from elemental analyses*, Resour Consverv Recycl 5 (1991) 329-341.

[16] K Annamalai, JM Sweeten, SC Ramalingam, *Estimation of gross heating values of biomass fuels*, Trans ASABE 30 (1987) 1205-1208.

Chapter 4

Effects of Processing Conditions

This chapter reports the results of the investigation of several experimental variables that may affect the hydrothermal liquefaction (HTL) of microalgae. The variables we studied had not been sufficiently investigated by other researchers, and we sought to fill in the gaps in the current literature. In the first section, we discuss in detail how different recovery solvents affect the reported yields and composition of the HTL products. The following three sections examine how procedural variations in the feedstock preservation, reactor headspace, and biomass loading affect the yield of biocrude. The fifth section discusses how variations in time and temperature affect the elemental content and distribution among the product fractions from HTL of microalgae. The final section examines the energy distribution among the product fractions and the return on investment for energy required for HTL of microalgae.

4.1. Solvent Selection

This section discusses how the composition of the biocrude depends on the solvent that is used to recover it from the reactor. The research discussed in this section was completed in collaboration with Jake Dickinson. We collected and analyzed the gas, biocrude, dissolved aqueous solids, and insoluble residual solids arising from the HTL of *Nannochloropsis* sp. at 350 ºC for 60 min. We also determined how the solvent used to recover the biocrude affected the yields and compositions of the product fractions. We used both non-polar solvents (hexadecane,

decane, hexane, cyclohexane) and polar solvents (methoxycyclopentane, dichloromethane, and chloroform).

Our research elucidates how the yields and compositions of the product fractions depend on the solvent used. We studied dichloromethane [1-3], chloroform [4], hexane [5], and cyclohexane [6] because they have been used in previous liquefaction studies. We included decane and hexadecane because these straight-chain alkanes mimic the main compounds expected to exist in a potential recycle stream of upgraded algae biocrude that has undergone deoxygenation and some cracking reactions. These solvents could also allow identification and quantification of volatile compounds in the biocrude that would co-elute with the light solvents that are more commonly used. Methoxycyclopentane was included as a greener alternative to chlorinated solvents that exhibits similar polarity [7].

In addition to elucidating the influence of different solvents, the present work is noteworthy because we collected and analyzed all of the product fractions from HTL. Previous studies have focused primarily on the biocrude and perhaps the gas fractions, but no previous research on algae liquefaction has analyzed and quantified directly the amount of material in all four of the product fractions, including the dissolved-aqueous solids (water-soluble products) and residual solids. Our analyses include gravimetric yields measured directly (not inferred by assuming mass balance closure), elemental analysis, and, where possible, quantitative molecular characterization of the product fractions.

4.1.1. Procedure for Solvent Selection

This sub-section outlines the specific procedure for the data presented in this section (4.1) only. We reacted 19.4 g of a 20 - 25 wt % microalgae slurry of Nanno3600 in a 31 mL reactor for 1 h at 350°C. After the reaction, we opened the reactors and added 10 mL of the desired

solvent, pre-weighed, to each reactor. The reactors were then resealed and slowly rotated end over end (10 rpm) at room temperature for 120 min. We performed this step to provide extensive contact between the solvent and reactor wall, where much of the biocrude resided. After rotation, the reactors were placed into an oven at 70 °C for 180 min to break an emulsion that formed when using decane and hexadecane. After heating, we cooled the reactors for 60 min at room temperature. The reactors were opened and their contents poured into a centrifuge tube. We attempted to improve the recovery of any viscous materials by resealing and reheating the reactors to 70 °C, and reopening them while still hot. The remaining contents, if any, were poured into the same centrifuge tube. This reheating step sometimes provided recovery of additional liquid products, but only when using decane and hexadecane as solvents.

We centrifuged the tubes at 3220 relative centrifugal forces for 10 min to separate the organic, aqueous, and solid phases. The organic and aqueous layers were decanted, leaving behind the solids. The organic and aqueous layers, both in one tube, were centrifuged again, and the lower phase was removed via Pasteur pipette. The liquefaction and workup procedure was performed with 3 or 4 replicates for each solvent. The values reported herein are the means and the uncertainties reported are the standard deviations. After separating the products and removing the solvent we measured the yields and elemental composition. We characterized the biocrude using elemental analysis and GC-MSD, GC-FID, and EI-MS techniques as described in chapter 3.

An aliquot of 0.2 – 1.0 mL of aqueous phase was frozen in liquid nitrogen and lyophilized for 22 h using a Labconco Freezone 2.5 freeze dryer set at –40 °C and 0.120 mbar. Aliquots of organic phase (500 μL) were dried under flowing N_2 for 6 h, except for the decane sample (200 μL), which was dried for 26 h, and the hexadecane sample, which was not dried. The appropriate

drying times were determined by periodically measuring the mass until there was no measurable change. The mass of material remaining after solvent removal was determined for the aliquots of the organic and aqueous phases and then used to calculate the gravimetric yields of biocrude and dissolved aqueous solids. Residual solids were dried by flowing N_2 over the solids for 6 h. The gravimetric yield of solids was calculated directly from the mass of the solids after drying. Lastly, samples of microalgae, biocrude, residual solids, and dissolved aqueous solids were sent to Atlantic Microlab, Inc. for elemental analysis (C, H, and N). We measured the concentration of ammonia in the aqueous phase with a HACH® Nitrogen-Ammonia reagent set.

For experiments with hexadecane as the solvent, we determined the biocrude mass as the difference between the mass of hexadecane added to the reactor and the mass of water-free organic phase obtained after separating the product fractions. We determined the water content of the biocrude and hexadecane mixture using a Mettler Toledo Karl Fischer titrator with Aquastar® Composite 2K, pyridine free reagent, and high purity (>99.8%) toluene and methanol. A 1:1 mixture of the organic phase and isopropanol was used to break any remaining emulsion and then 200 μL of sample was injected into the titrator. Isopropanol blanks were also analyzed and the water content was found to be within the error of the measurements. The water content of the hexadecane and biocrude phase was 5.1 ± 0.9 wt %, and the biocrude yield has been corrected for this value.

4.1.2. Control Experiment

To determine the effectiveness of the post-reaction procedures and to quantify systematic mass losses from sample transfers and solvent evaporation, we performed control experiments with a simple three-component synthetic crude algal biocrude. The synthetic biocrude consisted

of 100 mg of palmitic acid, 50 mg of cholesterol, and 10 mg of tetracosane dissolved in 1 mL of chloroform. These components represent those identified in the biocrude from previous work with this alga [1,8]. This solution was deposited into the reactors, and the solvent was evaporated by flowing N_2 into the open reactors for 1 h. We chose this method to mimic the post liquefaction conditions in the reactor, in which the biocrude adheres to the reactor walls. We next added 19.4 mL of deionized water and 10 mL of solvent to each reactor. Duplicate experiments were performed for each solvent. We sealed the reactors and followed the workup procedure described above. The recovery of palmitic acid, cholesterol, and tetracosane was determined using GC-FID.

Table 4.1 shows the percentage of each compound recovered with each of the solvents in this study. With the exception of hexadecane, each solvent recovered at least 84% of each compound. The recoveries of palmitic acid and cholesterol were highest when using the chlorinated solvents and methoxycyclopentane (i.e., the polar solvents). The recovery of tetracosane was around 85% in all of the solvents except for hexadecane. The losses can be attributed to the failure of the solvent to completely remove the compounds from the reactor walls or to dissolve all of the material present in the reactor. Low recovery with hexadecane is likely due to its high molecular weight and reduced molar volume, which may prevent it from fully dissolving the synthetic biocrude components [9]. Since the methods used here to recover the components in the synthetic biocrude are similar to those used to recover the biocrude from algae liquefaction, we anticipate hexadecane being the poorest solvent for these components in the biocrude and the polar solvents being the best.

Table 4.1. Recovery (%) with different solvents of components in the synthetic biocrude

	Palmitic Acid	Tetracosane	Cholesterol
Hexadecane	74 ± 3	63 ± 0	76 ± 3
Decane	88 ± 1	84 ± 1	90 ± 9
Hexane	85 ± 1	86 ± 4	89 ± 8
Cyclohexane	89 ± 0	84 ± 1	87 ± 1
Methoxycyclopentane	92 ± 1	88 ± 3	93 ± 5
Chloroform	91 ± 2	88 ± 1	93 ± 1
Dichloromethane	95 ± 4	85 ± 4	93 ± 6

4.1.3. Gravimetric Yields of Liquefaction Product Fractions

Figure 4.1 shows the yields of the four liquefaction product fractions obtained using different solvents. Each yield was calculated as the mass of each dry product phase relative to the mass of the algae solids (dry basis) added to each reactor. The biocrude, which ranged from 30 – 39 wt % yield, and the dissolved aqueous solids, which ranged from 29 – 36 wt % yield, were always the most abundant products. Residual solids (4 – 9 wt % yield) and gases (7 wt % yield) were less abundant. Biller and Ross reported yields within these ranges for biocrude, residual solids, and gases from *Nannochloropsis* sp. liquefaction with dichloromethane as solvent [10]. Figure 4.1 verifies that the yield of a given product fraction varies from solvent to solvent, but this variation is within bounds of < 9 wt %. Of course, the gas yield is independent of the solvent.

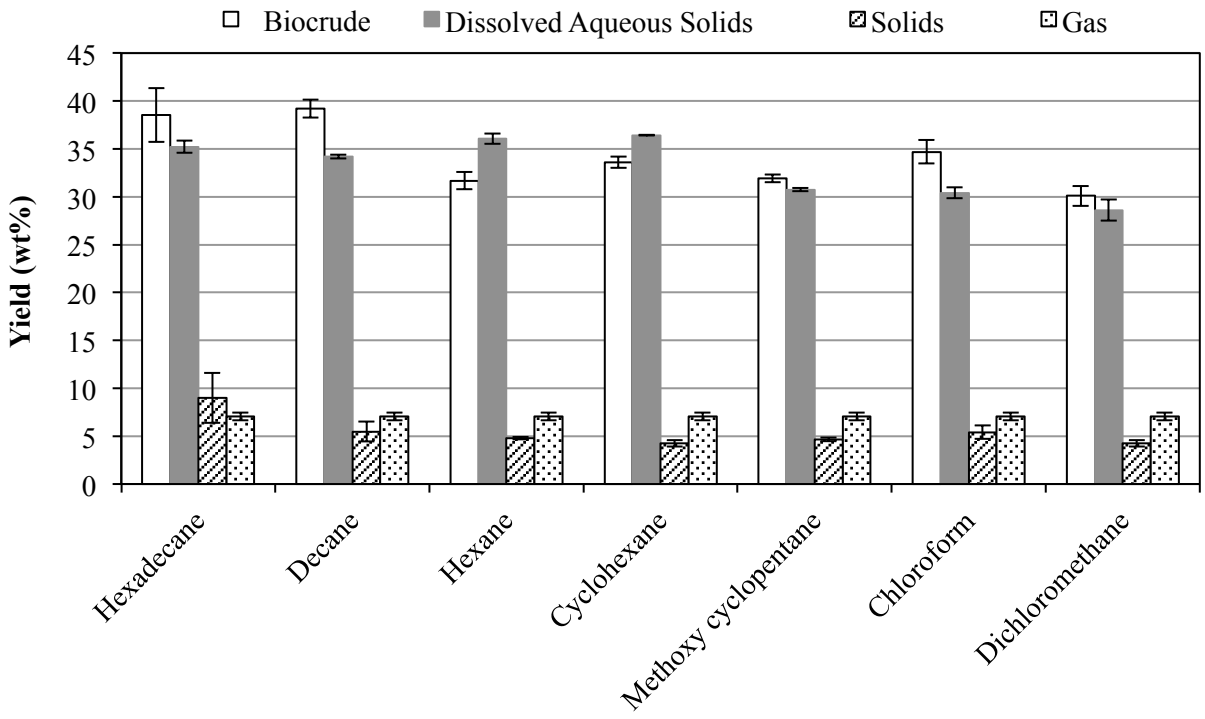

Figure 4.1. Yields of liquefaction product fractions with different solvents

The yield of residual solids was higher with the straight-chain alkane solvents, and it increases as the carbon number of the solvent increases. The high yield of solids does not appear to be accompanied by lower yields of biocrude or dissolved aqueous solids.

The yield of dissolved aqueous solids was always comparable to the yield of biocrude. These aqueous-phase products include the water-soluble compounds that formed during liquefaction, salts that were present in the algae slurry media, and any water-soluble metals or minerals present in the algae. The use of a non-polar solvent increased aqueous product yields when compared to the polar solvents. In fact, using hexane and cyclohexane resulted in more mass being partitioned to the aqueous solids than to the biocrude. Hexadecane and decane show the same high yields of dissolved aqueous solids as did hexane and cyclohexane, but there is not the same concomitant decrease in the yield of biocrude. The yield of biocrude from hexadecane

might be high because a different method was used to quantify it. The yield from decane would be high if some residual decane remained in the biocrude, even after the extensive efforts to remove all of the solvent. Given the low vapor pressure of decane, this is possible.

Table 4.2. NH_3 content in aqueous phase after liquefaction

	NH_3 conc. (mg / mL)	NH_3 Yield (mg / g Dry Algae)	% N in Dry Algae
Hexadecane	12 ± 1	46 ± 4	55 ± 5
Decane	11 ± 0.1	42 ± 0.4	49 ± 0.4
Hexane	12 ± 1	43 ± 2	50 ± 3
Cyclohexane	10 ± 1	40 ± 1	48 ± 1
Methoxycyclopentane	12 ± 1	44 ± 2	52 ± 3
Chloroform	12 ± 0.1	44 ± 0.4	52 ± 0.4
Dichloromethane	12 ± 1	44 ± 2	52 ± 3

In addition to the solids that survive the lyophilization procedure, the aqueous phase also contained ammonia. It had an ammonia scent, along with a foul smell from other compounds. The aqueous phase had a strong odor indicating that some of the aqueous-phase products had a high volatility and escaped into the vapor phase. Thus, the ammonia concentration that would be measured in the aqueous phase would necessarily represent a lower bound. The actual amount of ammonia initially present immediately after liquefaction would have been even higher. We determined the ammonia content of the aqueous phase recovered from the HTL experiments, and Table 4.2 shows the results. Nearly half of the N in the algal biomass is converted into ammonia

that partitions into the aqueous phase. The ammonia concentration in the aqueous phase is independent of the solvent selected to extract the biocrude.

Previous studies of HTL of Nanno3600 at 350 °C for 60 min reported that the yields of biocrude, recovered with dichloromethane, were 43 wt % and 35 wt % [1,8]. The present biocrude yield using dichloromethane was 30 wt %. The different methods used in these studies to recover the biocrude probably play a role in obtaining these different yields. For example, Brown et al. used three separate 15 mL aliquots of dichloromethane (45 mL total) to recover the biocrude from 0.9 g algae (dry weight) [1]. The present study used just a single 10 mL aliquot of solvent to recover biocrude from ~ 4 g of Nanno3600 biomass (dry weight). Additionally, some of the differences in the biocrude yields are likely due to the batch-to-batch variation of the purchased algae.

The overall recovery of total mass (algae paste and solvent) in the present liquefaction experiments is 95 ± 1 wt %. Only about 15% of this total mass is dry algal biomass, however, and 74 – 94 wt % of the initial algal mass appears in the products that we recovered. Some mass loss is unavoidable in the multiple transfers that take place during product workup. Other material losses likely occur during the lyophilization procedure used to isolate the dissolved aqueous solids. Some ammonia is likely lost due to volatilization during sample handling and product recovery. Char that was insoluble in both organic solvent and water or some biocrude may have remained within the reactor (likely adhering to the reactor wall) as yet another source of mass loss. That some material remained within the reactor was evident during reactor cleaning after an experiment. Solvents and brushes used to clean the reactor walls always returned discolored by a dark material. Finally, we know that some CO_2 was dissolved in the aqueous phase and hence not detected by the gas analysis. On the basis of Henry's Law, we

calculate that the mass of dissolved CO_2 (assumed as CO_2 only) was at least 6 wt % of the initial mass of the algae (dry basis) loaded into the reactor. The actual amount of dissolved CO_2 could be even higher, because the aqueous phase also contained ammonia, which can react with CO_2 and thereby increase the amount of CO_2 absorbed into the aqueous phase. Although the production of CO_2 may appear to be counter-productive, this yield of CO_2 accounts for roughly 40% of the oxygen from the biomass.

4.1.4. Gas Analysis

Table 4.3. Composition and yields (mg/g dry algae) of gas phase products

Gas	mol %	Yield
Hydrogen	10 ± 3	0.4 ± 0.1
Methane	1.8 ± 0.4	0.6 ± 0.1
Carbon Dioxide	74 ± 14	68 ± 4
Ethene	0.4 ± 0.2	0.2 ± 0.1
Ethane	0.7 ± 0.2	0.4 ± 0.1

Table 4.3 shows the composition (mol %) and mass yield of H_2, CH_4, CO_2, C_2H_4, and C_2H_6 from HTL. No O_2, N_2, CO, or C_3 gases were detected. The gas composition is similar to that obtained previously using the same feedstock and reaction conditions. Duan and Savage report a composition of 80 mol % CO_2 and 15 mol % H_2 [8]. Likewise, Brown et al. report a composition of 66 mol % CO_2 and 30 mol % H_2 [1]. Overall, 88 ± 15 mol % of the gas phase was accounted for with this analysis, and it consisted of a large proportion of CO_2. NH_3, N_2O, NO_2, and HCN

are not detectable when using the methods described previously. Water is expected to be present, but only in its saturation composition of about 2.5 mol %.

4.1.5. Elemental Analysis

The dried *Nannochloropsis* sp. microalgae was 41.89, 5.64 and 6.95 wt % C, H, and N respectively. This elemental composition is very similar to that reported in other studies with *Nannochloropsis* sp., both in our lab [1,8] and that of others [10]. We did not measure S or O, but they have been reported previously as 0.5 and 25.1 wt %, respectively [1]. The H/C and N/C atomic ratios are 1.60 and 0.14, respectively.

Table 4.4. Elemental content (wt % and atomic ratio) of the biocrude

Solvent	Biocrude				
	C	H	N	H/C	N/C
Hexadecane	N/A*	N/A	N/A	N/A	N/A
Decane	68.80	9.37	4.44	1.6	0.06
Hexane	70.45	9.80	4.04	1.7	0.05
Cyclohexane	64.87	9.76	3.87	1.8	0.05
Methoxycyclopentane	72.27	9.70	4.06	1.6	0.05
Chloroform	73.68	9.85	4.62	1.6	0.05
Dichloromethane	75.76	10.57	4.52	1.7	0.05

*Biocrude in hexadecane could not be separated for elemental analysis

Table 4.5. Elemental content (wt % and atomic ratio) of the dissolved aqueous solids

Solvent	Dissolved Aqueous Solids				
	C	H	N	H/C	N/C
Hexadecane	16.32	2.53	1.32	1.8	0.07
Decane	15.74	2.67	1.31	2.0	0.07
Hexane	15.76	2.58	1.18	2.0	0.06
Cyclohexane	14.59	2.40	1.26	2.0	0.07
Methoxycyclopentane	13.71	3.24	0.93	2.8	0.06
Chloroform	13.87	2.60	0.95	2.2	0.06
Dichloromethane	13.75	2.54	1.02	2.2	0.06

Table 4.6. Elemental content (wt % and atomic ratio) of the solids

Solvent	Solids				
	C	H	N	H/C	N/C
Hexadecane	29.73	6.55	2.12	2.6	0.06
Decane	13.42	3.30	1.73	2.9	0.11
Hexane	18.32	4.25	2.79	2.8	0.13
Cyclohexane	13.04	4.42	3.17	4.0	0.21
Methoxycyclopentane	11.82	3.79	2.69	3.8	0.20
Chloroform	20.39	5.43	2.4	3.2	0.10
Dichloromethane	21.10	4.47	2.70	2.5	0.11

Tables 4.4 - 4.6 summarize the elemental compositions and the H/C and N/C ratios for each of the product fractions. The biocrude always had a higher wt % of C, H, and N than did the dissolved aqueous solids and the residual solids. The biocrudes were enriched in C and H, but depleted in N relative to the original alga feedstock. This preferential partitioning of C and H into and N away from the biocrude is both desirable and consistent with previous reports of HTL of microalgae at similar conditions [1,3,8,10-12]. The biocrude H/C ratios are modestly higher than those in the dry algae, and the N/C ratio is reduced to nearly one third of its value in the dry feedstock. The polar solvents produced biocrudes with the highest C content and dissolved aqueous solids with the lowest C content. This outcome for the biocrude can be rationalized on the basis of past research that showed that chloroform-recovered biocrude contained large, carbon-rich molecules similar to resins and asphaltenes [4]. Such compounds would be insoluble in non-polar solvents. The elemental composition of the biocrude recovered with dichloromethane was nearly the same as that reported in our earlier work [1,8] with the same alga processed at the same liquefaction conditions. In these earlier studies, the C, H, and N contents of the biocrudes were 75.3, 10.2, and 4.18 wt % and 76.0, 10.3, and 3.9 wt % [1,8].

The residual solids typically have higher H/C and N/C ratios than the dissolved aqueous solids. To the best of our knowledge, only one other lab has provided information about the elemental composition of both of these product fractions from algae liquefaction [1,4,8]. The H/C ratio of around 2.0 for the dissolved aqueous solids is consistent with these materials containing some organic acids, which have been reported as aqueous-phase byproducts from hydrothermal treatment of algal biomass [13].

The elemental compositions of the algae feedstock and the product fractions were used to calculate the distributions of elements in the various product fractions. The distribution of each

element in each fraction is calculated as its mass in that product fraction relative to its mass in the algae feedstock. Figures 4.2 - 4.4 display the results.

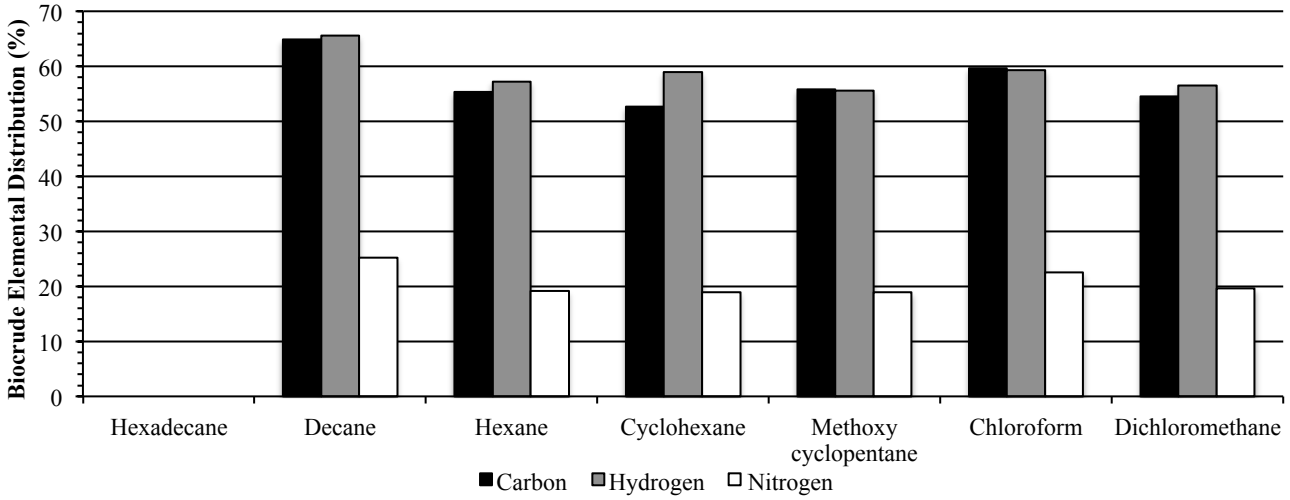

Figure 4.2. Percentage of C, H, and N in algae distributed to the biocrude

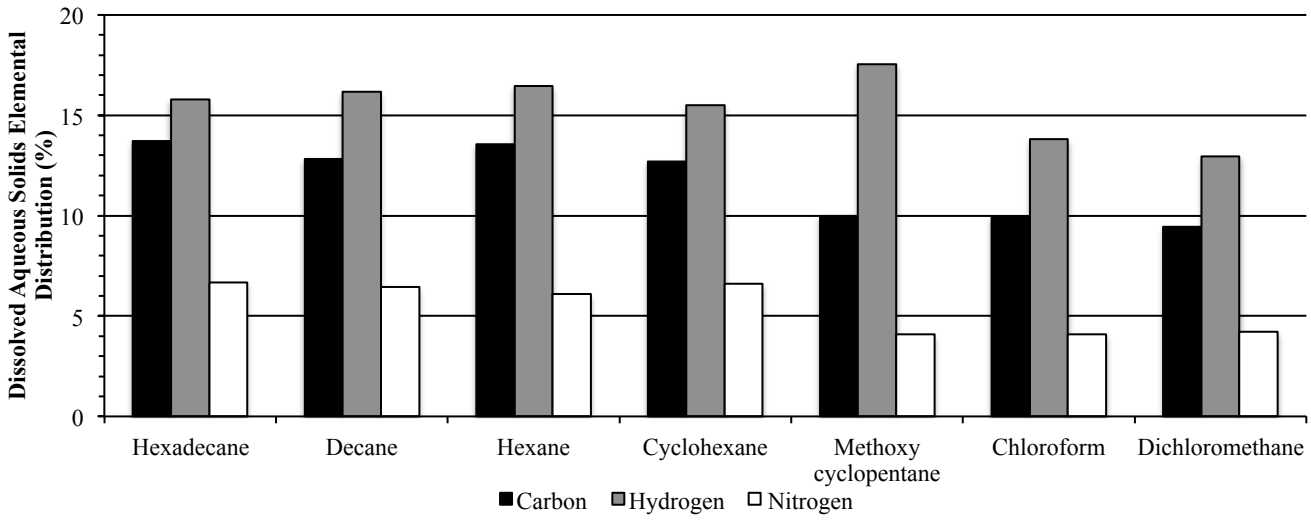

Figure 4.3. Percentage of C, H, and N in algae distributed to dissolved aqueous solids

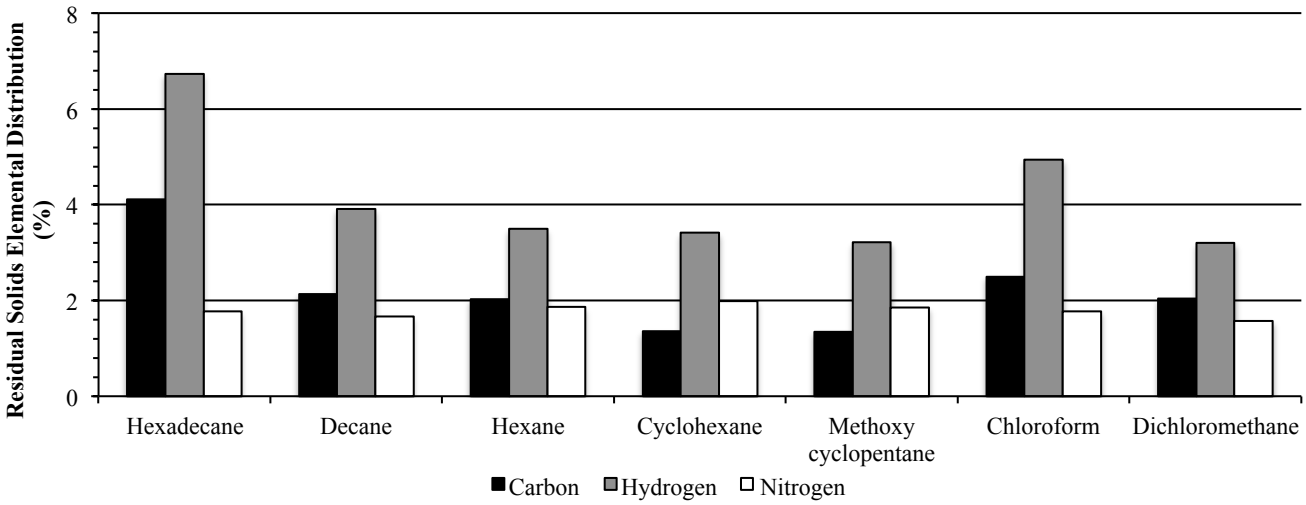

Figure 4.4. Percentage of C, H, and N in algae distributed to residual solids

Figure 4.2 shows that the biocrude typically contained 50 - 65% of the amount of C and H and about 20% of the N originally present in the algae feedstock. In fact, the majority of the C and H that we recovered resided in the biocrude fraction. The C and H distributed to the biocrudes were nearly identical for a given solvent, and there was not much variation from solvent to solvent. Figure 4.3 shows that the C, H, and N distributed to the dissolved aqueous solids were typically around 12, 15, and 5%, respectively. These values are only about one fourth as large as the yields in the biocrude. The polar solvents had lower C and N distributions than the hydrocarbon solvents. Figure 4.4 shows that the distribution of C, H, and N in the residual solids are even lower. Inspecting Figures 4.3 and 4.4 further shows that the H distribution in the dissolved aqueous solids and in the residual solids always exceeds the C distribution. The N distributions were always the lowest of the three in the dissolved aqueous solids, whereas they were comparable to the C yields in the residual solids.

Table 4.7. C, H, N, and mass balance for liquefaction products

Solvent*	% Recovery			Mass Balance (wt %)	Modified % Recovery			Modified Mass Balance (wt %)
	C	H	N		C	H	N	
Decane	80	99	82	90	100	104	100	104
Hexane	71	91	78	84	100	97	100	102
Cyclohexane	67	91	76	85	100	97	100	106
Methoxycyclopentane	67	90	76	79	100	97	100	99
Chloroform	72	92	80	82	100	97	100	100
Dichloromethane	66	87	78	74	100	93	100	95

*Biocrude in hexadecane could not be dried for elemental analysis, mass balance was 94 wt %.

Knowledge of the C, H, and N yields in each of the four product fractions (biocrude, dissolved aqueous solids, solids, gas) and the ammonia concentration in the aqueous phase permits calculation of the overall recovery of each element. This calculation was not made for the experiment with hexadecane, as we had no elemental analysis for the biocrude in that case.

Table 4.7 shows that the atom recovery always exceeded 66% for C, 87% for H, and 76% for N. The recoveries were about the same for all of the solvents save decane, which led to the highest recovery of C, H, and N. Table 4.7 also presents the overall mass balance in terms of mass of material recovered in the four product fractions plus ammonia relative to the dry weight of algae loaded into the reactor. The mass balance is higher with the non-polar solvents (e.g., 90 wt % with decane and 94 wt % with hexadecane) than it is with the polar solvents (e.g., 74 wt % with dichloromethane).

The data in Table 4.7 permit a rough test of hypotheses mentioned earlier in this chapter for the mass balances being less than 100 wt %. We assume that the losses from carbon can be

accounted for by dissolved CO_2 in the aqueous phase and carbonaceous char that remains unrecovered in the reactors. We calculated the amount of dissolved CO_2 from Henry's Law and the known CO_2 yield. We then closed the C balance by assuming that all of the remaining unrecovered C atoms were resident in char, which was assumed to contain only carbon. We assume that the nitrogen losses are exclusively NH_3 vapors lost during the experimental protocol. Making these assumptions about the missing C and N atoms leads to the modified element and mass balances shown in the right half of Table 4.7. The modified H recovery and mass balance both close to within a few percent for all of the solvents. Thus, the hypothesis that the missing C is primarily dissolved CO_2 and char and that the missing N (and H) is primarily lost NH_3 is consistent with the data we obtained. The modified H recovery and modified mass balance being lower for dichloromethane indicate that char and NH_3 alone might not account for all of the missing material. We suspect that this solvent did not remove all of the biocrude from the reactor and that this missing biocrude perhaps accounts for the remainder of the material. Recall that dichloromethane gave the lowest biocrude yield of any of the solvents and that the yield was lower than those we had obtained in the past when working with the same algae strain. In section 4.5 we show that via direct measurement of the C and N in the aqueous phase we are able to close the balances of those elements.

4.1.6. Biocrude Composition

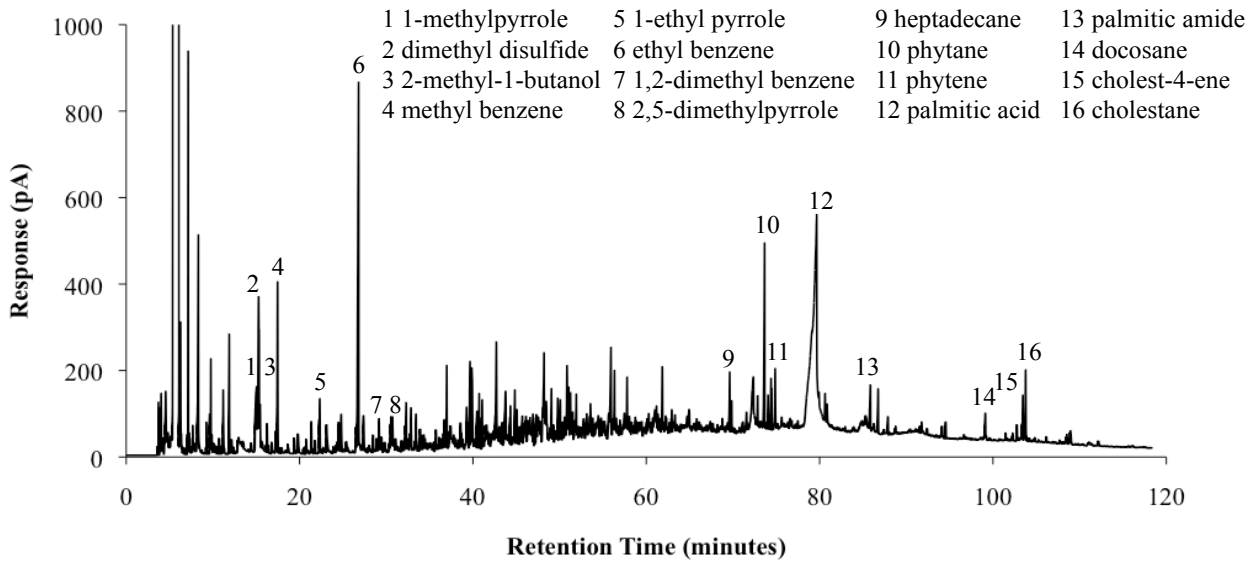

Figure 4.5. Chromatogram of biocrude recovered with dichloromethane and an HP-5 column

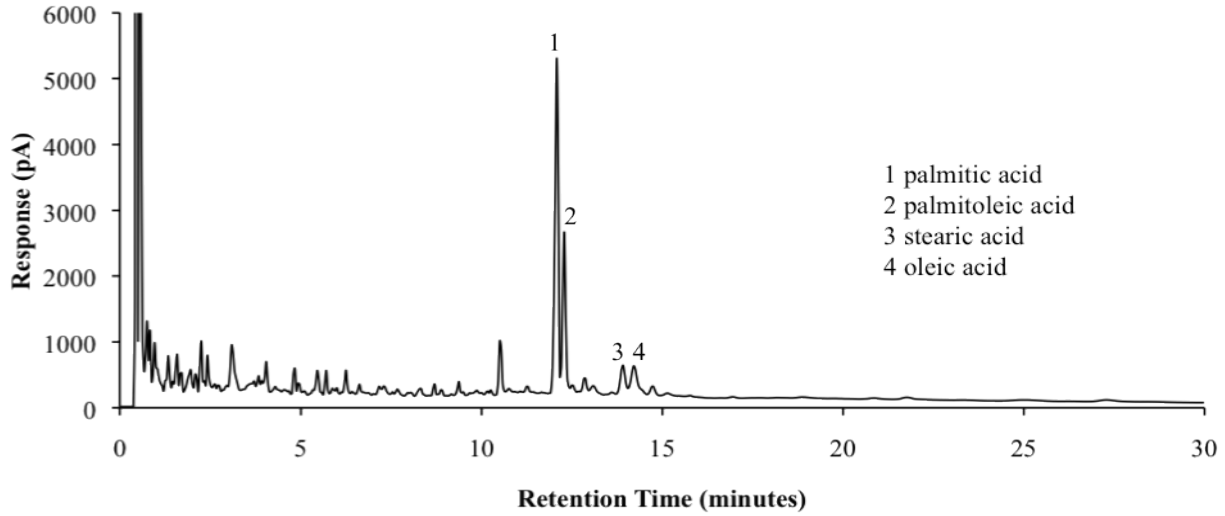

Figure 4.6. Chromatogram of biocrude for fatty acid analysis using chloroform and a Nukol capillary column

All of the biocrudes were analyzed chromatographically to gain information about their molecular compositions. Figures 4.5 and 4.6 show chromatograms of two biocrudes analyzed with two different gas-chromatography (GC) columns. We have quantified 19 molecular components in the crude algal biocrude for the first time. We apportioned the identified compounds into three different classes: light ends, aliphatics, and fatty acyls. We classify compounds that have boiling points less than 150 °C as the light ends. Examples include 1-methylpyrrole, dimethyl disulfide, 2-methyl-1-butanol, methyl benzene, 1-ethyl pyrrole, ethyl benzene, 1,2-dimethyl benzene, and 1,5-dimethyl pyrrole as shown in Figure 4.5. The biocrude also contained aliphatic compounds such as heptadecane, phytane (3,7,11,15-tetramethyl hexadecane), phytene (2,6,4,10-tetramethyl 2-hexadecene and 3,7,11,15-tetramethyl 2-hexadecene), docosane, cholestane, and cholestene. The fatty acyls in the biocrude are palmitic (hexadecanoic), palmitoleic (hexadecenoic), stearic (octadecanoic), and oleic (octadecenoic) acids, as well as palmitic amide (hexadecanamide).

Table 4.8 displays the yields of each compound we identified along with the total yield of each class of compounds in the biocrude. To the best of our knowledge, these data are the first to give quantitative information about the absolute yields of individual molecules in algal biocrude from HTL. Previous work provided only information about the relative abundance of different components [1,3,4,8]. The compounds in the biocrude that have been quantified in this work account for roughly 62% of the total peak areas found in the chromatograms, but less than 22 ± 8 wt % (on average) of the biocrude mass. Adding in the 38% of the total peak area that was not identified would increase the GC-elutable portion of the biocrude to roughly 35% of the total. Thus, it seems that the biocrude contained a significant proportion (~ 65%) of high-molecular-weight compounds that are not amenable to analysis by capillary-column GC.

Table 4.8. Yields (mg/g dry algae) of biocrude compounds recovered with different solvents

		Hexadecane	Decane	Hexane	Cyclohexane	Methoxy cyclopentane	Chloroform	Dichloromethane
Light Ends	1-Methyl Pyrrole	0.66±0.16	0.95±0.01	1.01±0.02	1.23±0.04	NQ	1.28±0.02	1.24±0.12
	Dimethyl Disulfide	2.65±0.76	2.75±0.04	4.50±0.20	1.99±0.10	NQ	7.49±0.36	6.88±1.52
	2-Methyl-1-Butanol	0.79±0.09	0.70±0.03	1.08±0.52	0.87±0.10	NQ	0.88±0.09	0.69±0.04
	Toluene	0.88±0.23	0.239±0.001	1.23±0.04	1.24±0.02	NQ	1.50±0.01	1.48±0.11
	1-Ethylpyrrole	0.53±0.06	NQ	0.66±0.06	0.63±0.01	0.48±0.01	0.67±0.01	0.68±0.05
	Ethyl Benzene	3.79±0.45	3.40±0.12	4.33±0.19	4.33±0.05	4.54±0.03	4.96±0.04	4.80±0.47
	o-Xylene	0.98±1.21	NQ	0.32±0.01	0.36±0.01	0.358±0.002	0.27±0.01	0.32±0.04
	2,5 Dimethyl Pyrrole	0.54±0.06	NQ	0.52±0.01	0.567±0.002	0.77±0.01	0.56±0.11	0.57±0.11
	Total	10.8±1.5	8.05±0.13	13.6±0.6	11.2±0.2	6.15±0.03	17.6±0.4	16.7±1.6
Aliphatics	Phytane	1.69±0.16	0.88±0.72	1.31±0.02	1.29±0.03	1.40±0.05	1.37±0.05	1.38±0.16
	Phytene	2.02±0.08	1.30±0.48	1.51±0.22	1.54±0.11	1.69±0.01	1.68±0.08	1.85±0.65
	Heptadecane	0.15±0.26	0.25±0.18	0.31±0.00	0.36±0.01	0.39±0.02	0.34±0.02	0.31±0.05
	Docosane	0.11±0.10	0.139±0.001	NQ	NQ	0.14	0.153±0.004	0.10±0.09
	Cholest-4-ene	0.48±0.07	0.28±0.17	0.36±0.01	0.40±0.01	0.37±0.02	0.323±0.001	0.34±0.01
	Cholestane	0.75±0.08	0.41±0.28	0.56±0.01	0.59±0.02	0.65±0.01	0.58±0.01	0.61±0.03
	Total	5.19±0.34	3.27±0.94	4.05±0.22	4.18±0.12	4.64±0.06	4.45±0.09	4.59±0.68
Fatty Acyls	Palmitic Amide	2.69±1.98	0.58±0.09	0.50±0.14	0.67±0.25	0.44±0.01	1.22±0.27	0.70±0.03
	Palmitic Acid	4.96±0.57	8.88±3.96	17.3± 4.2	11.2±2.9	13.3±1.4	30.9±2.2	26.4±1.8
	Palmitoleic Acid	4.72±0.48	10.6±6.2	14.3±2.8	15.0±1.5	16.0±1.1	15.2±1.2	13.6±0.5
	Stearic Acid	8.56±0.20	9.76±1.01	12.7±3.4	10.0±1.5	11.4±1.4	25.2±1.1	22.4±1.4
	Oleic Acid	12.3±0.2	12.6±1.0	14.3±1.6	13.1±1.2	14.1±0.4	17.5±0.4	15.8±0.4
	Total	33.2±2.1	42.7±7.5	59.4±6.3	50.4±3.8	55.7±2.2	90.0±2.8	79.9±2.4

NQ: Not quantifiable

The molecules categorized as light ends include N-, O-, and S-containing compounds in addition to aromatic hydrocarbons. Dimethyl disulfide and ethylbenzene are the most abundant of the light ends. Dichloromethane and chloroform, two of the polar solvents, extracted the highest amounts of light ends in the biocrude. The yields of light ends vary by about a factor of two over the range of solvents studied. Most of this variation is due to the low yields of light ends in decane and methoxycyclopentane. Most light-end compounds were not detectable in methoxycyclopentane because the solvent eluted at the same time as the compounds of interest. The yields were low in decane because the use of the least volatile solvents considered in this work (hexadecane and decane) led to poor chromatographic resolution of compounds that eluted just before the solvent. Most of the light-end compounds eluted shortly before the decane solvent, and they were not chromatographically resolved and hence not quantified. Solvent effects did not influence the light-end peaks in hexadecane because the elution time between light ends and solvent was long enough to allow for chromatographic development of the solute in the column.

The total yields of aliphatic compounds shown in Table 4.8 do not vary significantly from solvent to solvent, but the three polar solvents produced modestly higher recoveries of aliphatic compounds than the non-polar solvents. The most abundant aliphatic compounds are phytyl chains and cholesterol derivatives. Straight-chain alkanes were also present but only at 10 – 20% of the concentration of the other aliphatic compounds. The branched alkanes and the cholesterol derivatives had a higher yield in hexadecane than in the other solvents.

We identified and quantified four free fatty acids (palmitic, palmitoleic, stearic, oleic) in the algae liquefaction biocrude. There are also some free fatty amides present, but in lower concentrations. The free fatty acyls make up the majority (~ 80%) of the material quantified by

GC-FID. Solvent selection significantly affects the yields of free fatty acyls, with the chlorinated solvents producing the highest yields of free fatty acyls in the biocrude. In contrast, hexadecane and decane provided the lowest yields. This outcome is likely due to these solvents being unable to dissolve fully all of the free fatty acyls.

4.1.7. High Molecular Weight Compounds

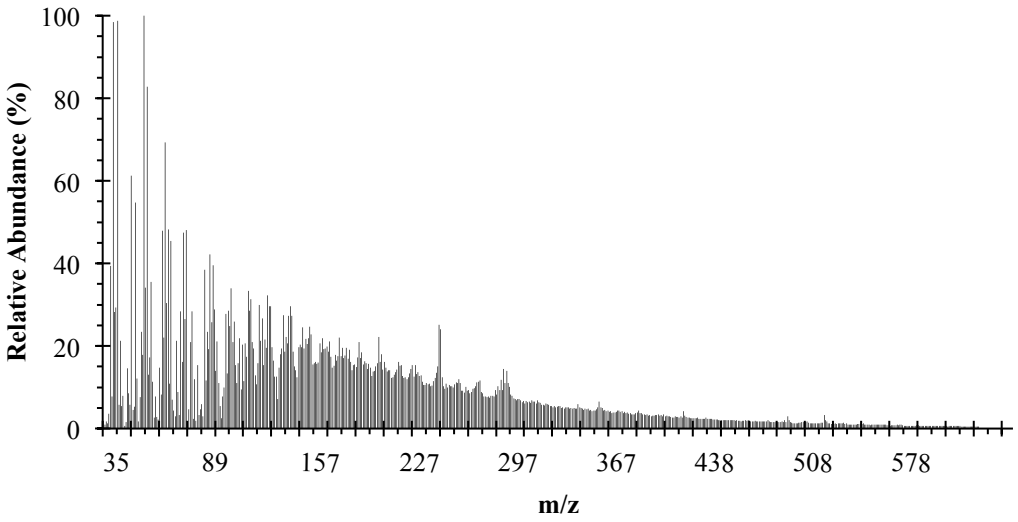

Figure 4.7. EI mass spectrum of biocrude recovered using dichloromethane

As noted in the previous section, GC analysis quantified at most 22 wt % of the compounds in the biocrude. It is likely that much of the remaining material consists of high-molecular-weight compounds that do not elute from a GC column. We used magnetic-sector mass spectrometry to test this hypothesis that higher-molecular-weight compounds are present in the biocrude. Figure 4.7 shows the mass spectrum obtained using electron-impact ionization for the biocrude sample that was recovered using dichloromethane. The sample shows peaks, albeit at low abundance, at mass/charge (m/z) ratios exceeding 500. Electron-impact methods lead to

fragmentation of the compound(s) of interest, so the peaks in Figure 4.7 probably do not correspond to molecular ions. The distribution of fragmented compounds is indicative of the presence of aliphatic compounds instead of aromatic compounds in the sample. Inspection of the insertion probe after taking the mass spectrum revealed that much of the material remained on the probe, indicating that the compounds were not volatilized and thus not detected by the MS. This result nevertheless confirms the hypothesis that the biocrude contained a large proportion of high-molecular-weight compounds. If these compounds could not be liberated from the MS probe by heating to 300 °C, under vacuum, they clearly would not be able to enter and/or elute from a capillary GC column.

4.2. Feedstock Preservation

One effect that has not been discussed thoroughly in the literature is how preservation techniques for algae might affect the results of hydrothermal processing. Heilmann et al. recently demonstrated that the results for hydrothermal treatment of fresh algal slurry and freeze-dried then rehydrated slurry were identical [14]. We extended this study to include frozen slurry and oven-dried algae. Specifically, we examined how the yield of biocrude was affected by the various preservation techniques. We tested frozen, freeze-dried, and oven-dried samples of Nanno3600. The frozen algae were used as received. Samples of the frozen algae were used for freeze drying and oven drying. We froze one set of samples in liquid nitrogen and then placed it in a Labconco freeze dryer for 24 h. We dried a different set of samples in a temperature controlled oven set to 105 °C for 72 h, following guidelines established by ASTM E 1756 for determining the solid content of biomass [15]. The frozen sample was already diluted to 20 wt % biomass solids so it was reacted as-is, after thawing. The freeze-dried and oven-dried samples

were rehydrated to 20 wt % biomass slurry before reaction. We loaded 1.1 g of slurry into 1.7 mL reactors and heated them at 350°C for 1 h.

Table 4.9. Biocrude yields after preservation of microalgae

Treatment	Biocrude Yield (wt %)
Frozen	32 ± 1
Frozen/Oven Dried	34 ± 2
Frozen/Freeze Dried	32 ± 2

Table 4.9 shows that the method of preservation did not affect the biocrude yield for the experiments. Therefore it does not matter how this alga is preserved prior to HTL. The results showed that the difference in yield averages were not statistically significant, based on one-way analysis of variance (ANOVA) hypothesis testing. The error reported is one standard deviation.

4.3. Reactor Headspace

Limited attention has been given to the selection of reaction atmosphere and initial headspace pressure in the reaction vessel for biomass liquefaction [8,16]. However, the results showed both increases and decreases of biocrude yield when the reactor headspace is pressurized with a gas before reaction. To validate the result for algae liquefaction, we tested both air and helium in the reactor headspace at increasing pressure values (0, 30, 60, 90 psig). We loaded 4.1 mL reactors with 2.7 g of Nanno3600 slurry (20 wt %). We used the procedure described in section 3.3.1 to fill the reactor with either helium or air at a given pressure. We then heated the reactors to

350 °C for 1 h and used the procedure described in section 3.4 to recover the products, substituting chloroform for dichloromethane.

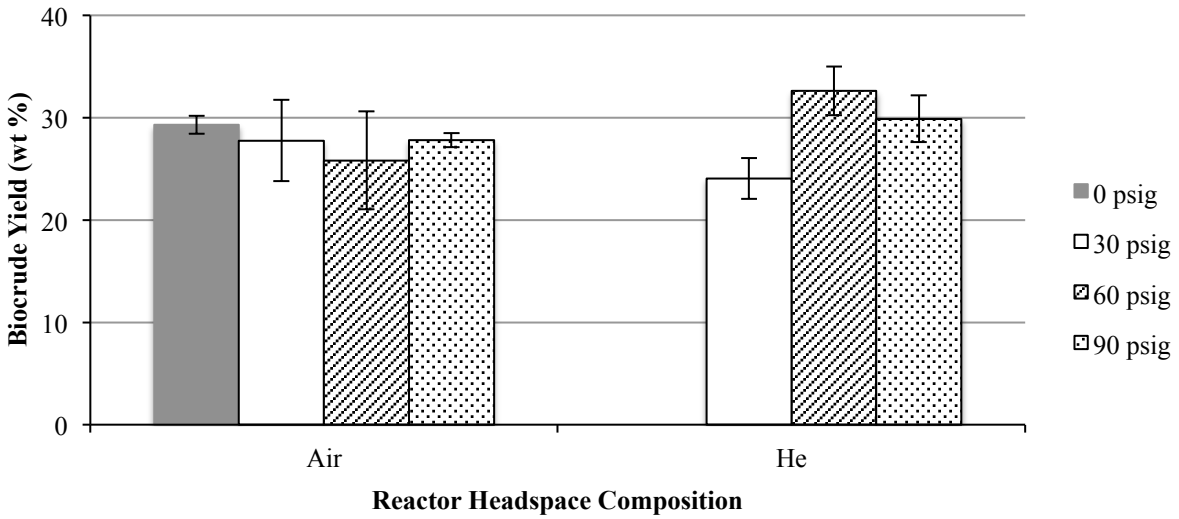

Figure 4.8. Effect of headspace composition on biocrude yield

Figure 4.8 shows the biocrude yield for each gas and at varying pressures between 0 - 90 psig. Contrary to the results of Yin et al. for manure liquefaction, we found that increasing the initial reactor headspace pressure did not affect biocrude yield [17]. We confirmed the results of He et al., concluding that there is little to no difference in biocrude yield between air and an inert reactor headspace composition [16]. Although air might be considered a reactive gas because of the oxygen content, it does not significantly change the biocrude yield. With the exception of the experiment of helium at 30 psig, there is no significant difference between the various experiments.

4.4. Biomass and Water Loading

We evaluated the effect of varying the solids concentration in the biomass slurry. We prepared various dilutions of alga slurry using the 35 wt % *Nannochloropsis* sp. slurry from Reed Mariculture Inc. (section 3.1.2). We loaded 4.1 mL reactors with 2.3 - 3.4 g of biomass slurry. The total amount of water remained constant at 2.2 g. The solid concentration of the slurry ranged from 5 - 35 wt %. We treated the reactors for 60 min at 350 °C and then followed the workup as described in section 3.4, omitting analysis of the gas products.

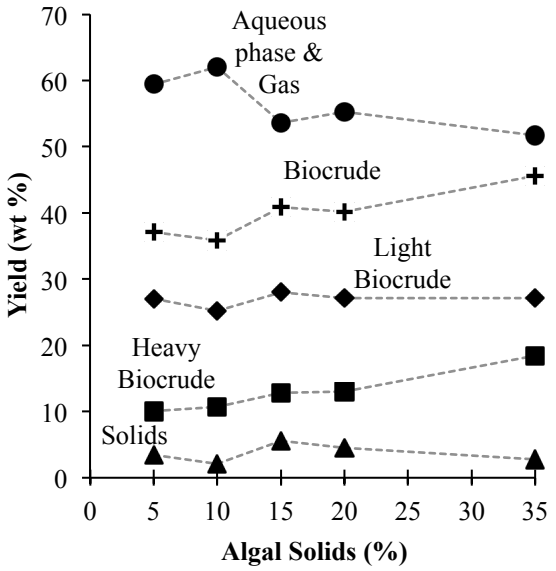

Figure 4.9. Effect of algae loading on yield of product fractions

Figure 4.9 depicts the change in yields of the liquefaction product fractions with respect to variation of the loading of algal solids. The biocrude yield increases from 36 - 46 wt % as the algae concentration in the slurry increases from 5 - 35 wt %. These results differ from those of Jena et al., which showed no significant variation in the biocrude yield when biomass loading was varied from 10 - 50 wt % concentrations of *Spirulina* in water [18]. Thus, it seems that

different species of algae might behave differently during HTL. The apparent increase in the combined yields of biocrude with increasing loading is due to the rising yield of heavy biocrude. It is possible that at higher biomass concentration more polymerization reactions take place, forming compounds that would reside in the heavy biocrude. The yield of light biocrude remains relatively constant in Figure 4.9. Although higher loadings resulted in higher biocrude yields, Peterson et al. suggest that for hydrothermal processes to be energy and economically efficient, the target biomass loading is 15 - 20 wt % [19]. The yields of aqueous-phase products and gas are determined by difference and decrease with increased loading. The yield of solids remains relatively unchanged at 4 ± 1 wt %, across all loadings tested.

We also varied the water loading in the reactor at 400 °C. We used a 15 wt % slurry of *Nannochloropsis* sp. in 4.1 mL reactors. We loaded the reactors with enough slurry to correspond to water density values of 0.3, 0.4, and 0.5 g/mL based on the volume of the reactor. We then heated each reactor to 400 °C and held the temperature for 10, 20, 30, and 40 min. The yields of the product fractions from experiments at different water densities, but otherwise identical conditions, were so close to one another that the small differences are very likely within the experimental error. Therefore, we report only the results from one water density (0.5 g/mL) to compare results from supercritical and subcritical conditions in this chapter and in chapters 5, 6, and 7. Yields of the product fractions at lower water density values (0.3 and 0.4 g/mL) are available in the Appendix (Table A.1).

4.5. Elemental Content and Distribution

This section provides information about the elemental composition of the product fractions formed at different times and temperatures for HTL. We loaded 4.1 mL reactors with 1.3 - 3.6 g

of 15 wt % slurry of *Nannochloropsis* sp. We followed the procedures in section 3.3 to adjust the loading according to reaction conditions. We varied reaction temperature at 250, 300, 350, and 400 °C. At 400 °C we adjusted the loading so the water density inside the reactor would be 0.5 g/mL. We also varied the batch holding time at a given reaction temperature between 10 - 90 min. After reaction we followed the work-up procedure outlined in section 3.4. We used this procedure to collect the data presented in sections 4.5 and 4.6.

4.5.1. Elemental Content

The *Nannochloropsis* sp. was 51 wt % C, 7 wt % H, 9 wt % N, 0.6 wt % S, 0.6 wt % P and 28.8 wt % O (by difference). The ash content of the alga was 3 wt %. Qualitative analysis using inductively coupled plasma optical emission spectroscopy (ICP-OES) showed traces of Co, Mn, Fe, Cu, Zn, Mo, Cr, Mg, Al, Na, K, Ca, and Cl present in the alga.

Figure 4.10 shows the variation of the wt % of C, N, S, and O in the light biocrude with time and temperature. The H content of the light biocrude (10.4 ± 0.4 wt %) is independent of both time and temperature and hence not presented here. As shown in Figure 4.10a, the C composition of the light biocrude varies slightly from as low as 73 wt % at 250 °C to as high as 77 wt % at 400 °C, but there is no clear trend with respect to time. The C wt % generally being 75 ± 1 wt % is consistent with fatty acids and other hydrocarbons being dominant in the biocrude [20]. Palmitic acid, a major component of biocrude from this alga, is 75 wt % C which is similar to the average C composition of the light biocrude [1].

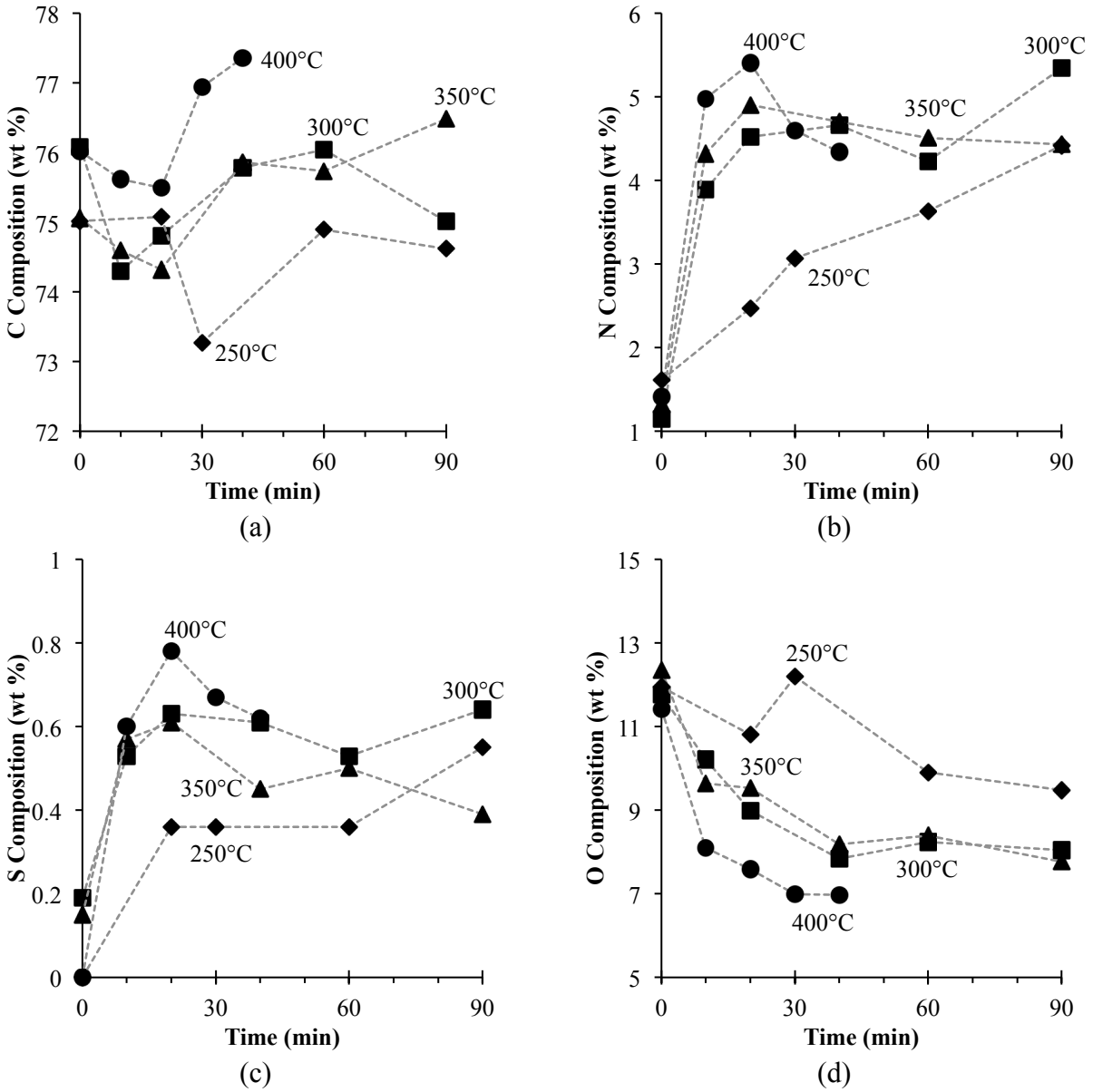

Figure 4.10. Elemental composition a) C, b) N, c) S, and d) O in the light biocrude at 250 °C (◆), 300 °C (■), 350 °C (▲), and 400 °C (●)

Figure 4.10b shows that the N composition is both time and temperature dependent. The N composition is initially low, around 2 wt %, but increases to approximately 5 wt %. Increasing temperature increases the rate at which the N composition reaches this 5 wt % value. Garcia Alba et al. documented a similar trend in the N content of biocrude produced at 300 °C [21]. The increase of the N content in the biocrude is undesired, reaffirming the need to develop methods

to remove the N from the light biocrude. Many pyrroles and indoles are common in biocrudes and likely contribute to the N content of the light biocrude since they are difficult to decompose at these conditions [10,20].

Figure 4.10c shows that there is some variation in the S content with time and temperature. The S content is highest at 400 °C and lowest at 250 °C. Even so, the S content is relatively low (< 0.8 wt %) and not detectable initially. Sulfur in the light biocrude is likely from dimethyl disulfide, which accounts for the majority of the sulfur found in the microalgae [20].

Figure 4.10d shows that the O content in the light biocrude decreases as time and temperature increase. The terminal value of the wt % of O is strongly dependent on the temperature, ranging from approximately 9 wt % at 250 °C to 7 wt % at 400 °C. Reducing the O content in the biocrude is important because doing so increases its energy content.

Figure 4.11 shows the C, N, S, and O wt % of the heavy biocrude. Figure 4.11a shows that the composition of C increases with both time and temperature. The C composition of the heavy crude was always lower than that of the light biocrude produced at the same conditions. Figure 4.11b shows that the N composition in the heavy biocrude settles to a time independent value of about 7 ± 1 wt %, which exceeds that of the light biocrude. The S wt %, shown in Figure 4.11c is not a strong function of time at any of the temperatures investigated, and it has its lowest values at the intermediate liquefaction temperatures. Figure 4.11d illustrates how the composition of O decreased as time progressed. Increasing temperature also resulted in a lower O content after 20 min. The terminal value of the O content of the heavy biocrude formed at a given temperature was higher than the corresponding value in the light biocrude. Jena et al. also determined the elemental content of heavy biocrude from a different alga, showing similar values for C, N, and

O composition but nearly three times the S composition [18]. The higher S composition may be inherent to the algal species.

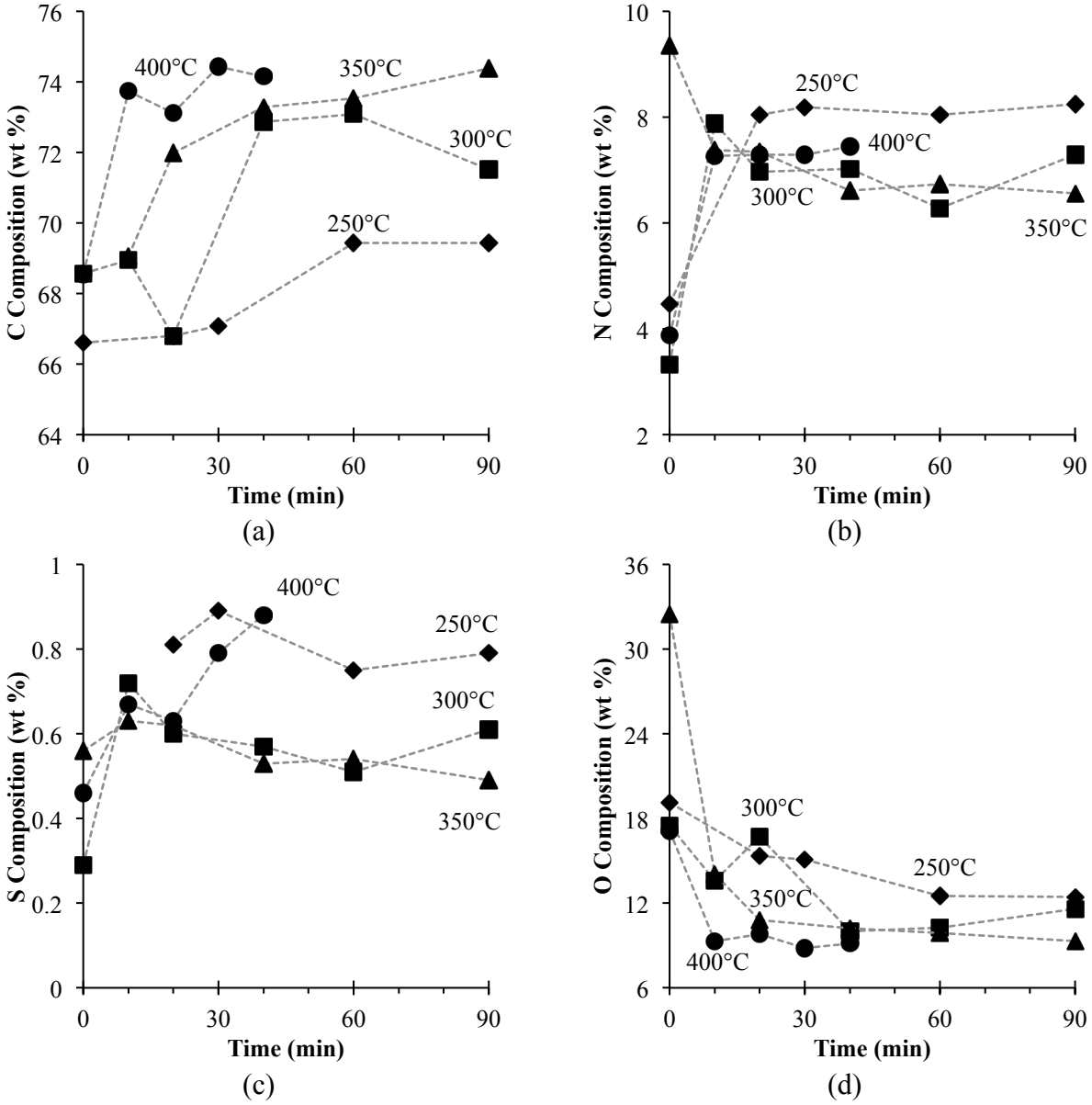

Figure 4.11. Elemental composition a) C, b) N, c) S, and d) O in the heavy biocrude at 250 °C (◆), 300 °C (■), 350 °C (▲), and 400 °C (●)

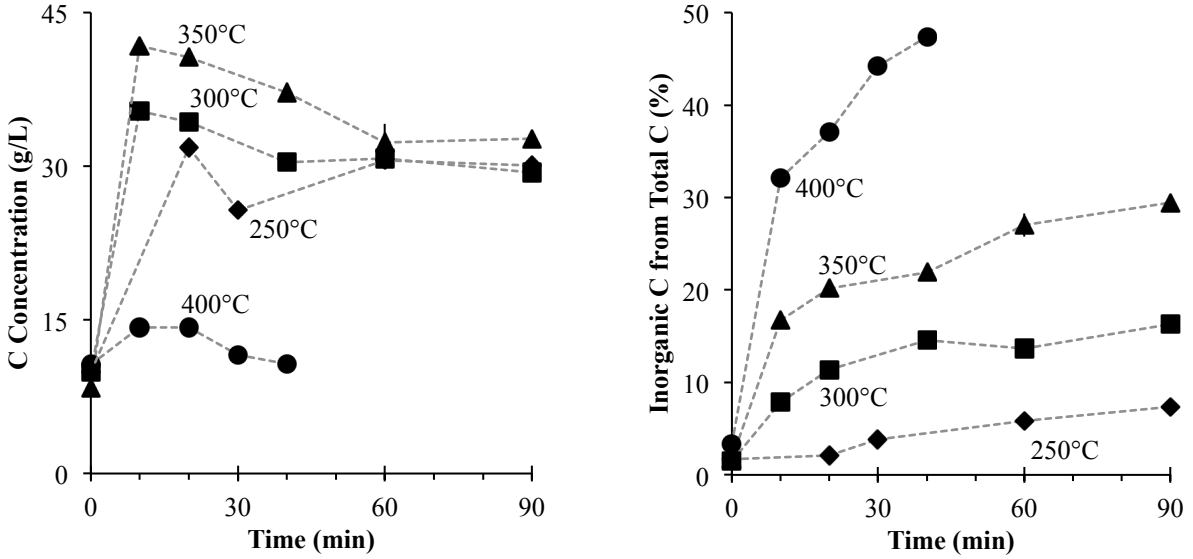

Figure 4.12. Concentration of C (a) and % of C present as inorganic carbon (b) in the aqueous phase at 250 °C (◆), 300 °C (■), 350 °C (▲), and 400 °C (●)

Figure 4.12a, which shows the concentration of C in the aqueous phase produced after HTL, illustrates that the C concentration at a given temperature is highest at the shortest reaction time and then gradually decreases as time increases. Figure 4.12a also shows that more C is released into the aqueous phase at a fixed time as temperature increases, up to 350 °C. At supercritical conditions, the C concentration is roughly half that of subcritical conditions, perhaps because at the higher temperature, C containing compounds in the aqueous phase are decomposed more easily into volatile compounds. Figure 4.12b shows that increased time and temperature also increase the portion of total carbon in the aqueous phase that is inorganic carbon, up to 47% at the most severe conditions, that is at higher temperatures or longer reaction times.

Preliminary analysis of the aqueous phase via high-performance liquid chromatography revealed the presence of citric acid, glucose (trace), glycerol, lactic acid, acetic acid, and pyroglutamic acid. These compounds only account for ~30% of the total organic C in the aqueous phase, so a continued investigation is still needed.

Table 4.10. N concentration in the aqueous phase (g/L)

Time (min)	250 °C	300 °C	350 °C	400 °C
0	2	2	1	2
10	-[a]	11	11	12
20	10	11	13	13
30	11	-	-	11
40	-	11	12	11
60	11	12	12 ± 2	-
90	11	12	14	-

[a]No data available

The N concentration in the aqueous phase is 11 ± 1 g/L after a short amount of hydrothermal treatment, regardless of temperature (Table 4.10). Since most of the intracellular nitrogen (> 90%) in marine microalgae resides in proteins [22], it appears that many of those proteins are readily decomposed into water-soluble amino acids and ammonia.

Table 4.11 shows the C composition of the solids is 52 ± 1 wt % at 0 min, which is similar to the C composition of the dried biomass feedstock. Upon experiencing liquefaction conditions, the C composition drops to as low as 5.18 wt % at 300 °C, indicating that most of the organic material has been transferred from the solid algal biomass to the other product fractions. At 250 °C, the C content is relatively high, only dropping as low to as 31.7 wt %. Table 4.11 also shows that the N composition in the solids is approximately 10 wt % initially and then drops to < 5 wt % by the end of the reaction. We did not include the data for sulfur in Table 4.11, as S in the solids is undetectable after 20 min. Sulfur was 0.6 wt % in the initial biomass.

Table 4.11. Carbon and nitrogen composition (wt %) of the solids

Time (min)	250 °C		300 °C		350 °C		400 °C	
	C	N	C	N	C	N	C	N
0	53.2	10.5	51.0	9.21	51.2	9.98	52.7	10.1
10	-[a]	-	21.4	3.77	22.6	3.22	12.6	1.29
20	45.6	10.8	11.4	2.12	16.9	2.26	8.88	1.44
30	42.5	8.71	-	-	-	-	18.3	2.34
40	-	-	10.1	1.29	23.9	2.55	16.6	2.19
60	43.8	6.41	5.18	0.88	-	-	-	-
90	31.7	4.59	7.18	1.31	35.8	2.41	-	-

[a]No data available

4.5.2. Elemental Distribution

Having reported gravimetric yields and elemental composition (wt %) for each of the product fractions, we now discuss how the reaction conditions affected the fraction of the initial C, N, and P that is distributed to each product fraction.

Summing the mass of C in the biocrude, gases, solids, and aqueous phase and comparing that value with the mass of C in the initial algal biomass permits calculation of the C balance in each experiment. The average C balance is 97 ± 14% from all of the reaction conditions. The large standard deviation comes from the C balance being lower from the reactions at supercritical conditions. As previously mentioned, there is a significant quantity of volatile compounds produced at supercritical conditions that is likely lost during transfers or cannot be analyzed with the gas phase products.

Table 4.12. Carbon (%) distributed to the light and heavy biocrudes

Time (min)	Light Biocrude				Heavy Biocrude			
	250 °C	300 °C	350 °C	400 °C	250 °C	300 °C	350 °C	400 °C
0	9.0	9.7 ± 0.4	13 ± 1	7.0	1.2	3.4 ± 1.8	4.5 ± 1.1	3.7
10	-[a]	25 ± 5	26 ± 3	34	-	34 ± 5	34 ± 5	22
20	24	25 ± 7	28 ± 4	38	23	30 ± 8	29 ± 5	18
30	24	-	-	33	24	-	-	17
40	-	27 ± 5	34 ± 2	33	-	30 ± 6	28 ± 3	16
60	27	30 ± 2	35 ± 2	-	32	30 ± 1	24 ± 3	-
90	19	30 ± 5	37 ± 1	-	28	26 ± 4	26 ± 1	-

[a]No data available

Table 4.12 shows that the fraction of the C in the algae that is partitioned to the light biocrude tends to increase with the reaction severity. That is, at a fixed reaction time, the amount of the initial C that appears in the light biocrude tends to increase with temperature. Likewise, at a fixed temperature, the amount tends to increase with time. After reaching its highest value of 38% at 400 °C and 20 min, the percentage of initial C in the light biocrude appears to decrease, which suggests decomposition of some of the compounds, perhaps to gases.

The data in Table 4.12 for the heavy biocrude shows a similar maximum value (34 ± 5% in this case) but at much milder conditions (300 and 350 °C, 10 min). As the reaction severity increases beyond this point, the fraction of initial C partitioned to the heavy biocrude decreases. This region is also where the fraction of initial C partitioned to the light biocrude increases, which suggests that some of the larger molecules in the heavy biocrude are being converted to smaller ones that appear in the light sub-fraction.

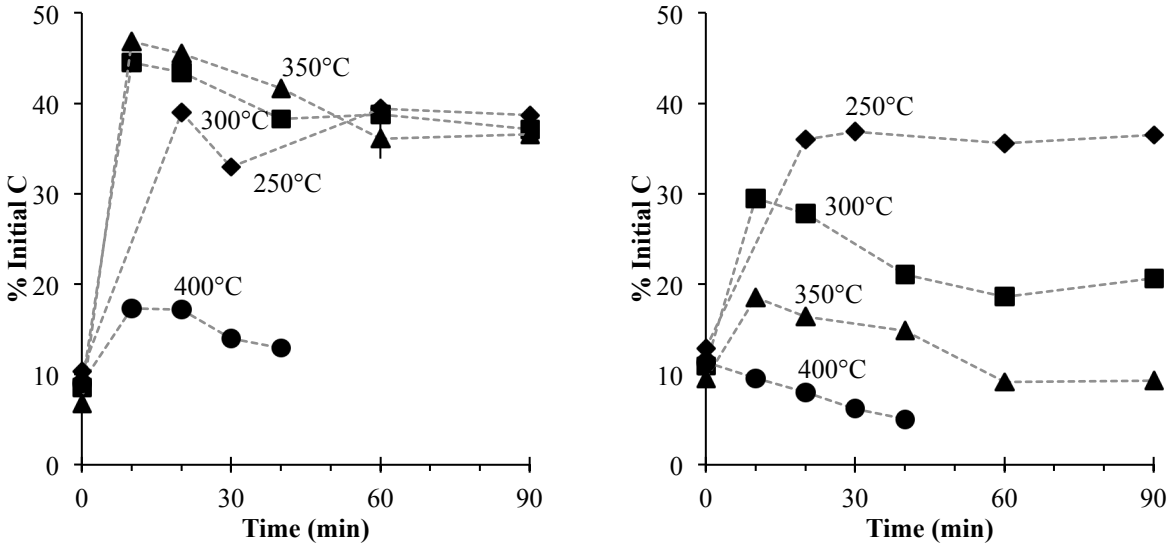

Figure 4.13. Carbon distribution in a) the aqueous phase and b) the water-soluble products at 250 °C (◆), 300 °C (■), 350 °C (▲), and 400 °C (●)

Figure 4.13a shows that much of the initial C appears in the aqueous phase. At subcritical conditions, approximately 40 - 45% of the C resides in the aqueous phase. Much less C is in the aqueous phase from liquefaction at supercritical conditions. Figure 4.13b shows that the percent of the initial C that resides in the dried aqueous phase (water soluble products) varies much more significantly with time and temperature than did the results in Figure 4.13a. It seems that at increasing temperatures and longer times, more and more of the C-containing compounds in the aqueous phase are lighter products that escape during evaporation of the water.

The results presented thus far show that > 95% of the initial C is distributed to the biocrude and the aqueous phase. The small balance of the remaining C is distributed to the gas and solid products. Less than 4% of the C from the biomass is converted into gas phase products at subcritical conditions, mainly as CO_2. At temperatures above 250 °C, the recovery of C in the solids is < 1%.

Table 4.13. Nitrogen (%) distributed to the light and heavy biocrudes

Time (min)	Light Biocrude				Heavy Biocrude			
	250 °C	300 °C	350 °C	400 °C	250 °C	300 °C	350 °C	400 °C
0	1.1	0.8 ± 0.03	1.3 ± 0.1	0.7	0.5	0.9 ± 0.5	4.8 ± 1.2	1.2
10	-[a]	7.6 ± 1.5	8.5 ± 1.0	13	-	22 ± 3	21 ± 3	13
20	4.5	8.8 ± 2.3	11 ± 1	16	16	18 ± 5	17 ± 3	10
30	5.7	-	-	11	17	-	-	10
40	-	9.4 ± 1.9	12 ± 1	11	-	17 ± 3	15 ± 2	9.0
60	7.4	9.6 ± 0.6	12 ± 1	-	21	15 ± 1	13 ± 1	-
90	6.3	12 ± 2	12 ± 1	-	19	15 ± 2	13 ± 0.5	-

[a]No data available

Similar to the calculation of the C balance, summing the masses of N in the biocrude, solids, and aqueous phase and comparing that value with the mass of N in the initial algal biomass permits calculation of the mean N balance for these experiments: 104 ± 9%. Table 4.13 shows that the amount of the original N in the algae that is partitioned to the light biocrude levels out at about 11% after reaching moderate liquefaction conditions. Conversely, the N recovery in the heavy biocrude initially increases, reaches a maximum of 26%, and then decreases with time at each of the three highest temperatures investigated. Although there is a significant reduction in the amount of N partitioned in the heavy biocrude as time progresses at the higher temperatures, the absence of a corresponding increase in the light biocrude indicates that the N-containing compounds are not simply transferred to the light biocrude.

Table 4.14. Nitrogen (%) distributed to the aqueous phase

Time (min)	250 °C	300 °C	350 °C	400 °C
0	14	12	8	17
10	-[a]	75	67	83
20	66	-	-	81
30	76	79	83	71
40	-	78	74	67
60	75	80	69 ± 10	-
90	82	81	84	-

[a]No data available

Table 4.14 shows that about two-thirds of the initial N is immediately distributed into the aqueous phase, even at the mildest liquefaction conditions. Although there is some variation, the N distribution is always 75 ± 9%, regardless of the conditions used. Ideally, all of the N would be distributed to the aqueous phase so that it could possibly be recovered and re-used for algae cultivation. Also, if all of the N were distributed to the aqueous phase, then there would be none in the biocrude, which would also be a desirable outcome.

Figure 4.14 shows that the portion of N in the aqueous phase that is present as ammonia generally increases with temperature for a fixed reaction duration. For example, at 20 min, the amount of aqueous-phase N present as ammonia is 19, 45, 49, and 54% at 250, 300, 350, and 400 °C, respectively. This result indicates that, at higher temperatures, the reactions that convert organic nitrogen to ammonia become more favorable during HTL. The results in Figure 4.14 also show that only a portion of the aqueous-phase N is present as ammonia, in contrast to what

others had previously assumed [10]. Most of the ammonia is likely derived from the decomposition of proteins.

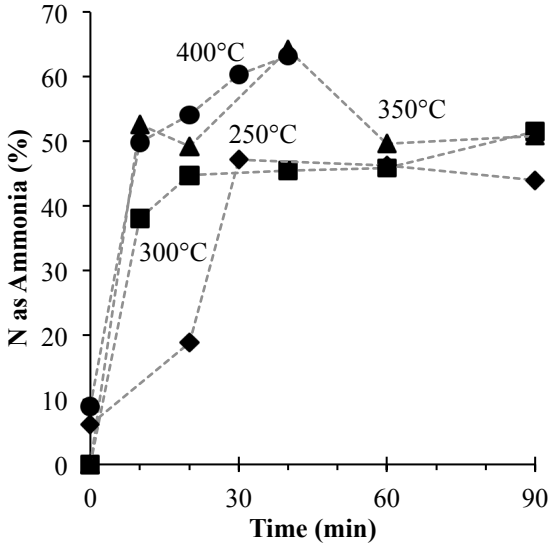

Figure 4.14. Percent of total nitrogen as ammonia in the aqueous phase at 250 °C (◆), 300 °C (■), 350 °C (▲), and 400 °C (●)

At 250 °C, < 5% of the N is in the solids and at higher temperatures, < 1% of the N is distributed to the solid phase. Although N containing gases are not easily detected in the gas phase, Ross et al. identified HCN, N_2O and NO_x in their experiments [3]. It is likely that they are present here only at very low concentrations since > 99% of the initial N in the algae appears in the biocrude and aqueous phase.

Phosphorus is an important element for algal cultivation and its limited quantities emphasize the need to recover and recycle it for sustainable production of algal biofuels [23]. The P content of the algal feedstock is 0.6%. We used this value to calculate the fraction of P distributed to the aqueous phase, shown in Table 4.15. This table illustrates that more than half of the initial P partitioned into the aqueous phase, except at the more severe processing conditions. At a given reaction time, the amount of P partitioned to the aqueous phase decreases with increasing

temperature. Clearly, using milder liquefaction conditions favors retention of phosphorus in the aqueous phase. Values determined for total phosphorus and phosphate were similar, demonstrating that most of the P in the aqueous phase is present as free phosphate. Garcia Alba et al. also reported that all of the P in the aqueous phase from the liquefaction of *Desmodesmus* sp. was in the form of phosphate [21]. The P content of the biocrude and solids produced at 350 °C for 60 min is 0.6 and 18%, respectively. These content values correspond to a P distribution of 26% to the biocrude and 24% to the solids. It is likely that at harsher reaction conditions more P may partition to the biocrude instead of to the solids or aqueous phase. This is the first time that P has been shown to be present in a biocrude formed via hydrothermal liquefaction of microalga.

Table 4.15. Phosphorus (%) distributed to the aqueous phase

Time (min)	P Distribution			
	250 °C	300 °C	350 °C	400 °C
10	-[a]	71	57	51
20	82	67	60	58
30	81	-	-	48
40	-	66	48	50
60	76	75	38 ± 3	-
90	85	74	44	-

[a]No data available

4.6. Energy Recovery and Return on Investment

Table 4.16. Biocrude energy metrics at different conditions

Time (min)	Energy distributed to the biocrude (%)				Energy Return on Energy Invested			
	250 °C	300 °C	350 °C	400 °C	250 °C	300 °C	350 °C	400 °C
0	11	14 ± 2	19 ± 2	12	-	-	-	-
10	-[a]	75 ± 8	64 ± 6	63	-	8.7 ± 1.1	6.9 ± 0.7	5.6
20	51	75 ± 11	62 ± 7	63	8.7	8.1 ± 1.5	6.7 ± 0.7	5.6
30	51	-	-	56	8.8	-	-	5.0
40	-	76 ± 9	67 ± 4	54	-	8.5 ± 1.2	7.3 ± 0.5	4.8
60	64	64 ± 3	67 ± 4	-	11	8.9 ± 0.3	7.0 ± 0.4	-
90	51	62 ± 7	69 ± 2	-	8.7	8.3 ± 1.0	7.4 ± 0.2	-

[a]No data available

Table 4.16 shows that over half of the chemical energy in the algal biomass is recovered almost immediately in the biocrude, even under very mild reaction conditions. At 300 °C, about 75% of the energy in the algae is recovered in the biocrude fractions, regardless of whether liquefaction proceeded for 10, 20, or 40 min. A similar insensitivity to reaction time is also apparent in the data from liquefaction at 350 °C. This result suggests that short reaction times might be sufficient for hydrothermal liquefaction of algae, if the main objective is to convert the wet algae paste to a smaller amount of energy-dense biocrude that retains most of the chemical energy. Garcia Alba et al. reported similar values for energy recovery from a biocrude produced from *Desmodesmus* sp. at 300°C [21]. Brown et al. demonstrated that 67 - 90% of the energy in the alga is recovered in the biocrude and gas products [1]. The heating value of the biocrude produced in these experiments, as estimated from the Boie formula, ranged from 34 to 37 MJ/kg,

values that are in accord with those reported previously for hydrothermal liquefaction of this alga [1].

We calculated the energy return on energy invested (EROEI) of a hypothetical liquefaction reactor by dividing the amount of chemical energy in the biocrude produced at a given set of liquefaction conditions with the amount of energy needed to heat and pressurize the algae paste from 20 °C and 1 atm to those liquefaction conditions. We used the steam tables to determine the enthalpies of the feed and effluent streams as saturated liquids and assumed conservatively that the algae paste had the same enthalpy as water. A well-engineered, large-scale HTL process would incorporate heat integration such that the hot reactor effluent would be used to heat the feed stream. We assumed that 80% of the heat in the effluent can be recovered in this way. Table 4.16 shows that the EROEI exceeds unity at all conditions investigated. Even at the most harsh reaction conditions investigated; there is approximately a fivefold increase in the energy return. Keep in mind that this calculation deals only with the liquefaction reactor. The EROEI for an entire process would be lower as additional energy inputs would be required for other unit operations (e.g., mixing, separations).

4.7. Conclusions

This work is the first to quantify directly the amount and composition of material in each of the four product fractions formed by hydrothermal liquefaction of microalgae. Doing so accounted for up to 94 wt % of the initial mass of the dry algae loaded into the reactor (with hexadecane as solvent). Accounting for products observed but not quantified (dissolved CO_2, char, NH_3 losses) led to mass balances ranging from 95 – 106 wt % for the different solvents employed. Solids dissolved in the aqueous phase and solids insoluble in both water and the

organic solvent contained largely inorganic material, but the H/C atomic ratios typically exceeded 2, which suggests the presence of some organic compounds in these product fractions. This work also confirms the presence of high-molecular-weight compounds in the biocrude fraction.

With the experimental protocol used here, the choice of solvent used to recover biocrude from HTL of microalgae affects the biocrude yield and composition. Non-polar solvents gave modestly higher gravimetric yields but yielded biocrudes with lower carbon content, and thus lower energy density. Polar solvents gave lower yields but a much higher fatty-acid content. Solvent choice also had an effect on the carbon content of the dissolved aqueous solids. The polar solvents produced solids that were lower in both C and N relative to those recovered with nonpolar solvents. For a given solvent and given microalgae strain, the yield of biocrude that is recovered can depend on the specific lot of algae used and the specific conditions used to recover the biocrude. A lower oil yield was obtained when using a lower ratio of solvent to algae.

The method of drying and storing *Nannochloropsis* sp. is not a significant factor affecting the yield of biocrude. Increasing the solid concentration of the slurry results in a moderate increase of the yield, but there are economic and energetic factors to consider to concentrate algal slurries above 20 wt %.

The lowest HTL temperature examined (250 °C) led to the partitioning of more than 80% of the initial phosphorus into the aqueous phase, primarily as phosphate. The P content of the aqueous phase generally decreased as the reaction severity increased (e.g., higher temperature, longer time) and it is possible that more P is being partitioned to the biocrude. The behavior for N was different, as the amount partitioned to the aqueous phase (primarily as ammonia) first increased, reached a maximum of 80 – 85%, and then decreased as the reaction temperature

increased. Thus, it appears that there is a tradeoff to be considered as mild conditions gave the highest P recovery in the aqueous phase, whereas moderate conditions led to the highest N recovery. High recoveries of both are desired to facilitate nutrient recycling.

The water density used for liquefaction at 400 °C had little effect on the yields of the different product fractions. The biomass loading (wt %) did have an effect, however. Liquefaction with higher loadings produced higher yields of biocrude, primarily by increasing the amount of the heavy crude fraction produced.

The molecular forms of N and P compounds in the aqueous phase are important for nutrient recycling as well, with ammonia and phosphate being the most desirable molecules bioavailable to algae [24]. While we confirmed that most P is in the form of free phosphate, only an average of 48% of the N present in the aqueous phase was ammonia. Bacteria have been shown to grow poorly, yet convert a large amount of organic N to ammonia in low organic C/N ratio (< 10 wt %) growth media [25]. The average organic C/N ratio of the aqueous phase was 1.57, so growing a microbial side-culture with it may facilitate ammonia regeneration before it is recycled to the algae operation [25].

Up to 75% of the chemical energy resident in the algal biomass can be recovered in the biocrude and in most cases the energy in the biocrude is at least 5 times greater than the unrecovered energy needed to produce it. The oxygen content in the biocrude decreased with increasing reaction severity. The nitrogen content, on the other hand, increased with the reaction severity until it reached a limiting value. Neither heteroatom is desired in the biocrude. The present results show that liquefaction conditions can be selected to produce bio-oil with either relatively low oxygen or nitrogen content, but not both simultaneously.

The results reported in this chapter are specific to the *Nannochloropsis* sp. used in the experiments. This alga has a very high protein content and modest lipid content, as reported by the supplier to be 59 and 14 wt %, respectively. HTL of other species, which have less protein and more lipid would probably provide biocrude in higher yield and with a lower N content.

References

[1] TM Brown, P Duan, PE Savage, *Hydrothermal Liquefaction and Gasification of Nannochloropsis sp*, Energy Fuels 24 (2010) 3639-3646.

[2] Y Dote, S Sawayama, S Inoue, T Minowa, S-Y Yokoyama, *Recovery of liquid fuel from hydrocarbon-rich microalgae by thermochemical liquefaction*, Fuel 73 (1994) 1855-1857.

[3] AB Ross, P Biller, ML Kubacki, H Li, A Lea-Langton, JM Jones, *Hydrothermal processing of microalgae using alkali and organic acids*, Fuel 89 (2010) 2234-2243.

[4] YF Yang, CP Feng, Y Inamori, T Maekawa, *Analysis of energy conversion characteristics in liquefaction of algae*, Resour Conserv Recycl 43 (2004) 21-33.

[5] T Matsui, A Nishihara, C Ueda, M Ohtsuki, N Ikenaga, T Suzuki, *Liquefaction of micro-algae with iron catalyst*, Fuel 76 (1997) 1043-1048.

[6] C Song, H Hu, S Zhu, G Wang, G Chen, *Nonisothermal catalytic liquefaction of corn stalk in subcritical and supercritical water*, Energy Fuels 18 (2004) 90-96.

[7] K Watanabe, N Yamagiwa, Y Torisawa, *Cyclopentyl Methyl Ether as a New and Alternative Process Solvent*, Org Process Res Dev 11 (2007) 251-258.

[8] P Duan, PE Savage, *Hydrothermal Liquefaction of a Microalga with Heterogeneous Catalysts*, Ind Eng Chem Res 50 (2011) 52-61.

[9] G Wypych, *Handbook of Solvents*, William Andrew: Toronto, Canada: 2001; 43

[10] P Biller, AB Ross, *Potential yields and properties of oil from the hydrothermal liquefaction of microalgae with different biochemical content*, Bioresour Technol 102 (2011) 215-225.

[11] P Duan, PE Savage, *Upgrading of crude algal bio-oil in supercritical water*, Bioresour Technol 102 (2011) 1899-1906.

[12] P Duan, PE Savage, *Catalytic treatment of crude algal bio-oil in supercritical water: optimization studies*, Energy Environ Sci 4 (2011) 1447-1456.

[13] D Zhou, L Zhang, S Zhang, H Fu, J Chen, *Hydrothermal liquefaction of macroalgae Enteromorpha prolifera to bio-oil*, Energy Fuels (2010)

[14] SM Heilmann, HT Davis, LR Jader, PA Lefebvre, MJ Sadowsky, FJ Schendel *et al.*, *Hydrothermal carbonization of microalgae*, Biomass Bioenergy 34 (2010) 875-882.

[15] ASTM E 1756, *Standard Test Method for Determination of Total Solids in Biomass*, (2008)

[16] BJ He, Y Zhang, Y Yin, TL Funk, GL Riskowski, *Preliminary characterization of raw oil products from the thermochemical conversion of swine manure*, Trans ASABE 42 (2001) 1865-1871.

[17] S Yin, R Dolan, M Harris, Z Tan, *Subcritical hydrothermal liquefaction of cattle manure to bio-oil: Effects of conversion parameters on bio-oil yield and characterization of bio-oil*, Bioresour Technol 101 (2010) 3657-3664.

[18] U Jena, KC Das, JR Kastner, *Effect of operating conditions of thermochemical liquefaction on biocrude production from Spirulina platensis*, Bioresour Technol 102 (2011) 6221-6229.

[19] AA Peterson, F Vogel, RP Lachance, M Fröling, MJ Antal Jr, JW Tester, *Thermochemical biofuel production in hydrothermal media: A review of sub-and supercritical water technologies*, Energy Environ Sci 1 (2008) 32-65.

[20] PJ Valdez, JG Dickinson, PE Savage, *Characterization of product fractions from hydrothermal liquefaction of Nannochloropsis sp. and the influence of solvents*, Energy Fuels 25 (2011) 3235-3243.

[21] L Garcia Alba, C Torri, C Samori, J van der Spek, D Fabbri, SRA Kersten *et al.*, *Hydrothermal Treatment (HTT) of Microalgae: Evaluation of the process as conversion method in an Algae Biorefinery Concept*, Energy Fuels 26 (2012) 642-657.
[22] SO Lourenço, E Barbarino, PL Lavín, M Lanfer, Ursula M, E Aidar, *Distribution of intracellular nitrogen in marine microalgae: Calculation of new nitrogen-to-protein conversion factors*, Eur J Phycol 2 (2004) 154-163.
[23] PH Pfromm, V Amanor-Boadu, R Nelson, *Sustainability of algae derived biodiesel: a mass balance approach*, Bioresour Technol 102 (2011) 1185-1193.
[24] L Garcia Alba, C Torri, D Fabbri, SRA Kersten, B (Wim), Derk W.F., *Microalgae growth on the aqueous phase from Hydrothermal Liquefaction of the same microalgae*, Chem Eng J 228 (2013) 214-223.
[25] F Touratier, JG Field, CL Moloney, *A stoichiometric model relating growth substrate quality (C:N:P ratios) to N:P ration in the products of heterotrophic release and excretion*, Ecol Modell 139 (2001) 265-291.

Chapter 5

Developing a Reaction Network

This chapter discusses the development of a reaction network to describe the conversion of algal solids from *Nannochloropsis* sp. into light and heavy biocrude, aqueous-phase products, and gas. As mentioned previously, there is limited discussion in the literature elucidating the reaction pathways that exist during hydrothermal liquefaction (HTL) of microalgae. Although some specific pathways have been described [1], a complete reaction network is lacking. The first section describes how variations in time and temperature affect the yields of the product fractions from the hydrothermal liquefaction of *Nannochloropsis* sp. The second section describes development of a reaction network, while the third section discusses the study of the reaction pathways within the first proposed network. The final section proposes a new reaction network based on the investigation of the reaction pathways.

5.1. Investigating Variations of Time and Temperature

Previous investigations of batch holding time and reaction temperature have been limited, examining only a few variations in time or temperature [2-5]. These studies also used large bench-scale reactors (> 10 mL) with heat-up times on the order of minutes or tens of minutes, bringing into question whether or not such studies [2-5] can be treated as being from isothermal reactions for use in kinetic modeling. This section describes the distribution of the product

fractions from the hydrothermal liquefaction of *Nannochloropsis* sp. at various times and temperatures. We reacted a 15 wt % slurry of *Nannochloropsis* sp. at 250, 300, 350, and 400 °C at holding times between 10 - 90 min in 4.1 mL reactors [6]. The heat-up time of the reactor is roughly 3 min. We collected and directly measured the yields of the solids, light and heavy biocrudes, and water-soluble products. After reaction we followed the work-up procedure outlined in section 3.4. We used this procedure to collect the data presented in sections 5.1 and 5.2.

Table 5.1. Average initial content of product fractions in the feedstock

product fraction	initial content* (wt %)
gas	0
light biocrude	6.5 ± 1.8
heavy biocrude	2.7 ± 1.5
solids	68 ± 5
water-soluble products	21 ± 2
total	98 ± 6

*dry basis

Table 5.1 shows the yield of each product fraction obtained from the original algal biomass using the procedure described in section 3.4.2 for measuring the initial values of the product fractions. The yields varied, presumably because modestly different amounts of slurry were used to load reactors at the different reaction temperatures. The results show that some biocrude and aqueous-phase products can be obtained from the algae simply by extraction using the outlined procedure. Of course, much higher biocrude yields are available through liquefaction.

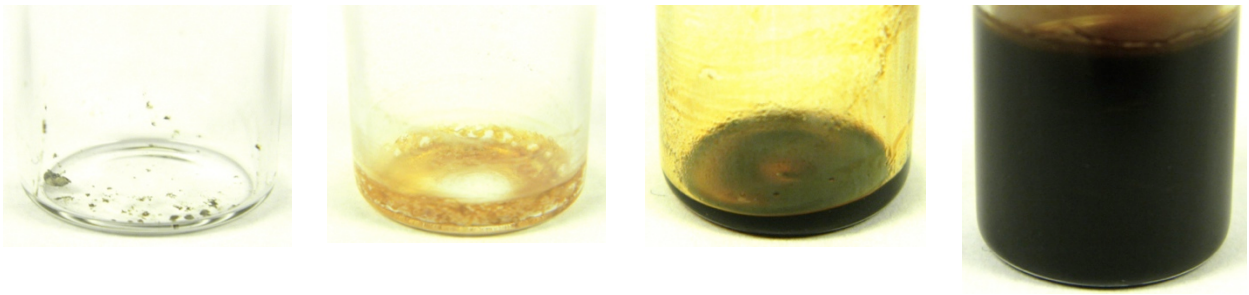

(a) (b) (c) (d)

Figure 5.1. Liquefaction product fractions: a) solids, b) water-soluble products, c) light biocrude, and d) heavy biocrude produced at 350 °C for 60 min

Figure 5.1a shows that the solids appear as a gray powder. At lower reaction temperatures or times the solids showed more green hues suggesting compounds such as chlorophyll from the cells may be present and intact in the solids. The aqueous phase was always amber in color with a strong odor of ammonia. The amber color intensified as time and temperature increased and the solution was always semi-transparent. Figure 5.1b shows that when the aqueous phase was dried, the water-soluble products maintained a similar amber color. The water-soluble products were malleable and soft with a similar foul odor. Both biocrudes (light and heavy) were dark-brown as shown in Figure 5.1c and 5.1d, respectively. The volume of heavy biocrude cannot be inferred from the photograph since the highly viscous product adheres to the walls of the vial when dried.

The total yield of biocrude (light plus heavy), illustrated in Figure 5.2, is between 30 - 50 % at 300 and 350 °C. Although some biocrude is lost during drying, the loss generally comprises < 3% of the total biocrude yield [14]. There is little variation in the biocrude yield with time after 10 min at 350 °C. The yields at 250 and 400 °C were almost always lower than the yields at 300 and 350 °C, which is consistent with previous work with this alga [7]. Above the critical point of water (374 °C) there is a decrease in the overall yield of biocrude at longer times, perhaps because some of the biocrude is thermally converted to smaller gaseous molecules.

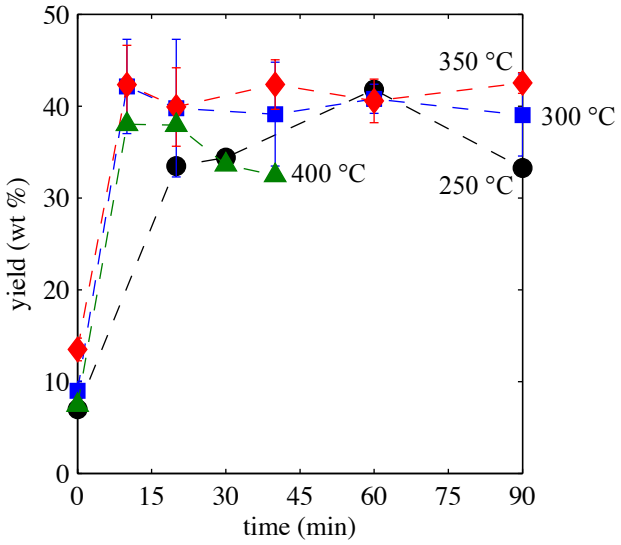

Figure 5.2. Yield of biocrude at 250 °C (●), 300 °C (■), 350 °C (◆), and 400 °C (▲)

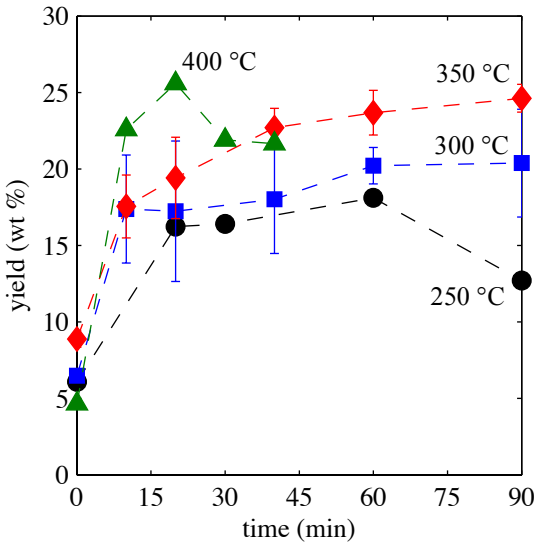

Figure 5.3. Yield of light biocrude at 250 °C (●), 300 °C (■), 350 °C (◆), and 400 °C (▲)

Figure 5.3 shows that the yield of light biocrude at a fixed time often increases with temperature. These results are consistent with the trend suggested by Jena et al. [3]. The highest yield of light biocrude is 25 wt % at 400 °C and 20 min. The yield then drops as time progresses. At 300 °C the light biocrude yield is fairly constant with time variations. The yield of light crude produced at 350 °C shows a steady increase with increasing time. The yield is lowest at 250 °C. Analysis of the light biocrude via gas chromatography, as described in section 3.5.4. showed the presence of fatty acids, chlorophyll derivatives, and cholesterol derivatives, as had been reported from previous analyses of biocrude from this alga [7].

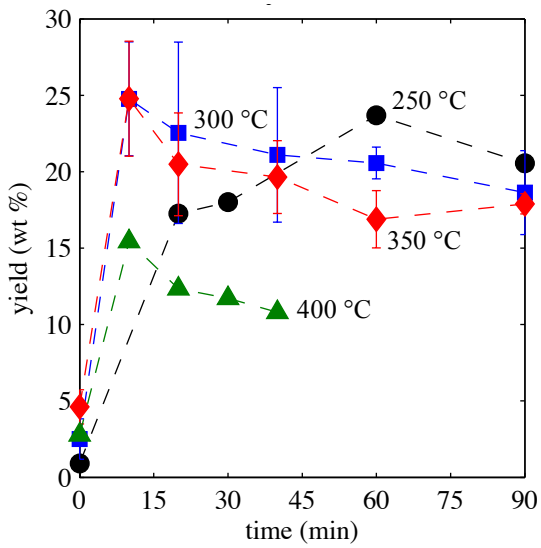

Figure 5.4. Yield of heavy biocrude at 250 °C (●), 300 °C (■), 350 °C (◆), and 400 °C (▲)

Figure 5.4 shows that the yield of heavy biocrude is initially higher than that of the light biocrude at 300 and 350 °C. Above 300 °C, increasing temperature produces less heavy biocrude and the yield of heavy crude decreases as time increases. The initial increase in the yield of heavy biocrude at 250 °C and its subsequent decrease at the more severe reaction conditions may

discount the previous assumption of free radical polymerization forming large amounts of high molecular weight compounds during liquefaction [1,8]. Polymerization may still take place, but it may not be a dominant reaction, allowing for the conversion of other heavy biocrude components into gas, light biocrude, and aqueous-phase products.

There appears to be some interconversion of material in the light and heavy biocrude fractions as the reaction progresses. At 350 °C and 20 min, and at higher temperatures, the yield of light biocrude surpasses the yield of heavy biocrude. The increasing yield of the light biocrude, shown in Figure 5.3, coupled with the concomitant decrease of heavy biocrude, suggests the transformation of heavy biocrude compounds into light biocrude compounds.

Figure 5.5 shows the total yield of products distributed to the aqueous phase. This yield is determined as the difference between 100 wt % and the sum of the yields of the other product fractions (biocrude, gas, and solids). About 51 ± 5 wt % of the initial mass of algae resides in the aqueous phase after the reaction. The change in yield of products distributed to the aqueous phase is almost entirely independent of the liquefaction temperature. As time increases, so does the yield of the aqueous phase products, but only slightly. These results suggest that the products in the aqueous phase primarily come directly from the algal biomass and that compounds originally partitioned into the biocrude fraction that get converted into aqueous-phase products account for only a small amount of the material.

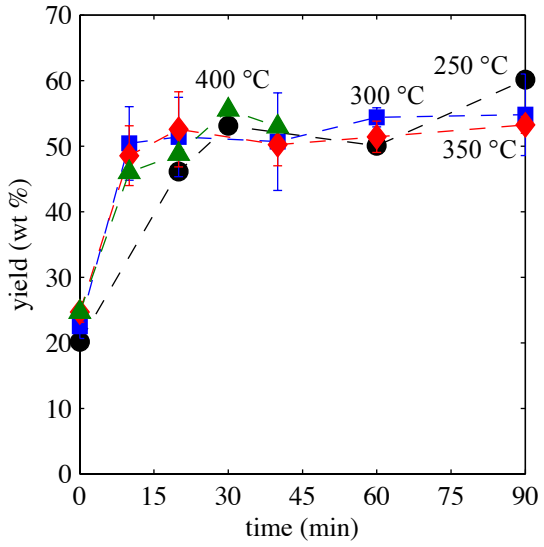

Figure 5.5. Yield of aqueous-phase products at 250 °C (●), 300 °C (■), 350 °C (◆), and 400 °C (▲)

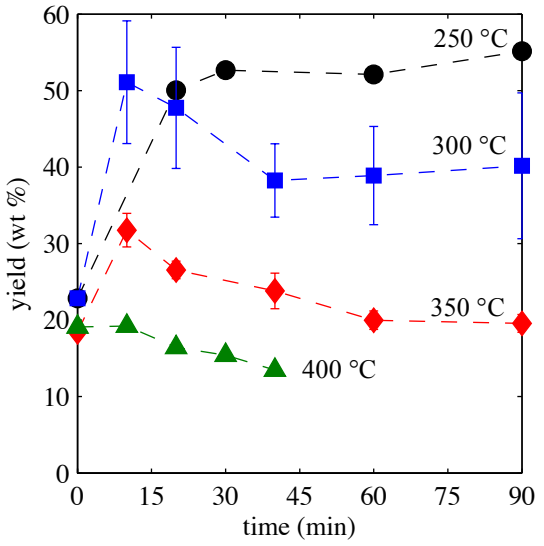

Figure 5.6. Yield of water-soluble products at 250 °C (●), 300 °C (■), 350 °C (◆), and 400 °C (▲)

Figure 5.6 illustrates that the yield of the water-soluble products quickly increases to about 50 wt % at both 250 and 300 °C. In fact, the yields of water-soluble products at 250 °C, which were determined directly, are on average within 1 wt % of the yield of aqueous-phase products in Figure 5.5, which was determined by difference. These yields being essentially equal at the mild liquefaction conditions lends credence to calculating the total yield of aqueous-phase products by difference. At 250 °C we accounted for, on average 100 ± 4 wt % of the initial biomass in all of the products. The yield of water-soluble products in Figure 5.6 decreases with time at 300, 350, and 400 °C. Presumably, the compounds in the aqueous phase decompose into highly volatile constituents that are not recovered [9]. We determined the yield of these volatiles formed in the aqueous phase as the difference between 100 wt % and the sum of the yields of the other product fractions (biocrude, gas, solids, and water-soluble products).

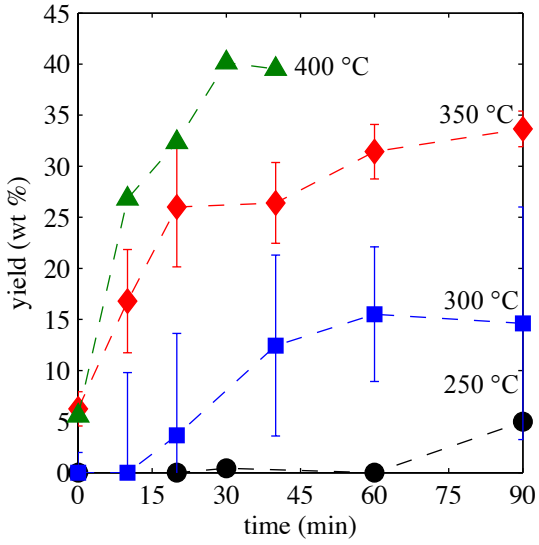

Figure 5.7. Yield of volatiles at 250 °C (●), 300 °C (■), 350 °C (◆), and 400 °C (▲)

Figure 5.7 shows that the yield of the volatiles is nearly the mirror image of the yield of the water-soluble products. The yield of volatiles increases steadily with both time and temperature.

These trends are consistent with the hypothesis that the volatiles, which are lost during the drying of the aqueous phase, come from the decomposition of compounds originally partitioned into the aqueous phase very early in the reaction. Thus, there appear to be significant reactions taking place within the aqueous phase itself, wherein large compounds with low vapor pressure are converted into lighter products.

Figure 5.8 illustrates that the yield of gases (H_2, CO, CH_4, CO_2, C_2H_4, C_2H_6) increases as both time and temperature increase. At 250 °C, < 1 wt % of the algae is converted into gas, but the yield reaches 13 wt % at 400 °C. Similar to previous results, at least 77 mol % of the product gases is composed of CO_2 at supercritical conditions [7,10]. At subcritical conditions, > 93 mol % of the gas product is CO_2. Although there is some value in flammable gases such as H_2, CH_4, C_2H_4, and C_2H_6 they are in small concentrations (below 14 mol % combined at 400 °C, and below 7 mol % at subcritical conditions).

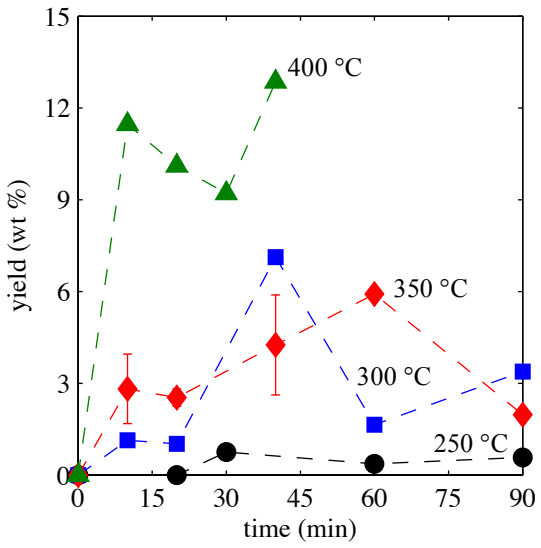

Figure 5.8. Yield of Gas and at 250 °C (●), 300 °C (■), 350 °C (◆), and 400 °C (▲)

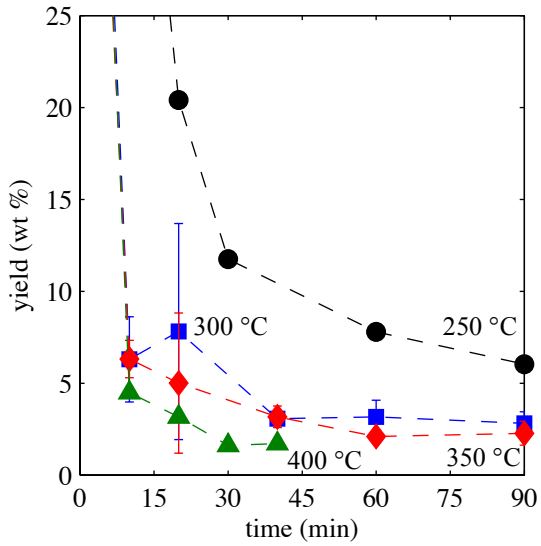

Figure 5.9. Yield of Solids at 250 °C (●), 300 °C (■), 350 °C (◆), and 400 °C (▲)

The initial algal biomass is composed primarily of solid material that is insoluble in both water and dichloromethane. Figure 5.9 shows that as time progresses, more of the solid material is transformed into the other product fractions. The yield of solids decreases rapidly at short reaction times and the rate of this initial decrease increases with temperature. At 250 °C the yield of solids drops below 8 wt % after 60 min of reaction time. The yield of solids is just 3 wt % after 60 min of treatment at higher temperatures. Note that there is no region where the yield of solids increases with time and temperature. This result suggests that over-reaction of the biocrude to produce large dichloromethane-insoluble compounds does not occur to any appreciable extent at the conditions investigated. After a short period of hydrothermal treatment, it is likely that the intracellular contents of the alga are released so that there is a sharp decrease in yield of solids and sharp increase in the yields of water-soluble products and light and heavy biocrude fractions.

5.2. Proposed Network

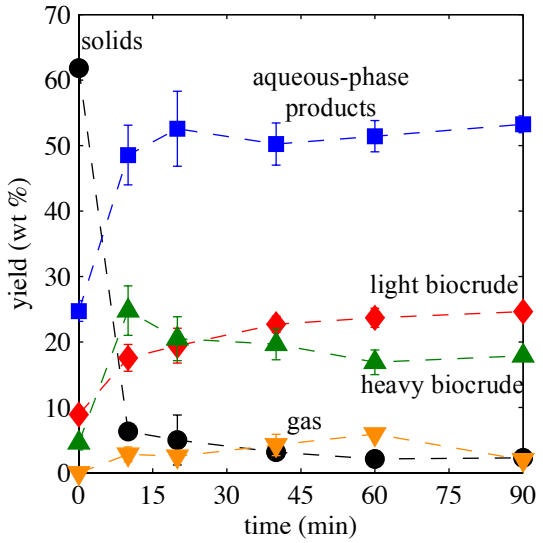

Figure 5.10. Temporal variation of yields of light biocrude (◆), heavy biocrude (▲), aqueous-phase products (■), solids (●), and gas (▼) at 350 °C

Figure 5.10 illustrates the product fractions as they change with time at 350 °C. These data, along with those at the other temperatures, can be used to deduce a potential reaction network for the HTL of microalgae. Most of the initial algal biomass exists as materials classified as solids in our protocol. As the reaction begins, the yields of gases, volatiles, aqueous-phase products, light biocrude, and heavy biocrude increase as the yield of solids decreases, suggesting direct reaction paths from the solids to all of the other product fractions. The reaction of solids to aqueous-phase products likely represents the release of intracellular proteins and carbohydrates and their subsequent decomposition in the hydrothermal environment. The pathway from solids to light and heavy biocrudes presumably represents the decomposition of the cell wall as the phospholipids are hydrolyzed. Any intracellular lipids are also released and hydrolyzed as the reaction progresses. It is likely that the aqueous-phase products and biocrudes contribute to the continued formation of gases as the reaction severity increases, thus suggesting at least a minor pathway from these product fractions to gas production. The biocrude contributes some gaseous

compounds that are formed during cracking reactions [10], although it is not clear whether they originate from the light or heavy biocrude or both. The simultaneous rise in light biocrude yield as the heavy biocrude yield decreases suggests a pathway between these two product fractions. The path from heavy to light biocrude may be reversible if polymerization reactions occur as has been assumed [8]. Light and possibly heavy biocrude probably contribute to the aqueous-phase products as triglycerides and phospholipids are hydrolyzed and water-soluble glycerol and phosphates are formed. Reactions such as these could account for the slight increase in the yield of aqueous-phase products with increasing time. Using the aforementioned observations and assumptions, we offer Figure 5.11 as a potential reaction network, showing the dominant reaction directions and paths for the hydrothermal liquefaction of this microalga.

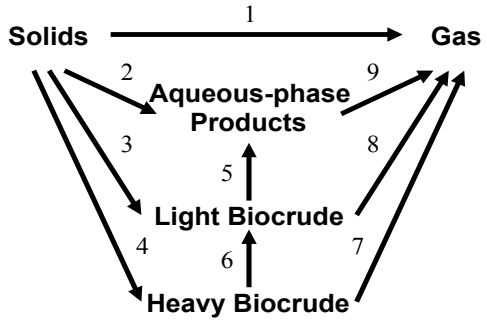

Figure 5.11. Potential reaction network for hydrothermal liquefaction of algae

5.3. Investigating Reaction Pathways

This section details the results of the hydrothermal treatment of the isolated product fractions to study the reaction pathways, further probing and refining the reaction network developed in the previous section (Figure 5.11). By studying how each product fraction reacted during the hydrothermal treatment, we can suggest reaction pathways that occur during liquefaction.

We loaded approximately 130 mg of each of the isolated product fractions (solids, light and heavy biocrude) and 2.18 mL of water into a 4.1 mL batch reactor. We generated the isolated product fractions from a 15 wt % slurry of *Nannochloropsis* sp., following the procedure outlined in section 3.1.2. The loading mimics the concentration of the products from previous liquefaction experiments [6]. The reactor was built as described previously and included a valve for gas recovery and analysis [6]. For the reaction with aqueous-phase products, we simply loaded 2.18 mL of the aqueous-phase mixture to each batch reactor. We placed the sealed reactors in a pre-heated sandbath set to 350 °C and kept them at temperature for 10, 20, 30, and 40 min. We then followed the work-up procedure described previously in section 3.4 to collect, separate, and quantify each of the product fractions, including analysis of the gases in the reactor headspace. The yield is defined as the mass of the product fraction per mass of the initial material added to the reactor. The reactors that were loaded with light and heavy biocrudes underwent a modified work-up to ensure complete recovery of the products from the reactor. After pouring the contents of the reactor into a test tube, we added 3 mL of dichloromethane to the reactor, capped it, and then placed it on a vortexer for 10 min at 1000 rpm. We then poured the dichloromethane phase into the test tube and repeated this twice.

Control experiments verified that 95 ± 7 wt % of the material deposited into the reactors can be recovered with the methods described when investigating the reactions of individual product

fractions. The control experiments also showed some partitioning (but always < 8 wt %) of the material originally in each product fraction into other product fractions even at room temperature. The partitioning probably occurs because fresh solvents, both organic and aqueous, come into contact with the product fraction. We take the results of the control experiments to represent the initial concentration of each of the product fractions in the reactor at 0 min.

5.3.1 Reaction of Solids

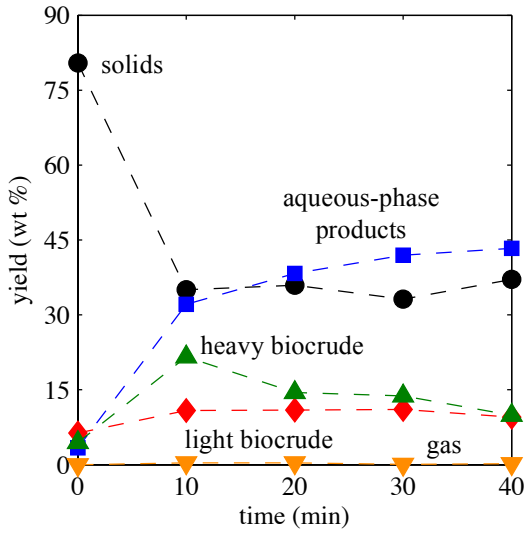

Figure 5.12. Temporal variation of product fractions from the hydrothermal treatment of solids at 350 °C

Figure 5.12 demonstrates that the reaction of the solid material recovered from a previous alga liquefaction experiment resulted in the formation of each of the product fractions. The yield of solids settles around 35 ± 2 wt % after 10 min of reaction and remains relatively unchanged thereafter. The solids added to the reactor were roughly 33 wt % ash (see Table A.2 in the Appendix for ash content of all product fractions), suggesting that the remaining solids are also largely ash. The yield of light biocrude is relatively constant at 11 wt % but it does increase from the initial value of 6 wt %. The yield of heavy biocrude produced from the solid phase is 22

wt % at 10 min and decreases to 10 wt % after 30 min of reaction time. Previous work showed that the remaining mass resides in the aqueous-phase products [6], so we assume the same is true here. The yield of aqueous-phase products increases as the yield of heavy biocrude decreases with time. Gas is a very minor product, always comprising < 0.4 wt % of the total products. The time-dependent trends for product formation from the solids are similar to the trends for the reaction of microalgae at the same temperature (Figure 5.10).

The results in Figure 5.12, which show that the solids produce aqueous-phase products, and light and heavy biocrudes, suggest a direct pathway from solids to each of these three product fractions. Although there is some gas produced from the reaction of the solids, its yield was low and the data do not permit its assignment either as a primary product from the solids or as a secondary product from the aqueous-phase products or biocrudes.

5.3.2 Reaction of Aqueous-phase Products

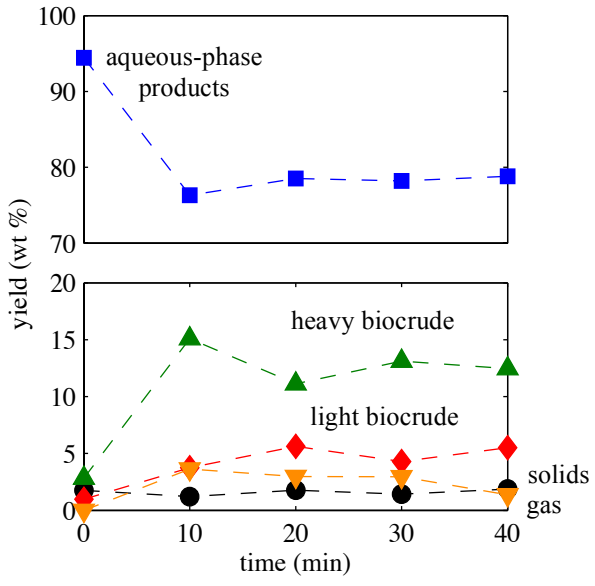

Figure 5.13. Temporal variation of product fractions from the hydrothermal treatment of aqueous-phase products at 350 °C

Figure 5.13 shows that about 23 wt % of the initial aqueous-phase products were quickly converted into the other products. The aqueous-phase products formed both biocrudes, with the yield of heavy roughly twice that of light. The yields of the biocrudes increase with increasing reaction time, but at longer reaction times the yield of heavy biocrude begins to decrease. The formation of biocrude from the aqueous phase has not been shown previously for this alga. The yield of solids is relatively constant at its initial value (below 2 wt %). More gas is produced from the aqueous-phase products than from the reaction of any other product fraction, with the yield ranging from 1 - 4 wt %. The product gas contains above 82 mol % CO_2 and below 10 mol % H_2, with the balance composed of CH_4, CO, and C_2H_4.

The results suggest a pathway to both light and heavy biocrudes from the aqueous-phase products. The existence of these paths is consistent with previous work suggesting the formation of biocrude components from the water-soluble components based on the molecular composition of the biocrude [1]. The formation of gas from the aqueous-phase products is likely one of the major contributors of gas during the liquefaction of microalgae and the other product fractions as well.

5.3.3. Reaction of Light Biocrude

Figure 5.14 shows that the reaction of the light biocrude produces aqueous-phase products in the highest yield (43 wt % at 40 min). The yield of heavy biocrude initially increases but then it decreases at longer times. Gas yields were always below 0.2 wt % and similar in composition to the gas phase produced during the treatment of aqueous-phase products. The yield of solids is relatively constant at its initial value of < 4 wt % in all cases.

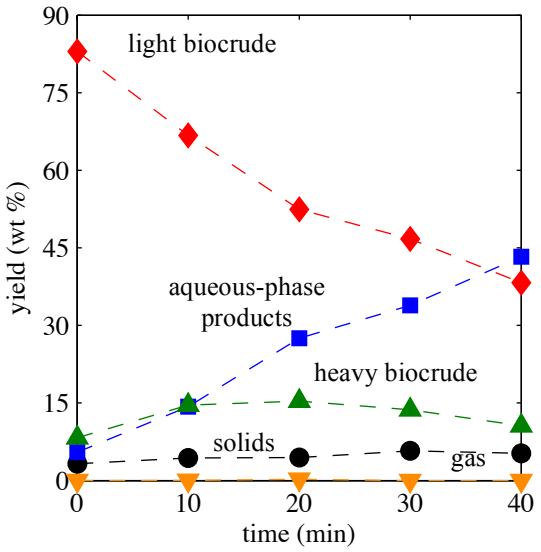

Figure 5.14. Temporal variation of product fractions from the hydrothermal treatment of light biocrude at 350 °C

The results in Figure 5.14 are consistent with pathways from the light biocrude leading to aqueous-phase products and heavy biocrude. Production of water-soluble products is a reasonable pathway since hydrolysis of lipids (mono-, di-, and triglycerides), which are hexane-soluble, produces glycerol, which is water-soluble and should contribute to the aqueous phase. The formation of heavy biocrude from light biocrude supports the previously hypothesized polymerization pathway to produce high-molecular-weight hexane-insoluble species [6]. The yield of gases was so low that the pathway from the light biocrude to the gas products is negligible. The small amounts of gas observed could have been formed as a secondary product from the aqueous-phase products. The formation of gas products from the light biocrude may not be as significant as previously suggested [6].

5.3.4 Reaction of Heavy Biocrude

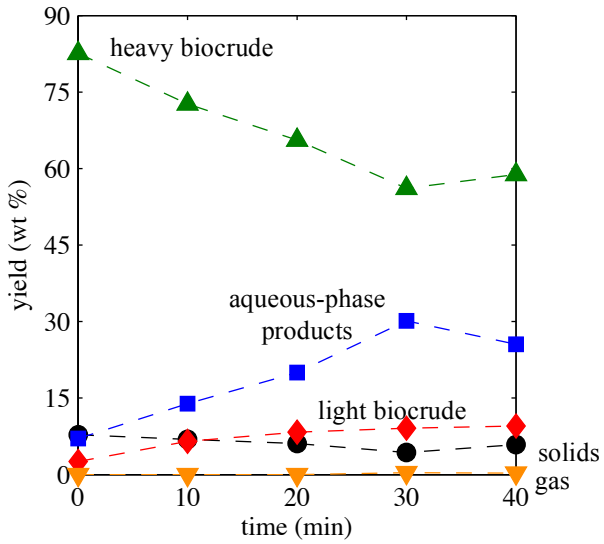

Figure 5.15. Temporal variation of product fractions from the hydrothermal treatment of heavy biocrude at 350 °C

Figure 5.15 shows that the reaction of the heavy biocrude results primarily in the formation of aqueous-phase products. The yield of the aqueous-phase products increases over time from 5 to 26 wt %. The formation of aqueous-phase products from heavy biocrude has not been advanced previously in the literature. The yield of solids from the heavy biocrude is 8 wt % initially and it decreases slightly to 6 wt % as time increases. This behavior suggests that there is no pathway for solids formation from heavy biocrude under the hydrothermal conditions considered in Figure 5.15. The heavy biocrude forms light biocrude and the yield steadily increases from 2 to 9 wt % during the reaction time.

The reaction of the heavy biocrude yields < 0.4 wt % gas products, but this product fraction is richer in fuel gases (H_2, CH_4, C_2H_4, and C_2H_6) than the gas produced by the aqueous-phase products. The yield of gas products increases slightly with increased reaction time. The molar ratio of the sum of H_2, CH_4, C_2H_6, and C_2H_4 to CO_2 for the reaction of heavy biocrude at 40 min

is 1.2:1. The molar ratio of the same gases for the reaction of aqueous-phase products at 40 min is 0.1:1. The aqueous phase may produce most of the CO_2 during the reaction while the heavy biocrude may produce most of the hydrocarbon gases, since that product fraction reacts and decomposes. This pathway to fuel gases from heavy biocrude, though operative, appears relatively minor because the majority of the gas product from the hydrothermal liquefaction of *Nannochloropsis* sp. was always CO_2 [6]. The pathway to gas from the heavy biocrude seems to be important for the formation of the hydrocarbon and H_2 gases, but it probably represents a minor pathway with respect to the overall yield of gases under liquefaction conditions. To summarize, Figure 5.15 provides evidence consistent with pathways to light biocrude and gas products from heavy biocrude, as previously hypothesized [6]. The results are also consistent with a reaction pathway to aqueous-phase products from the heavy biocrude that had not been previously advanced.

5.4. Refining the Reaction Network for the HTL of *Nannochloropsis* sp.

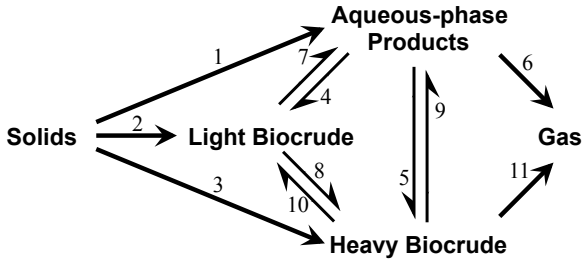

Figure 5.16. Reaction network for the hydrothermal liquefaction of *Nannochloropsis* sp.

Collecting together all of the pathways deduced from qualitative inspection of Figures 5.12-5.15 leads to Figure 5.16 as the reaction network for the hydrothermal liquefaction of *Nannochloropsis* sp. The network includes all of the pathways originally proposed in Figure 5.11,

with the exception of the formation of gas from the solids and from the light biocrude. Gas formation from these product fractions was much lower than that from the aqueous-phase products and the heavy biocrude. Hence, we neglect them in the reaction network. Figure 5.16 includes new pathways from aqueous-phase products to light biocrude and from light biocrude to heavy biocrude. The exchange of material between heavy biocrude and aqueous-phase products is also a new discovery from the present work. Thus, there are two reaction paths between aqueous-phase products and heavy biocrude. One is direct and the other proceeds through the light biocrude as an intermediate.

5.5. Conclusions

Hydrothermal liquefaction at 300 °C or higher converted ~ 95 wt % of the initial cellular material to water- and dichloromethane-soluble compounds, even at the shortest time examined in this study (10 min). At these short times, about half of the converted material partitioned to the aqueous phase and the other half to the biocrude. This high conversion at short times suggests that liquefaction at even shorter times should be examined. If effective, it may be possible to develop a hydrothermal liquefaction process that requires residence times of just a few minutes rather than tens of minutes. Such a process would require smaller equipment volumes and consequently lower capital costs.

The yield of heavy biocrude decreased with increasing reaction temperature. One potential pathway for the heavy material is its overreaction to form even heavier, insoluble solid material, as often happens in pyrolytic processes. This pathway does not appear to be important under the conditions examined, however, as the yield of solids (insolubles) monotonically decreased with time and produced yields below 3 wt % at the most severe conditions examined. Rather, the

increase in the yield of light biocrude that accompanies the decrease in yield of heavy crude as the reaction severity increases, suggests that the heavy biocrude converts to lighter, not heavier, material during this hydrothermal process.

The reaction network for the hydrothermal liquefaction of *Nannochloropsis* sp. includes formation of aqueous-phase products, light biocrude, and heavy biocrude as primary products from the initial algal biomass. Secondary reaction pathways interconnect each of these primary product fractions. Gases form from secondary reactions of aqueous-phase products and heavy biocrude, with the latter product fraction being the chief source of fuel gases.

The reaction network developed here strictly applies only to the alga used in the experiments, that is *Nannochlorpsis* sp. Additional work with other species is needed to determine whether the network can be generalized to other microalgae.

References

[1] C Torri, L Garcia Alba, C Samorì, D Fabbri, DWF Brilman, *I - Hydrothermal Treatment (HTT) of Microalgae: Detailed Molecular Characterization of HTT Oil in View of HTT Mechanism Elucidation*, Energy Fuels 26 (2012) 658-671.

[2] L Garcia Alba, C Torri, C Samori, J van der Spek, D Fabbri, SRA Kersten *et al.*, *I - Hydrothermal Treatment (HTT) of Microalgae: Evaluation of the Process As Conversion Method in an Algae Biorefinery Concept*, Energy Fuels 26 (2012) 642-657.

[3] U Jena, KC Das, JR Kastner, *Effect of operating conditions of thermochemical liquefaction on biocrude production from Spirulina platensis*, Bioresour Technol 102 (2011) 6221-6229.

[4] T Minowa, S-Y Yokoyama, M Kishimoto, T Okakura, *Oil production from algal cells of Dunaliella tertiolecta by direct thermochemical liquefaction*, Fuel 74 (1995) 1735-1738.

[5] YF Yang, CP Feng, Y Inamori, T Maekawa, *Analysis of energy conversion characteristics in liquefaction of algae*, Resour Conserv Recycl 43 (2004) 21-33.

[6] PJ Valdez, MC Nelson, HY Wang, X Lin, PE Savage, *Hydrothermal Liquefaction of Nannochloropsis sp.: Systematic study of process variables and the analysis of product fractions*, Biomass Bioenergy 46 (2012) 317-331.

[7] TM Brown, P Duan, PE Savage, *Hydrothermal Liquefaction and Gasification of Nannochloropsis sp*, Energy Fuels 24 (2010) 3639-3646.

[8] L Zhang, CC Xu, P Champagne, *Overview of recent advances in thermo-chemical conversion of biomass*, Energy Convers Manage 51 (2010) 969-982.

[9] P Biller, AB Ross, *Potential yields and properties of oil from the hydrothermal liquefaction of microalgae with different biochemical content*, Bioresour Technol 102 (2011) 215-225.

[10] PJ Valdez, JG Dickinson, PE Savage, *Characterization of product fractions from hydrothermal liquefaction of Nannochloropsis sp. and the influence of solvents*, Energy Fuels 25 (2011) 3235-3243.

Chapter 6

Quantitative Kinetic Model

The reaction network we present in Figure 5.16 provides a qualitative description of the reactions that take place and the origin of each product fraction during hydrothermal liquefaction (HTL). We used the reaction network from Figure 5.16 to develop a quantitative kinetic model and estimated its parameters using experimental results for the hydrothermal liquefaction of *Nannochloropsis* sp. at different temperatures and times. We developed the model to be able to predict the yields of product fractions based on a few initial parameters.

This chapter shows how the model accurately predicted previously published biocrude and gas yields for the hydrothermal treatment of *Nannochloropsis* sp., though predictions became poorer further outside the experimental parameter space used to determine the model parameters. The first section summarizes the mathematical formulation of the model and the correlation of the model with the data used to determine its parameters. The second section shows the ability of the model to predict the yields of liquefaction products from *Nannochloropsis* sp. The third and fourth sections describe sensitivity and rate analyses, respectively.

We used the experimental procedure described previously in section 3.3 to liquefy a 15 wt % slurry of *Nannochloropsis* sp. at 275 °C at 10, 20, and 30 min. The results from these experiments are presented in section 6.2 to validate the predictive capability of the kinetic model. Each experiment provides the yield (wt % dry-basis) of the four product fractions described previously and gases. The yield is defined as the mass of the product fraction per mass of alga added to the reactor.

6.1. Setup, Design, and Fitting Data

We used the reaction network shown in chapter 5 (Figure 5.16) as the basis for a kinetic model for the liquefaction of microalgae. Coupling the first-order (assumed for convenience) rate laws for each pathway with the design equation for an isothermal batch reactor leads to Equations 6.1 - 6.5, as the basis for the kinetics model. The total ash in this alga (3 wt %) [1] has been subtracted from the yield of the solids product fraction since we assume that the ash resides in the solids after hydrothermal treatment.

$$\text{Solids:} \quad \frac{dx_1}{dt} = -(k_1 + k_2 + k_3)x_1 \tag{6.1}$$

$$\text{Aqueous-phase Products:} \quad \frac{dx_2}{dt} = -(k_4 + k_5 + k_6)x_2 + k_1x_1 + k_7x_3 + k_9x_4 \tag{6.2}$$

$$\text{Light Biocrude:} \quad \frac{dx_3}{dt} = -(k_7 + k_8)x_3 + k_2x_1 + k_4x_2 + k_{10}x_4 \tag{6.3}$$

$$\text{Heavy Biocrude:} \quad \frac{dx_4}{dt} = -(k_9 + k_{10} + k_{11})x_4 + k_3x_1 + k_5x_2 + k_8x_3 \tag{6.4}$$

$$\text{Gas:} \quad \frac{dx_5}{dt} = k_6x_2 + k_{11}x_4 \tag{6.5}$$

We simultaneously solved the system of ordinary differential equations and estimated values for the rate constants (k_j) using a least-squares objective function. The residual, shown in Equation 6.6, is the summation of the squared differences, at a given liquefaction temperature, between the experimental yield for each product fraction (x_i) and the model value ($x_{i,m}$).

$$Residual = \sum_i \sum_t [x_i(t) - x_{i,m}(t)]^2 \tag{6.6}$$

The experimental yields are those we reported previously in section 5.1 for the hydrothermal liquefaction of *Nannochloropsis* sp. and those in the appendix that accompany this chapter. Since our goal is to model algae liquefaction, we used exclusively data from experiments with algae to determine the model parameters. We did not use the data from hydrothermal treatment of the individual isolated product fractions (Figures 5.12 - 5.15) since the reaction rates observed in those experiments could conceivably differ from those observed when starting with algae.

We used the MATLAB optimization function, 'fmincon', selecting the 'interior-point' algorithm to minimize the value of the residual at each temperature. We constrained the rate constants to be within 0 - 0.28 min^{-1}. The upper bound was constrained at 0.28 min^{-1} since this value was large enough to accommodate the fastest paths observed experimentally but small enough to avoid longer computational times. The optimized values of the rate constants for each reaction pathway at each temperature are included in the Appendix (Table A.3). We then used these optimized values to calculate the parameters for the Arrhenius equation, with standard error of the linear regression shown in Table 6.1 for each pathway.

Table 6.1. Arrhenius parameters

Path	Reaction	$E_{a,j}$ (kJ/mol)	A_j (min^{-1})
1	Solids → Aqueous-phase Products	27 ± 12	$10^{1.2 \pm 1}$
2	Solids → Light Biocrude	15 ± 5	$10^{0.09 \pm 0.4}$
3	Solids → Heavy Biocrude	41 ± 14	$10^{2.6 \pm 1.2}$
4	Aqueous-phase Products → Light Biocrude	26 ± 5	$10^{0.78 \pm 0.43}$
5	Aqueous-phase Products → Heavy Biocrude	2.9 ± 0.8	$10^{1 \pm 0.9}$
6	Aqueous-phase Products → Gas	66 ± 19	$10^{1.7 \pm 1.6}$
7	Light Biocrude → Aqueous-phase Products	17 ± 10	$10^{0.52 \pm 0.87}$
8	Light Biocrude → Heavy Biocrude	33 ± 10	$10^{0.39 \pm 0.91}$
9	Heavy Biocrude → Aqueous-phase Products	4.8 ± 2.7	$10^{0.35 \pm 0.22}$
10	Heavy Biocrude → Light Biocrude	45 ± 27	$10^{2 \pm 2.3}$
11	Heavy Biocrude → Gas	80 ± 6	$10^{4.3 \pm 0.4}$

The paths that form gases (pathways 6 and 11) have the highest activation energies (66 and 80 kJ/mol, respectively) in Table 6.1. Guan et al. investigated the formation of gas products from *Nannochloropsis* sp. via hydrothermal treatment; their data provide a basis for comparison of these activation energies [1]. Using the yields of carbon-containing gas in Figure 4a of Guan et al., we calculated the initial rate of gas formation at 450, 500, and 550 °C and subsequently determined the activation energy to be about 71 kJ/mol. This value is in good agreement with activation energies reported in Table 6.1 for gas formation for pathways 6 and 11, providing additional support for the values in Table 6.1. The activation energies for the other paths are all

lower and in some cases (e.g. paths 5 & 9) lower, than one would expect for a chemical reaction. These low values could simply be artifacts arising from the complexity of the system being modeled and the use of solubility-based criteria for assigning the various molecules to product fractions.

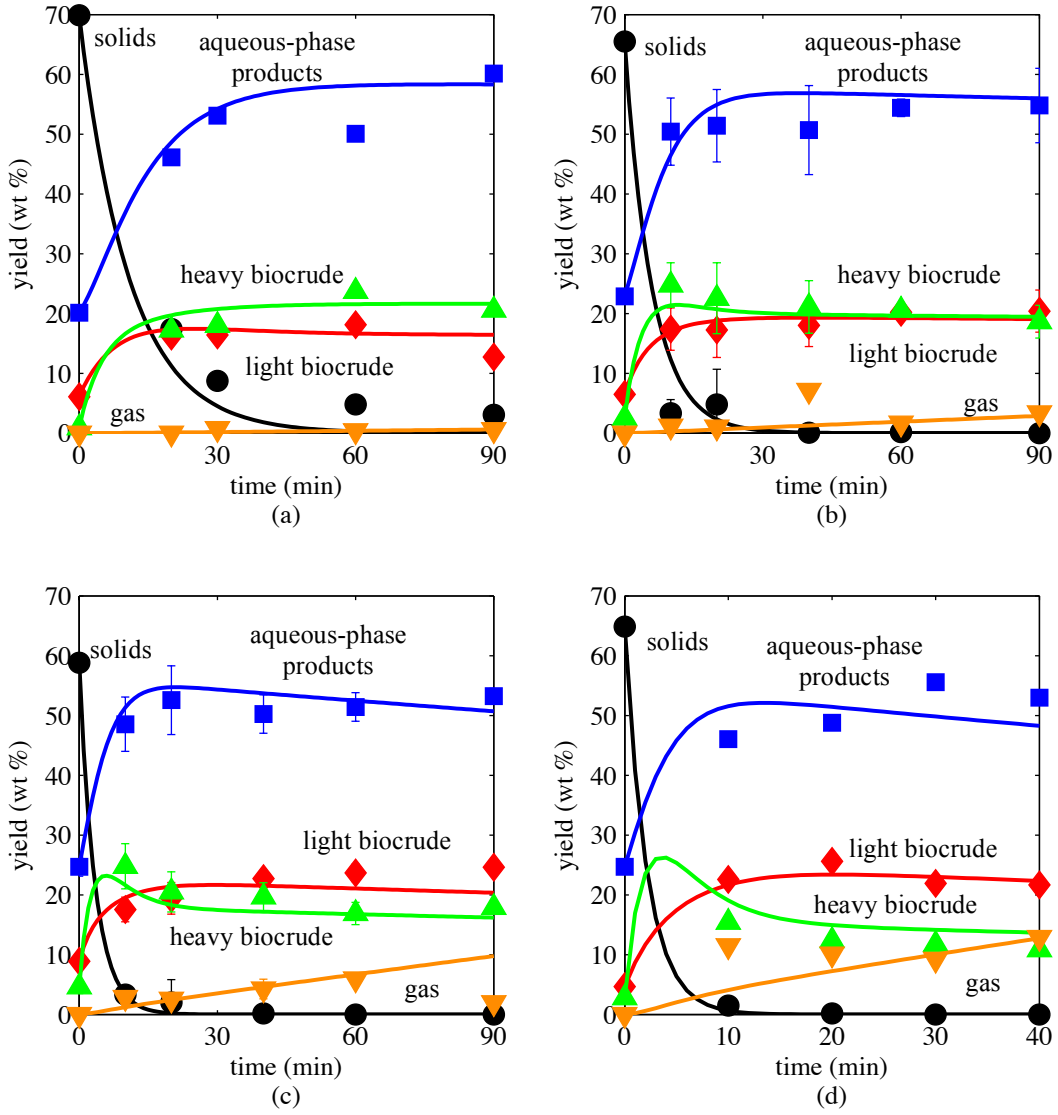

Figure 6.1. Yields of solids (●), aqueous-phase products (■), light biocrude (♦), heavy biocrude (▲), and gas (▼), and corresponding correlation with the model from the reaction at a) 250 °C, b) 300 °C, c) 350 °C , and d) 400 °C

Figure 6.1 shows the ability of the model, which is based on the 11-pathway network from Figure 5.16, to describe the data collected previously [2] and in this chapter for algae liquefaction. Agreement is very good at all four temperatures investigated as the experimental and model values are within a 5% absolute tolerance for all but six data points. This is the first quantitative kinetic model that has been developed for hydrothermal liquefaction of microalgae. The values of the rate constants at each of the temperatures presented here are in the Appendix (Table A.4).

6.2. Model Predictions

This section evaluates the predictive capability of the kinetic model. We compared the results of the model to the results from additional experiments and experiments from other researchers.

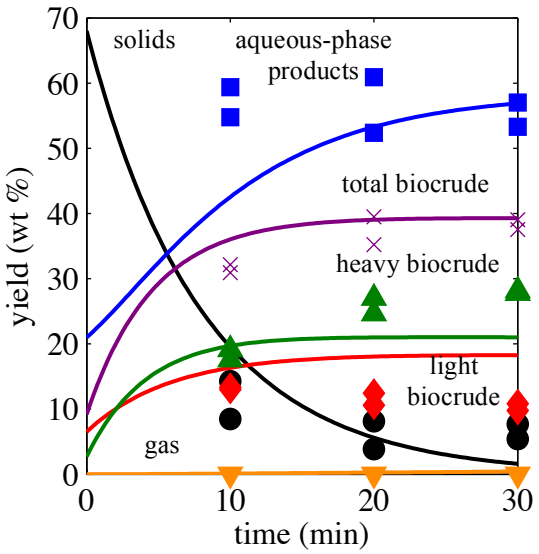

Figure 6.2. Yields of solids (●), aqueous-phase products (■), light biocrude (♦), heavy biocrude (▲),gas (▼), and (×) total biocrude and corresponding prediction from the model for the reaction at 275 °C

Having demonstrated that the model is consistent with the hydrothermal liquefaction data used to determine its parameter values, we next test its predictive capability. Figure 6.2 shows additional experimental results from the liquefaction of *Nannochloropsis* sp. at 275 °C and the ability of the model to predict the temporal variations of each of the product yields. None of these data were used to determine the model parameters. The model can reasonably capture the trends for all of the product fractions, and it accurately predicts the total biocrude yield.

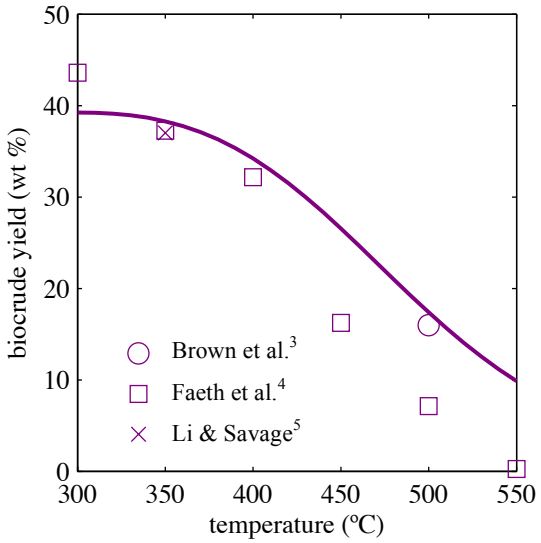

Figure 6.3. Prediction of biocrude yields from the liquefaction of *Nannochloropsis* sp. at 60 min and various temperatures [3-5]

Figure 6.3 shows, as discrete points, the yields (dry but not ash-free basis) of total biocrude from liquefaction of *Nannochloropsis* sp. for 60 min at different reaction temperatures, but the same biomass loading (15 wt %) used in the present experiments [3-5]. The solid curve is the yield predicted by the model at each temperature. The model does a very good job of predicting the published biocrude yields, even from reactors one or two orders of magnitude larger than the 4.1 ml reactors used here. Brown et al. used a 31 mL reactor [3] and Li and Savage used a 250 mL stirred reactor vessel [5]. The model is less successful at predicting the yields from Faeth et al. at supercritical temperatures (450 °C and above in Figure 6.3), but even here the model

accurately captures the trend in the data. The yields from Faeth et al. may be more difficult to predict because the water density in those experiments ranged from 0.13 - 0.24 g/mL for reactions at 450 - 550 °C. Those values all fall below the supercritical water density examined (0.5 g/mL) when determining the model parameters [2]. Additional work is needed to determine the influence of these lower water densities on biocrude yield from microalgae liquefaction at supercritical conditions.

A second reason for the difference between model prediction and experimental biocrude yield, especially at 550 °C, is the formation of char. The literature indicates that char formation is the norm under these high-temperature gasification conditions [1], but the hydrothermal liquefaction model includes no such pathway because it is unimportant under the liquefaction conditions investigated.

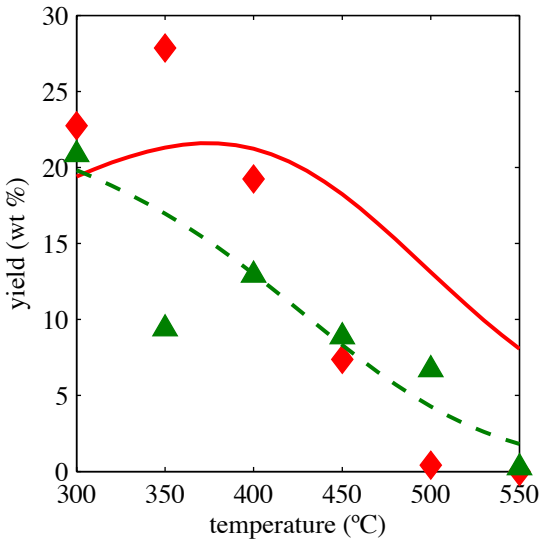

Figure 6.4. Predicted and experimental yields [4] of light biocrude (♦) and heavy biocrude yields (▲) from the liquefaction of *Nannochloropsis* sp. at 60 min

Figure 6.4 shows the yields of light and heavy biocrudes reported by Faeth et al. for the HTL of *Nannochloropsis* sp. for 60 min at 300 - 550 °C [4]. The model is able to capture the trends for how both light and heavy biocrude yields change with respect to temperature. Quantitative

agreement is poorer at the higher temperatures, where char formation and water density effects might be playing a role.

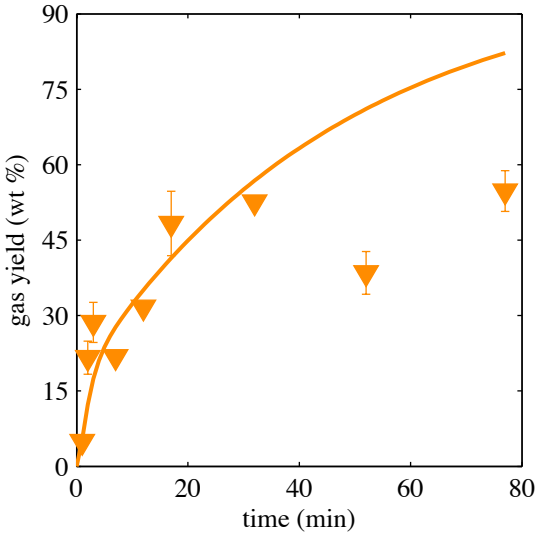

Figure 6.5. Prediction of gas yield from the gasification of *Nannochloropsis* sp. at 550 °C [1]

Figure 6.5 shows that the model is able to predict gas yields from the supercritical water gasification of *Nannochloropsis* sp. at 550 °C for reaction times up to 32 min. At longer reaction times, the experimental gas yields level off and other products are driven towards char formation. The absence of a char (solids) formation pathway in the reaction network (Figure 5.16) is the reason that the predicted yield for gas continues to increase.

Having demonstrated that the model is consistent with the experimental results used to determine its parameters and is able to predict literature results, we now use the model to explore the parameter space of HTL more completely. Figure 6.6 shows the yields calculated for each product fraction as a function of time (0 - 90 min) and temperature (200 - 400 °C).

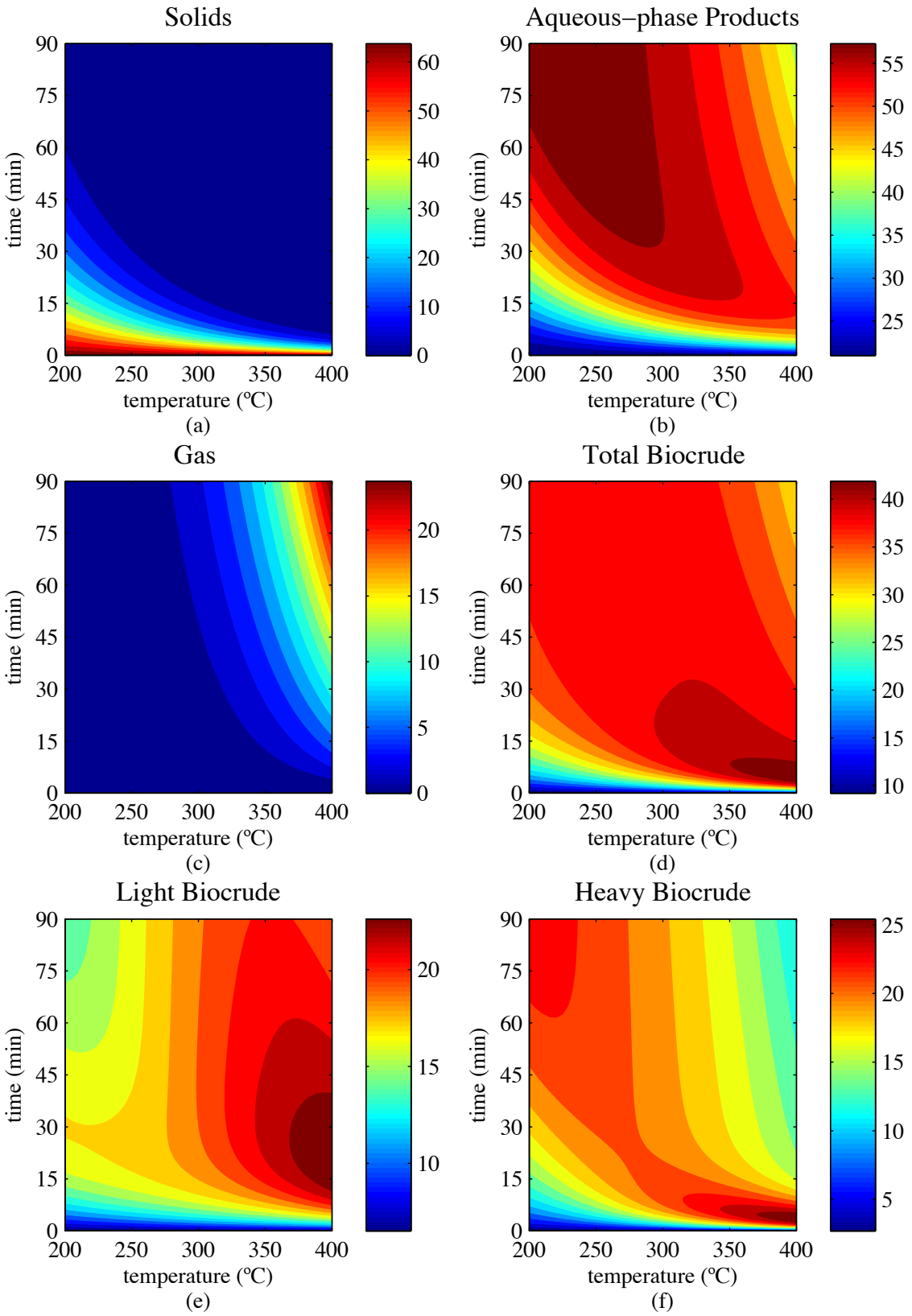

Figure 6.6. Prediction of yields of a) solids, b) aqueous-phase products, c) gas, d) total biocrude, e) light biocrude, and f) heavy biocrude from the HTL of *Nannochloropsis* sp.

The yield of solids (algal biomass), shown in Figure 6.6a, drops off very quickly and the solids are almost entirely consumed within 45 min, even at the lowest temperature (200 °C). Figure 6.6b shows that the yield of the aqueous-phase products settles around 60 wt % after 40 min of reaction. Figure 6.6c shows that the model predicts increased gas yields as the reaction time and temperature increase. Figure 6.6d demonstrates that the yield of total biocrude is maximized at 400 °C and 5 min. After 30 min of reaction at temperatures < 350 °C, biocrude yield reaches a nearly constant value. Longer reactions times do little to significantly increase the yield of biocrude. Figure 6.6e shows that the yield of light biocrude is highest at temperatures around 350 - 400 °C and at reaction times of 15-30 min. The maximum yield is 24 wt %. More light biocrude is produced at shorter times (< 20 min), and at higher temperatures (> 300 °C), suggesting that the time scale for liquefaction could be reduced to the order of minutes instead of tens of minutes [4]. Figure 6.6f shows that the yield of heavy biocrude is highest at temperatures above 300 °C, and reaches a maximum of 27 wt % within 4 minutes of reaction time. Longer reaction times at temperatures below 300 °C can also increase the yield of heavy biocrude.

6.3. Sensitivity Analysis

We analyzed the parameter sensitivity of the reaction network to determine how subtle changes in the rate constants could affect the results of the model. We calculated the normalized sensitivity coefficient $S_{ij}(t)$ by perturbing each of the rate constants individually (Δk_j) by 10% and recording the response in the yield of each product fraction ($\Delta x_i(t)$).

$$S_{ij}(t) = (\Delta x_i(t)/x_{i,m}(t))/(\Delta k_j/k_j) \quad (6.7)$$

A near-zero value for the sensitivity coefficient S_{ij} demonstrates that the value of the rate constant for path j does not strongly affect the yield of product fraction i. A value of $S_{ij} \geq 1$ signifies that the yield of the product fraction has a response equal to or greater than the relative perturbation of the rate constant. As a representative case, we present Figure 6.7, showing the results of the sensitivity analysis at 350 °C for the light and heavy biocrudes for the rate constants that most significantly affect their yields. At the other liquefaction temperatures the sensitivity coefficients show similar trends. Similar figures showing the sensitivity analyses at 250, 300, and 400 °C are in the Appendix (Figures A.1, A.2, A.3).

Figure 6.7a shows that the rate constant k_2 initially has the greatest influence on the yield of light biocrude. After 30 min, however, the yield of light biocrude is affected only by the rate constants for the reaction between the aqueous-phase products and the light biocrude (k_4, k_7).

Figure 6.7b shows that the yield of the heavy biocrude is initially most sensitive to the rate constant that is related to the formation of the heavy biocrude from the solids (k_3). At longer times, the most important rate constants (k_5, k_9) are for the pathway between heavy biocrude and the aqueous-phase products.

Figure 6.7c shows that the yield of the aqueous-phase products is less sensitive, more than half as much, to changes in the rate constants than are the yields of the light and heavy biocrudes. The rate constant k_1 only influences the yield of aqueous-phase products at reaction times shorter than 30 min, after which time all of the solids are consumed. At time longer than 30 min, k_4, k_5, and k_9 have a stronger influence on the yield, as was the case for the light and heavy biocrudes. The yield of the aqueous-phase products is insensitive to changes in the rate constant k_6, which consumes the aqueous-phase to produce gas. This rate constant had the smallest value of all the rate constants in the network.

Figure 6.7d shows that the gas yield is most sensitive to changes in k_{11}, which controls the rate of formation of gas from the heavy biocrude. The rate constants k_3, k_5, and k_9 are also influential.

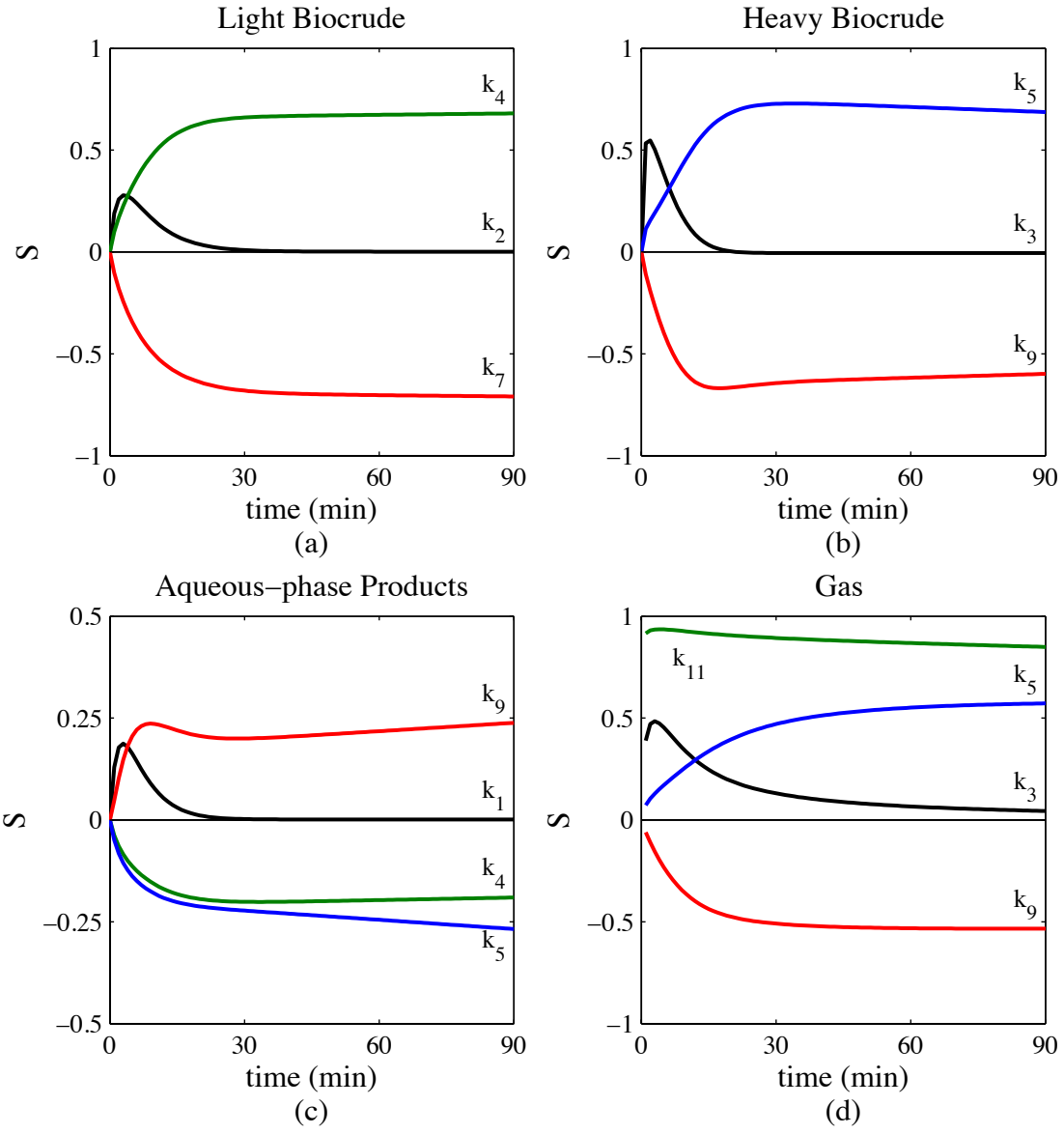

Figure 6.7. Sensitivity coefficients (S_{ij}) at 350 °C for a) light biocrude, b) heavy biocrude, c) aqueous-phase products, and d) gas

Sensitivity analysis showed that initially, at shorter reaction times (< 20 min), the rate constants controlling algae decomposition (k_1, k_2, k_3) are most influential to the biocrude yields. After the initial reaction period, the rate constants for the interconversion of aqueous-phase products and the light (k_4, k_7) and heavy biocrudes (k_5, k_9) are the most influential in controlling the yields of the light and heavy biocrudes.

6.4. Rate Analysis

We used net-rate analysis to complement the sensitivity analysis by determining the relative rates of each path in the network and the net direction of each two-way path. Rate analysis provides additional information about which pathways are fastest or slowest at a given time, providing a means to determine quantitatively the more important or dominant pathways during a reaction.

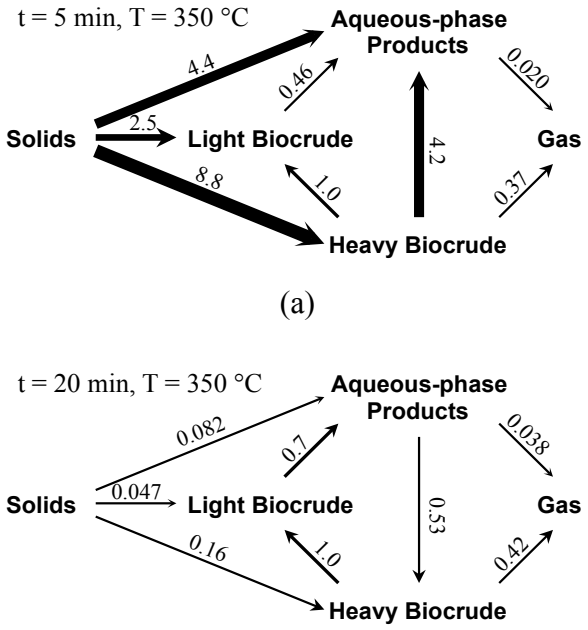

Figure 6.8. Net relative rates of each reaction at 350 °C, thickness of arrows represent magnitude of rate at a) 5 min and b) 20 min

We calculated the net rates for each of the pathways in Figure 5.16 at 350 °C and included their values in the Appendix (Table A.4). We normalized each net rate relative to that of the reaction between the light and heavy biocrudes. Figure 6.8 shows the net rates at 350 °C for all of the pathways in the reaction network at 5 and at 20 min. Figure 6.8a shows that the decomposition of solids and the formation of aqueous-phase products from the heavy biocrude are the fastest pathways at 5 min. After 20 min, when most of the biomass solids are consumed, however, Figure 6.8b shows that the fastest reactions are the three pathways exchanging products between the aqueous-phase products, the light biocrude, and the heavy biocrude. That is, interconversion of the different product fractions dominates, rather than the production of the fractions from the algal biomass.

Figure 6.8 also shows that although the paths between heavy and light biocrude and between aqueous-phase products and light biocrude exchange products in both directions, the net direction at both times examined is the same. In contrast there is a reversal in the net direction for the path connecting the aqueous-phase products and the heavy biocrude. At reaction times shorter than 18 min, aqueous-phase products are formed from the heavy biocrude. After 18 min the direction reverses and heavy biocrude is produced from the aqueous-phase products. The time of this shift in reaction direction varies with temperature, occurring at shorter times as the temperature increases. The result in Figure 6.8b complements the results from the sensitivity analysis that after 20 min of reaction, the more important rate constants are the ones that control the interconversion of products between the aqueous-phase products and light and heavy biocrudes.

6.5. Conclusions

A quantitative kinetic model based on the reaction network presented in Figure 5.16 dependably correlated the experimental results for algae liquefaction. It also accurately predicted published biocrude and gas yields from the hydrothermal treatment of this same alga, and the qualitative influence of temperature and time on these yields.

Analysis of the model results revealed that primary formation of the aqueous-phase products and biocrude from algal biomass are the dominant reaction paths only during the first few minutes of HTL. At longer times, interconversion of the product fractions dominates. The model predicts that the highest biocrude yield would be obtained at 400 °C for 5 min. These results suggest that reaction time on the order of a few minutes could be sufficient for liquefaction, as has been verified through related research from our lab [4].

The reaction network developed here strictly applies only to the alga used in the experiments. Additional work with other species is needed to determine whether the network can be generalized to other microalgae. Moreover, the kinetic parameters reported apply only to liquefaction with a 15 wt % biomass loading and temperatures, times, and water densities within the parameter space explained. Additional work is needed to determine the influence of biomass loading and water density at supercritical conditions on theses parameters. Finally, incorporating a char formation path in the network might enable development of a model that unifies hydrothermal liquefaction and hydrothermal gasification of algal biomass.

References

[1] Q Guan, PE Savage, C Wei, *Gasification of alga Nannochloropsis sp. in supercritical water*, J Supercrit Fluids 61 (2012) 139-145.

[2] PJ Valdez, MC Nelson, HY Wang, X Lin, PE Savage, *Hydrothermal Liquefaction of Nannochloropsis sp.: Systematic study of process variables and the analysis of product fractions*, Biomass Bioenergy 46 (2012) 317-331.

[3] TM Brown, P Duan, PE Savage, *Hydrothermal Liquefaction and Gasification of Nannochloropsis sp*, Energy Fuels 24 (2010) 3639-3646.

[4] JL Faeth, PJ Valdez, PE Savage, *Fast Hydrothermal Liquefaction of Nannochloropsis sp. To Produce Biocrude*, Energy Fuels 27 (2013) 1391-1398.

[5] Z Li, PE Savage, *Feedstocks for fuels and chemicals from algae: Treatment of crude bio-oil over HZSM-5*, Algal Research 2 (2013) 154-163.

Chapter 7

Effect of Biochemical Content

We modified the reaction network and kinetic model for hydrothermal liquefaction (HTL) described in chapter 6 to incorporate the biochemical content of the microalgae. Doing so permits the correlation of the model to other microalgae, regardless of species, depending on the initial concentrations of proteins, lipids, carbohydrates, and ash in the alga. Biller and Ross presented a formula for estimating biocrude yield, produced at 350 °C for 60 min, based on the protein, lipid, and carbohydrate concentrations in an algal feedstock [1]. Although their model was accurate for predicting the biocrude yield for some of microalgae, it was not consistent for cyanobacteria. The formula did not account for reaction temperature or holding time either, and was strictly limited to predicting the yield of biocrude only. In this chapter we present a modification of the model from chapter 6 that incorporates biochemical content in addition to time and temperature.

Before incorporating biochemical content, we simplified the model by combining the light and heavy biocrude fractions, reducing the number of pathways in the network and the number of parameters needed for the model. To generate data for parameter estimation for the generalized model for the HTL of microalgae, we hydrothermally treated 15 wt % slurries of *Chlorella protothecoides* and *Scenedesmus* sp. at 250, 300, 350, and 400 °C for 10 - 90 min and measured the yields of solids, gases, aqueous-phase products, and total biocrude. We used the

yields of the product fractions from all three microalgae to determine the rate constants and Arrhenius parameters of the modified kinetic model.

The first section of this chapter summarizes the results from the HTL of *C. prototheco*ides and *Scenedesmus* sp. The second section explains the modification of the reaction model and the network. The final section describes correlations of model results to data from the two microalgae.

7.1. Hydrothermal Liquefaction of *Chlorella prototheco*ides and *Scenedesmus* sp.

We hydrothermally treated 15 wt % slurries of *C. prototheco*ides and *Scenedesmus* sp. at 250, 300, 350, and 400 °C for 10 - 90 min in 4.1 mL reactors with gas sampling valves using the methods described in section 3.3. We recovered and measured the yield of each product fraction using the methodologies described in section 3.4. We compared the results to the HTL products from the *Nannochloropsis* sp. discussed previously in chapters 4 and 5.

7.2.1. Biochemical Content of the Feedstock

We used the procedures outlined in section 3.1 to determine the concentrations of proteins, carbohydrates, and lipids in each of the three microalgae we studied, which are reported in Table 7.1. Direct measurement of the lipids, proteins, and ash of *Nannochloropsis* sp. were within 5 wt % of the values reported by the manufacturer. The indirect calculation of carbohydrate concentration is 50% higher than that reported by the supplier. The protein and lipid content of *C. prototheco*ides is dramatically different when compared to *Nannochloropsis* sp., providing a comparison to understanding the effect of biochemical content on the HTL product fractions.

The *Scenedesmus* sp. is similar in composition to the *Nannochloropsis* sp. and provides a way to test the validity of the model using another microalga, but with a similar composition.

Table 7.1. Biochemical content (wt %, dry-basis) of *Nannochloropsis* sp., *Chlorella protothecoides*, and *Scenedesmus* sp.

	Protein	Carbohydrate	Lipid	Ash
Nannochloropsis sp.	56	32	9	3
Chlorella protothecoides	11	29	53	7
Scenedesmus sp.	50	31	8	11

7.2.2. Distribution of the Product Fractions

Figures 7.1 - 7.3 show the product fractions from *C. protothecoides* and *Scenedesmus* sp. Experiments at 350 °C were replicated three times. Figure 7.1 shows the yield of solids behaves similar to that of *Nannochloropsis* sp., the higher the temperature the faster the rate of decomposition. Figure 7.1a shows that at 250 °C the yield of solids increases at longer reaction times (> 20 min). At higher temperatures the solids usually appear as gray powders, but these solids were black and tar-like. It is possible that at these temperatures the biomass was carbonized [2] or more organic-solvent insoluble products were formed, resulting in a higher solid yield than shown previously for *Nannochloropsis* sp.

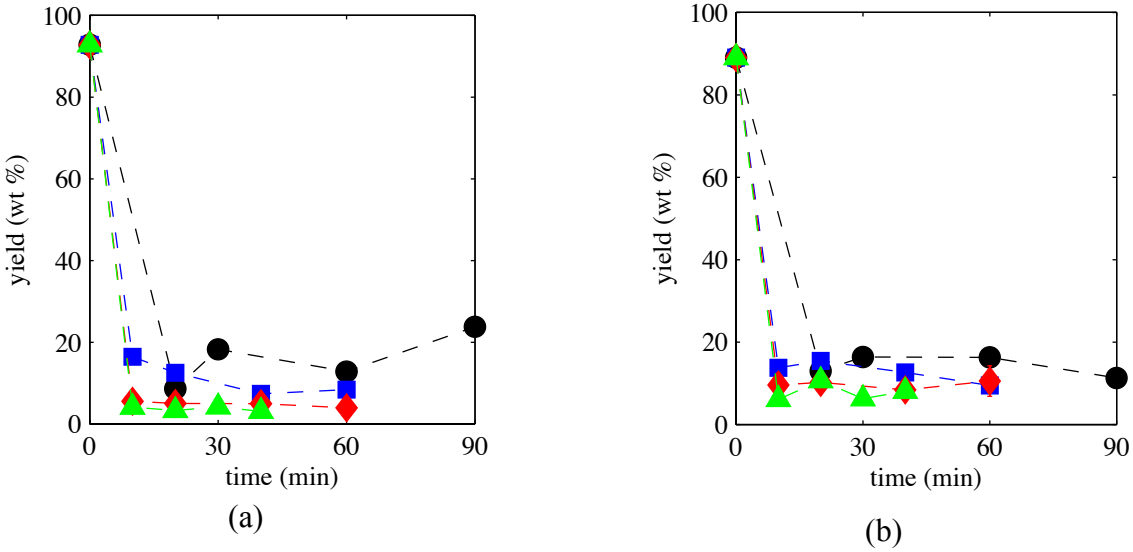

Figure 7.1. Yield of solids (wt %, dry-basis) at 250 °C (●), 300 °C (■), 350 °C (◆), and 400 °C (▲) from a) *C. prototheco*ides and b) *Scenedesmus* sp.

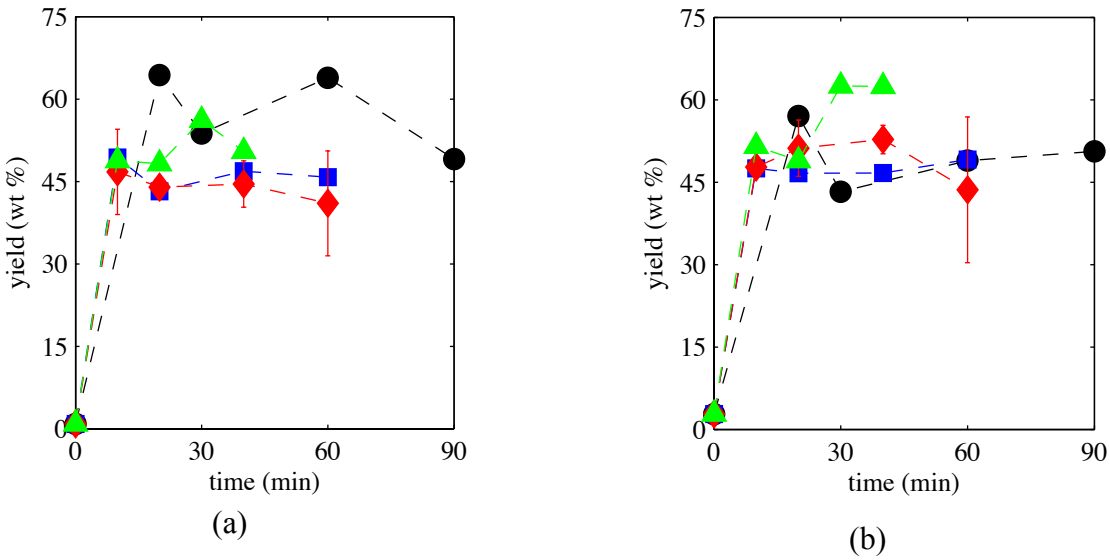

Figure 7.2. Yield of aqueous-phase products (wt %, dry-basis) at 250 °C (●), 300 °C (■), 350 °C (◆), and 400 °C (▲) from a) *C. prototheco*ides and b) *Scenedesmus* sp.

Figure 7.2 shows that the yield of aqueous-phase products is usually between 45 - 55 wt %, similar to the results from *Nannochloropsis* sp. At 250 °C, the average yield of the aqueous-phase products from *C. prototheco*ides is 58 ± 8 wt %. The increased yield in aqueous-phase products at 250 °C is likely due to the reduced yield of biocrude produced at that condition

(Figure 7.1). The aqueous phase from both algae was similar in appearance to the aqueous phase from *Nannochloropsis* sp. described in section 5.1, being amber in color and having a strong ammonia smell.

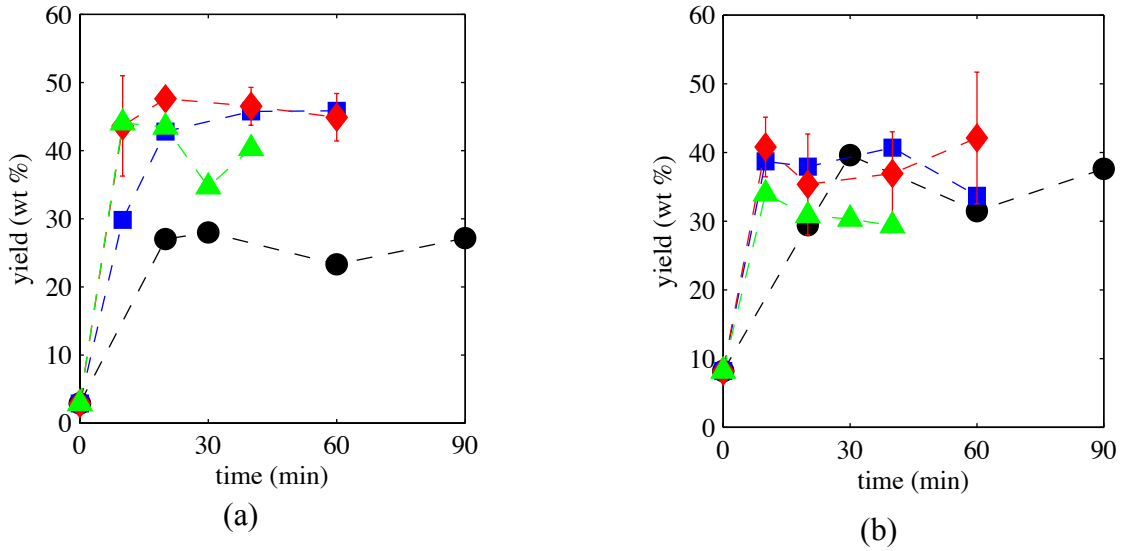

Figure 7.3. Yield of biocrude (wt %, dry-basis) at 250 °C (●), 300 °C (■), 350 °C (◆), and 400 °C (▲) from a) *C. protothecoides* and b) *Scenedesmus* sp.

Both biocrude products from *C. protothecoides* and *Scenedesmus* sp. were similar in appearance to one another and to the biocrude produced from *Nannochloropsis* sp. Both were very viscous and dark brown in color. Figure 7.3a shows the time and temperature dependence of the biocrude yield. With increasing reaction severity up to 350 °C the yield increases. At temperatures > 250 °C and as time increase, the yield of biocrude from *C. protothecoides* approaches 50 wt %, which is very close to the measured value of lipids in that alga. At the 250 °C reaction temperature, there is an increased solid yield, possibly retaining the lipids in that product fraction [3]. Although the C. protothecoides was richer in lipids compared to Nannochloropsis sp. and Scenedesmus sp., the yield of biocrude never exceeded 50 wt %.

Figure 7.3b shows that the yield of biocrude from *Scenedesmus* sp. at 250, 300 and 350 °C does not vary much with batch holding time. At 400 °C, the yield of biocrude decreases from 35 to 30 wt % with increasing time. It is possible that the more significant changes in biocrude yield occur at shorter time scales. The yield is nearly 4 times the initial mass of the lipid fraction in the biomass. The yields of gas products from both algae were scattered, showing no specific trends, but were always < 10 wt %, similar to the results from *Nannochloropsis* sp. Gas yields are presented in the Appendix (Figure A.4).

7.2. Incorporating Biochemical Content into the Reaction Network and Model

This section summarizes the changes we made to the reaction network and kinetic model to reduce the number of parameters, and extend applicability of the model to other alga by incorporating biochemical content. After examination of the results from the model described in chapter 6, we simplified the network to the new network shown in Figure 7.4.

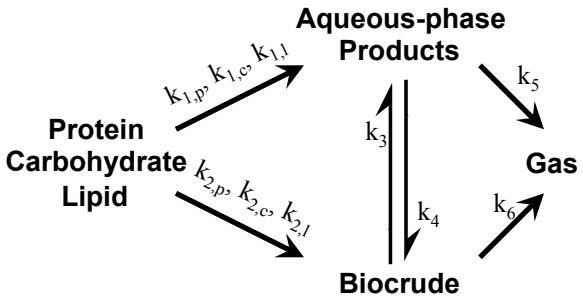

Figure 7.4. Reaction network incorporating biochemical content

Figure 7.4 shows the reduced reaction network with a combined product fraction for biocrude instead of separate product fractions for light and heavy biocrudes. Although there is some

exchange of material between the biocrude fractions, the more important metric is total yield of biocrude. From the rate and sensitivity analyses presented in chapter 6, the more important pathway to consider is the exchange of products between the biocrude fraction and the aqueous-phase products, not between biocrude fractions, hence, we can eliminate the pathways. Based on the reaction pathways in Figure 7.4, we present the balances in equations 7.1 - 7.6 as the basis for the modified reaction model.

$$\text{Proteins:} \quad \frac{dx_{1,\mathrm{p}}}{dt} = -\left(k_{1,\mathrm{p}} + k_{2,\mathrm{p}}\right)x_{1,\mathrm{p}} \tag{7.1}$$

$$\text{Lipids:} \quad \frac{dx_{1,\mathrm{l}}}{dt} = -\left(k_{1,\mathrm{l}} + k_{2,\mathrm{l}}\right)x_{1,\mathrm{l}} \tag{7.2}$$

$$\text{Carbohydrates:} \quad \frac{dx_{1,\mathrm{c}}}{dt} = -\left(k_{1,\mathrm{c}} + k_{2,\mathrm{c}}\right)x_{1,\mathrm{c}} \tag{7.3}$$

$$\text{Aqueous-phase Products:} \quad \frac{dx_2}{dt} = -(k_4 + k_5)x_2 + k_{1,\mathrm{p}}x_{1,\mathrm{p}} + k_{1,\mathrm{l}}x_{1,\mathrm{l}} + k_{1,\mathrm{c}}x_{1,\mathrm{c}} + k_3x_3 \tag{7.4}$$

$$\text{Biocrude:} \quad \frac{dx_3}{dt} = -(k_3 + k_6)x_3 + k_{2,\mathrm{p}}x_{1,\mathrm{p}} + k_{2,\mathrm{l}}x_{1,\mathrm{l}} + k_{2,\mathrm{c}}x_{1,\mathrm{c}} + k_4x_2 \tag{7.5}$$

$$\text{Gas:} \quad \frac{dx_4}{dt} = k_5x_2 + k_6x_3 \tag{7.6}$$

Equations 7.1 - 7.3 introduce new variables for the wt % of proteins ($x_{1,\mathrm{p}}$), carbohydrates ($x_{1,\mathrm{c}}$), and lipids ($x_{1,\mathrm{l}}$) of the solids, respectively. That is, the weight fraction of protein in the starting material ($x_{1,\mathrm{p}}$) is the product of the total solids fraction (x_1) and the dry ash-free fraction of protein in the microalgae (x_{p}). As we only measured the total solids (x_1) of the HTL products,

we used the relation shown in Equation 7.7 to relate each product fraction of proteins, carbohydrates, and lipids to the total solids. The amount of ash in the algae was subtracted from the solids (x_1) since most of the ash resides in the solids phase.

$$x_1 = x_{1,p} + x_{1,c} + x_{1,l} \tag{7.7}$$

For the decomposition of the proteins, carbohydrates, and lipids to produce aqueous-phase products or biocrude there are 6 total rate constants ($k_{1,p}$, $k_{1,c}$, $k_{1,l}$, $k_{2,p}$, $k_{2,c}$, $k_{2,l}$), assuming that each biomacromolecule decomposes at a different rate into different product fractions. Similar to the procedure described in section 6.1 we solved the set of differential equations while simultaneously estimating the values of the rate constants (k_j) by minimizing the least square objective function listed in Equation 6.6 for estimating the residual. We constrained the values of the rate constants from 0 - 0.35 min^{-1} to accommodate the fastest paths observed experimentally and to avoid excessive computational time.

7.3. Model Correlation

Figures 7.5 - 7.7 show the correlation of the model to the experimental data from the HTL of each alga at 300 °C. Figures 7.5 and 7.7 show the closest correlation between the model and the experimental values. Although two different cultures of algae were used, *Nannochloropsis* sp. and *Scenedesmus* sp., respectively, they were similar in biochemical composition. The model does not fit the data from *C. protothecoides* as closely, probably owing to the richer lipid content and protein deficiency relative to the other two algae.

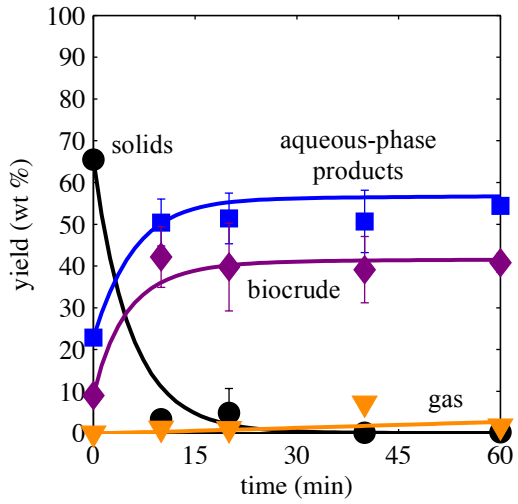

Figure 7.5. Correlation of model data with experimental yields from HTL of *Nannochloropsis* sp. at 300 °C

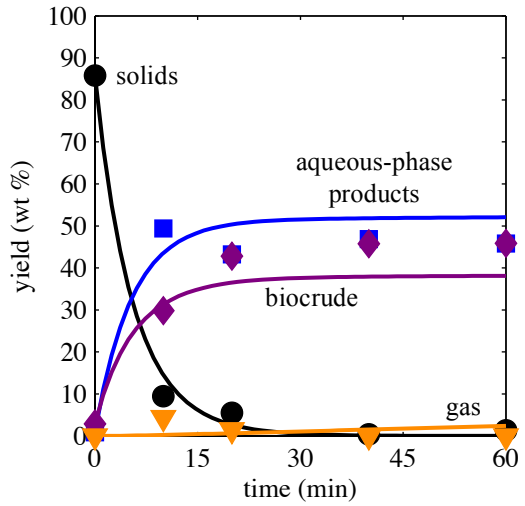

Figure 7.6. Correlation of model data with experimental yields from HTL of *C. protothecoides* at 300 °C

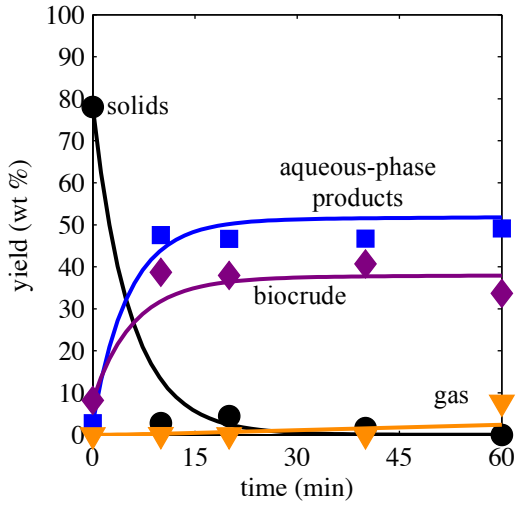

Figure 7.7. Correlation of model data with experimental yields from HTL of *Scenedesmus* sp. at 300 °C

Table 7.2 shows the values of the Arrhenius parameters and rate constants at 350 °C calculated by fitting the experimental data. Table A.5 in the Appendix shows the rate constants at 250, 300, and 400 °C. The activation energies for the formation of gas from biocrude and aqueous-phase products are roughly less than half of those reported previously in Table 6.1 for the similar pathways. The rate constants for gas formation are one to two orders of magnitude smaller than the other rate constants. Table 7.2 shows that the activation energies for the decomposition of proteins, carbohydrates, and lipids range from 7 - 49 kJ/mol. The decomposition of carbohydrates to the aqueous phase had a higher activation energy when compared to the decomposition of proteins and lipids as they are likely more difficult to decompose into the product fractions, as hypothesized by Biller and Ross [1].

Table 7.2. Arrhenius parameters from modified reaction network

Path (Fig. 7.4)	Reaction	$E_{a,j}$ (kJ/mol)	A_j (min^{-1})	k(350 °C) (min^{-1})
1,p	Protein → Aqueous-phase Products	7 ± 32	$10^{-0.4 \pm 2.8}$	0.085
1,c	Carbohydrate → Aqueous-phase Products	49 ± 23	$10^{3.6 \pm 2.1}$	0.27
1,l	Lipid → Aqueous-phase Products	8 ± 16	$10^{-0.1 \pm 1.5}$	0.16
2,p	Protein → Biocrude	41 ± 18	$10^{2.9 \pm 1.6}$	0.27
2,c	Carbohydrate → Biocrude	35 ± 7	$10^{2.3 \pm 0.6}$	0.26
2,l	Lipid → Biocrude	25 ± 12	$10^{-0.6 \pm 1.1}$	0.0018
3	Biocrude → Aqueous-phase Products	16 ± 7	$10^{0.7 \pm 0.6}$	0.26
4	Aqueous-phase Products → Biocrude	20 ± 7	$10^{1 \pm 1}$	0.21
5	Aqueous-phase Products → Gas	36 ± 23	$10^{-0.2 \pm 2}$	0.00058
6	Biocrude → Gas	38 ± 23	$10^{0.3 \pm 2}$	0.0014

Figure 7.8 shows the correlation of the model to all of the experimental data, with a majority of the data clustered on or near the parity line. Generally, the model shows a reasonable correlation with the yields of the product fractions, although there is some loss of accuracy in exchange for fitting several different types of microalgae. Figure 7.8 shows that the model does not favor a correlation towards a single species of microalga, as the correlated values corresponding to each microalga appear randomly distributed.

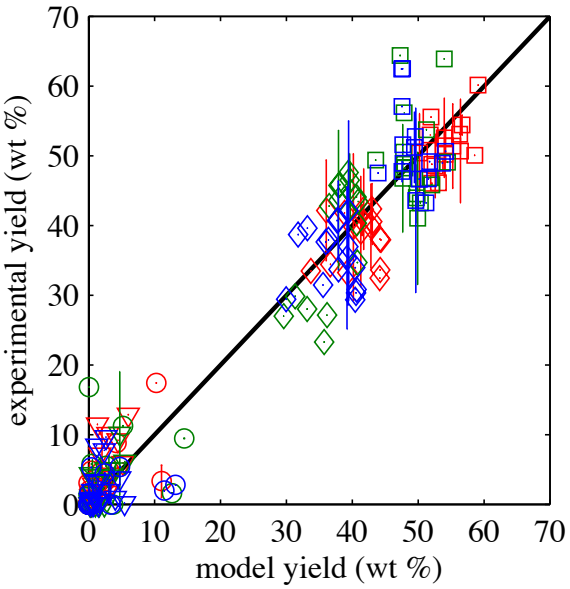

Figure 7.8. Parity plot of experimental and model values for yields of solids (●), aqueous-phase products (■), biocrude (◆), and gas (▼) for *Nannochloropsis* sp. (red), *C. protothecoides* (green), and *Scenedesmus* sp. (blue)

7.4. Conclusions

With the modified network presented in this chapter we are able to build upon the model presented in chapter 6. Figure 7.8 shows a reasonable correlation with the experimental data for the HTL of *Nannochloropsis* sp., *C. protothecoides*, and *Scenedesmus* sp. HTL of *Scenedesmus* sp. showed that the yield of biocrude was not dependent on reaction conditions after 10 min of hydrothermal treatment and shorter reaction times need to be investigated. Independent of reaction conditions or microalgal species, 40 - 50 wt % of the original biomass is converted to the aqueous-phase products. HTL at 250 °C of *C. protothecoides* yielded roughly half the amount of biocrude obtained at higher reaction temperatures.

Further investigation is needed to improve model accuracy. Additional data from the HTL of a different alga or one of the same alga presented here, but with a different biochemical content, could possibly improve the data fitting. We present a lumped model based on the solubility of

the products; another possible approach would be to measure the decomposition of lipids, proteins, and carbohydrates from the starting material and relate that to the rates of formation of the product fractions.

References

[1] P Biller, AB Ross, *Potential yields and properties of oil from the hydrothermal liquefaction of microalgae with different biochemical content*, Bioresour Technol 102 (2011) 215-225.

[2] RB Levine, AA Bollas, MD Durham, PE Savage, *Triflate-catalyzed (trans)esterification of lipids within carbonized algal biomass*, Bioresour Technol 111 (2012) 222-229.

[3] RB Levine, T Pinnarat, PE Savage, *Biodiesel Production from Wet Algal Biomass through in Situ Lipid Hydrolysis and Supercritical Transesterification*, Energy Fuels 24 (2010) 5235-5243.

Chapter 8

Hydrothermal Liquefaction of Bacteria and Yeast Monocultures

We cultivated *Escherichia coli*, *Pseudomonas putida*, *Bacillus subtilis*, and *Saccharomyces cerevisiae* and subjected the biomass to hydrothermal treatment at fast (rapid heating for 1 min) and isothermal (350 °C, 60 min) hydrothermal liquefaction (HTL) conditions. We studied the liquefaction of these microorganisms to determine the feasibility of hydrothermally treating bacteria and yeast to produce biocrude similar to the biocrude from microalgae. We examined how cellular structure and composition of the different organisms affected the product yield and characteristics after hydrothermal treatment.

E. coli and *S. cerevisiae* are bacterial and yeast species, respectively, that are frequently used in industrial bioprocesses. We selected *P. putida* because it is known to metabolize a diverse array of substrates, which makes it a good candidate for growth on complex waste streams [1]. *B. subtilis*, a widely studied Gram-positive bacterium [2], was included to investigate the impact of its differing cellular composition (particularly in the peptidoglycan-abundant cell wall) on liquefaction products when compared to the other two Gram-negative bacteria (*E. coli* and *P. putida*).

We report results showing how microorganism selection, growth media, cellular structure (Gram-positive vs. Gram-negative), and hydrothermal treatment conditions affect the yield and composition of the different product fractions. The first section lists the characteristics of the microorganisms we cultivated. The latter sections describe the results of the hydrothermal

treatment of the biomass, showing the yield, elemental composition, and selected molecular composition of the product fractions. We also report the heating value and energy recovery of the biocrudes and compare results among the various microorganisms. This research was in collaboration with Mike Nelson and Julia Faeth.

8.1. Feedstock Analysis

Table 8.1 shows the elemental and biochemical content of each biomass feedstock employed. There are but modest variations in the elemental composition of C, H, N, and S. The C and N wt % for *E. coli* are within 6 % relative difference of those reported previously [3,4]. Although the two *E. coli* cultures were cultivated using different growth media their C, H, N, and O contents were within 10 % of each other on a relative basis. The *E. coli* TB had a faster growth rate. *B. subtilis* and *P. putida* had the highest ash compositions of 13 and 11 wt %, respectively, whereas the other organisms had ash content below 7 wt %.

The *E. coli* grown with minimal media, *S. cerevisiae*, and *P. putida* had the highest lipid contents, but all were below 2.7 wt %. *E. coli* grown with TB and *B. subtilis* had lipid values below 0.6 wt %. The *E. coli* TB was grown in a nutrient-rich condition, so it is reasonable that the cells would accumulate less lipid content than the *E. coli* MM. Likewise, Gram-positive organisms such as *B. subtilis* have fewer lipids, possibly due to the lack of an outer membrane in the cell envelope compared to Gram-negative organisms. The carbohydrate content of each biomass sample varied between 4 and 17 wt %. All biomass samples were rich in protein (≥ 72 wt %). Compared to microalgae feedstocks typically subjected to HTL, the yeast and bacteria have a much lower lipid content and much higher protein and N content [5]. We calculated the

heating values of the biomass samples using the Boie formula. The heating values are very similar, ranging from 21 - 23 MJ/kg.

Table 8.1. Elemental (wt %), biochemical composition (wt %), and HHV (MJ/kg) of the biomass

	C	H	N	S	O	ash	lipid	protein	carbohydrate	HHV
E. coli TB	46.54	6.69	13.70	0.67	25.58	6.82 ± 0.02	0.57 ± 0.36	86	7	22
E. coli MM	47.32	6.88	13.17	0.58	27.15	4.9 ± 0.1	2.6 ± 0.1	82	10	23
P. putida	46.58	7.08	13.23	0.55	21.48	11	2.7 ± 0.7	83	4	23
B. subtilis	42.65	6.56	11.45	0.43	25.91	13.0 ± 0.4	0.55 ± 0.03	72	15	21
S. cerevisiae	46.47	7.31	12.04	0.47	29.03	4.68 ± 0.01	2.7 ± 0.6	75	17	22

8.2. Yields of Product Fractions

For conventional, isothermal HTL, we loaded 1.35 g of 12 wt % biomass slurry to each 1.7 mL Swagelok reactor. We sealed the reactors and placed them into a Techne Fluidized sand bath set at 350 °C. The reactors were submerged in the sand bath and agitated using a Burrell Wrist Action shaker for 60 min. For fast HTL reactions, done with rapid heating, we loaded the reactor with 0.30 g of 12 wt % biomass slurry. This water loading matched previous experiments in our laboratory [6]. After sealing the reactors, they were placed in a 600 °C sandbath for 1 min. As previously described by Faeth et al., we used dummy reactors fitted with a thermocouple to record temperature and calculate the heating rate [6]. In both cases, after the desired holding time had elapsed, we removed the reactors from the sandbath and quenched them in a room

temperature water bath. After the reactors cooled, we followed the recovery procedure described in section 3.4.

As a control experiment we exposed dried, unreacted biomass to fresh solvents at room temperature, following the procedure described in section 3.4.2. After exposure to dichloromethane and water, ≤ 4 wt % of the biomass partitioned to the organic phase as biocrude. The remaining biomass partitioned to the solid product fraction. Therefore, solvent extraction alone does not generate the biocrude in higher yields than are typical from hydrothermal treatment.

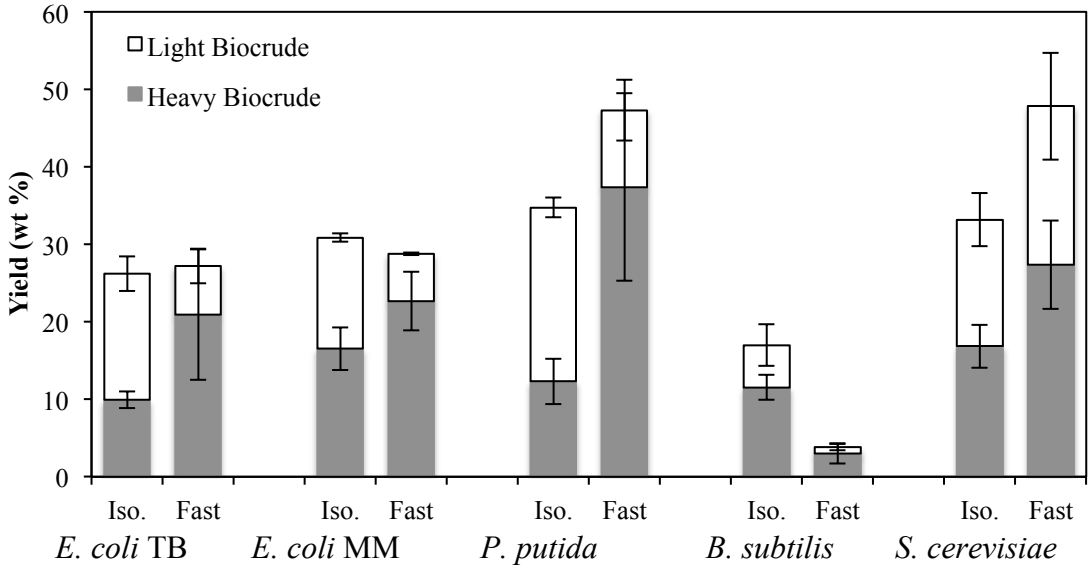

Figure 8.1. Yields of light and heavy biocrude (wt % daf) for each biomass and isothermal and fast HTL

Figure 8.1 shows the dry ash-free (daf) yields of light and heavy biocrudes for each organism at both hydrothermal treatment conditions. Yields of biocrudes are presented on a dry basis in the Appendix (Table A.6). The isothermal treatment at 350 °C for 60 min is common practice [7-11] so the present results from the yeast and bacterial biomass can be compared with those from

HTL of other feedstocks. We also used rapid heating or fast HTL by placing the reactor in a sand bath set to 600 °C for 1 min, which can increase the biocrude yield [6]. The average maximum temperature observed in the dummy reactor during fast HTL was 276 ± 41 °C, and the average heating rate of the reactors at fast liquefaction conditions was 216 ± 37 °C/min, with the uncertainty representing one standard deviation of the population.

B. subtilis showed the lowest total yield of biocrude for both conventional isothermal (17 ± 3 wt % daf) and fast (4 ± 1 wt % daf) liquefaction conditions; these low yields may be linked to its cellular structure. One contributing factor may be the different molecular composition of the cell envelope. Gram-positive bacteria, including *B. subtilis*, have a thick layer of peptidoglycans, which are polysaccharides cross-linked by polypeptides. These biomacromolecules likely hydrolyze to simple sugars and amino acids that would reside within the aqueous-phase product fraction. Past research has shown that continued hydrothermal processing of water-soluble amino acids and carbohydrates can form organic-solvent soluble products [12,13]. Such processes could account for the higher biocrude yield at isothermal HTL conditions observed in Figure 8.1 for *B. subtilis*.

Fast hydrothermal treatment of *P. putida* and *S. cerevisiae* produced the most biocrude, with yields of 47 ± 13 wt % and 48 ± 9 wt %, respectively. The higher yield of biocrude from *S. cerevisiae* may also be linked to the cell structure of the yeast, in this case improving the yield, unlike the result from *B. subtilis*.

The larger standard deviation in the yields from fast HTL probably arises from the lower biomass loadings. There is less material to recover in these experiments and transfer losses become more significant, on a relative basis, compared to conventional liquefaction [6]. The reaction conditions did not affect the total yield of biocrude for both types of *E. coli*. Figure 8.1

shows that fast liquefaction always produced a higher fraction of heavy biocrude than light biocrude, regardless of organism. This trend is also true for the fast liquefaction of the microalga *Nannochloropsis* sp. [6]. Figure 8.1 shows that, with the exception of *B. subtilis*, the yield of total biocrude produced at conventional HTL conditions did not vary much, ranging between 26 - 35 wt % daf for the different microorganisms.

Table 8.2. Yields of solid, aqueous-phase, and gas product fractions (wt % dry basis)

	Solids		Aqueous-phase Products		Gas	
	Iso.	Fast	Iso.	Fast	Iso.	Fast
E. coli TB	2.1 ± 0.5	8.5 ± 4.3	72 ± 2	66 ± 9	1 ± 0.1	-[1]
E. coli MM	5.0 ± 0.6	26 ± 3	64 ± 3	46 ± 5	1.2 ± 0.7	0.30
P. putida	1.8 ± 0.6	4.4 ± 2.0	64 ± 3	52 ± 11	3.8 ± 1.7	1.7
B. subtilis	3.6 ± 0.6	3.4 ± 1	81 ± 3	92 ± 2	1 ± 0.4	1.8
S. cerevisiae	4.6 ± 1.1	5.6 ± 0.3	62 ± 4	43 ± 9	1.9 ± 0.5	6.9

[1]under detection limit

Table 8.2 shows the yield of solids (water- and dichloromethane-insoluble), aqueous-phase-products, and gas for both isothermal and fast HTL of each organism. The aqueous phase was translucent amber in color for all of the different microorganisms. More than 42 wt % of the biomass is converted to aqueous-phase products. The solids were gray powders that settled at the bottom of the test tube. Solid yields were always below 9 wt %, with the exception of *E. coli* MM treated with fast HTL. *E. coli* differentially expresses genes that affect cell structure when grown in minimal versus rich medium [14]. The milder reaction conditions in fast HTL may not have been sufficient to break down certain components in the *E. coli* cell, especially when grown

in minimal media. The data in Table 8.2 suggest that the residual solids remaining after fast liquefaction likely form mostly aqueous-phase products when reacted under the harsher isothermal HTL conditions.

Table 8.2 shows that < 7 wt % of the biomass is converted to gas. The differences in the compositions of the gas products from HTL across the sources of biomass were not statistically significant. Therefore, Figure 8.2 shows the average composition of the gas phase from isothermal and fast HTL. The gas phase from isothermal HTL was on average 93 ± 6 mol % CO_2 with the balance being H_2, CO, CH_4, C_2H_4, and C_2H_6. The gas from fast HTL had significantly less CO_2, 64 ± 15 mol %, and significantly more CO, CH_4, C_2H_4, and C_2H_6. At harsher reaction conditions, CO_2 is a common product from the hydrothermal decomposition of amino acids [15].

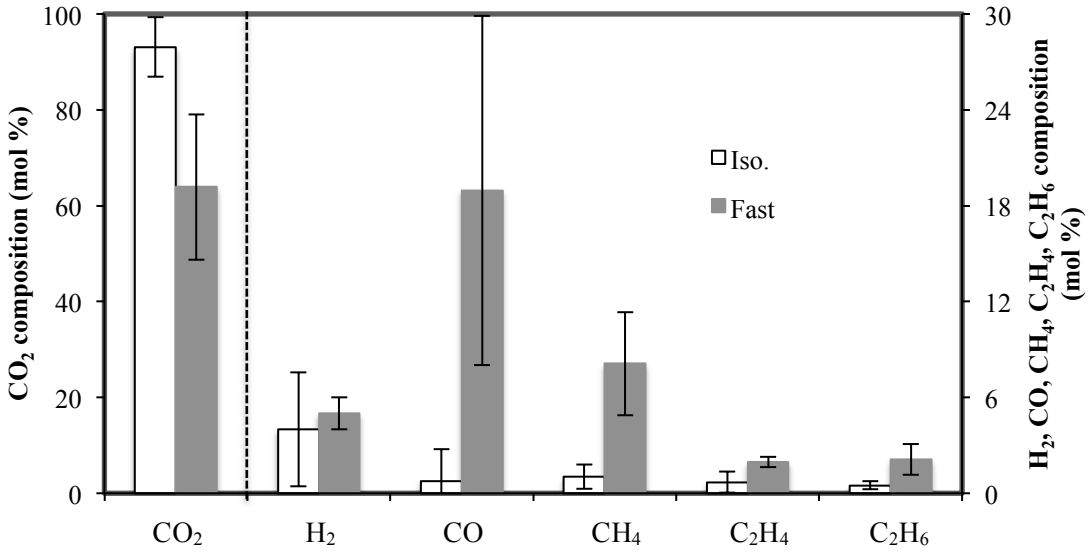

Figure 8.2. Average composition of the gas phase from isothermal and fast HTL

8.3. Elemental Composition of the Light and Heavy Biocrudes

Figure 8.3 shows the C, N, O, and S content (wt %) of the light and heavy biocrudes for each organism. Elemental ratios of H:C, N:C, O:C, and S:C in the light and heavy biocrudes are presented in the Appendix (Figure A.5). Figure 8.3a shows that regardless of the conditions of the hydrothermal treatment, the light biocrude always had a higher wt % C than the heavy biocrude, similar to the results obtained previously for HTL of *Nannochloropsis* sp. [6,16]. Fast HTL biocrudes, both light and heavy, always had a lower wt % C than the biocrudes from conventional isothermal liquefaction. Figures 8.3b and 8.3c show that the light and heavy biocrudes from fast HTL are always richer in N and O content than their counterparts from isothermal HTL. Previous results for HTL of *Nannochloropsis* sp. showed that increasing the reaction severity, that is, increasing holding time and/or increasing reaction temperature, reduces the O content in the biocrude [16]. The results in Figure 8.3c show the same trend. Even so, the N and O content in these biocrudes are roughly an order of magnitude greater than those in most petroleum crudes [17], and may present challenges to upgrade the biocrude to a hydrocarbon fuel. All of the biocrudes, however, have reduced O content compared to the original biomass.

Figure 8.3d shows that the S content in the biocrude varies among the different organisms, but it is always < 1 wt %, putting it within range of the S content of most petroleum crudes [17]. The heavy biocrude from fast liquefaction is always richer in S than the heavy biocrude from conventional liquefaction. The S content in the light biocrude from *S. cerevisiae* treated by fast liquefaction was the lowest at 0.15 wt %.

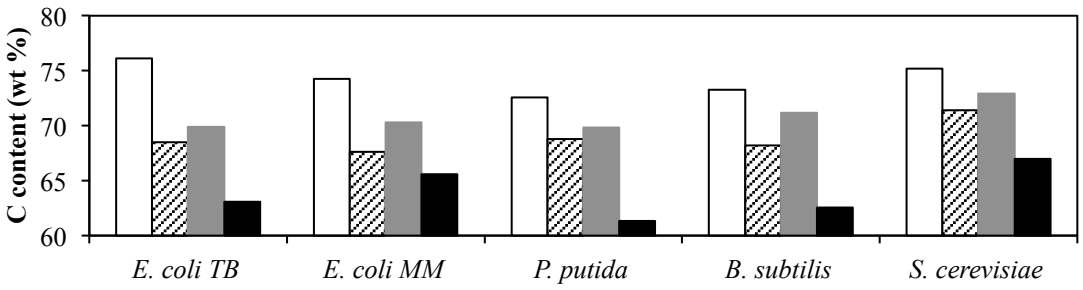

(a)

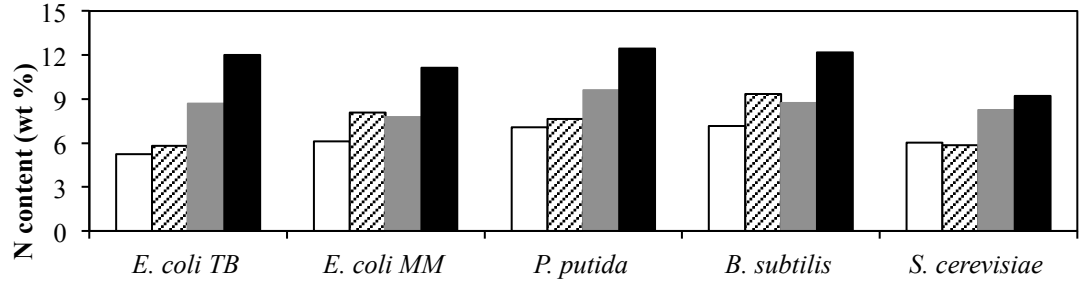

(b)

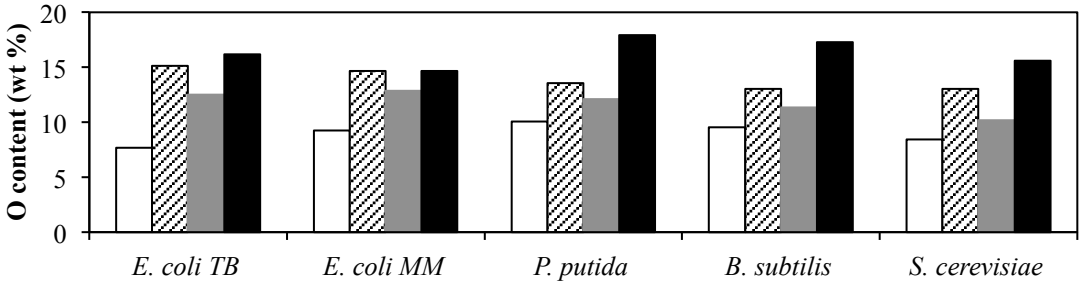

(c)

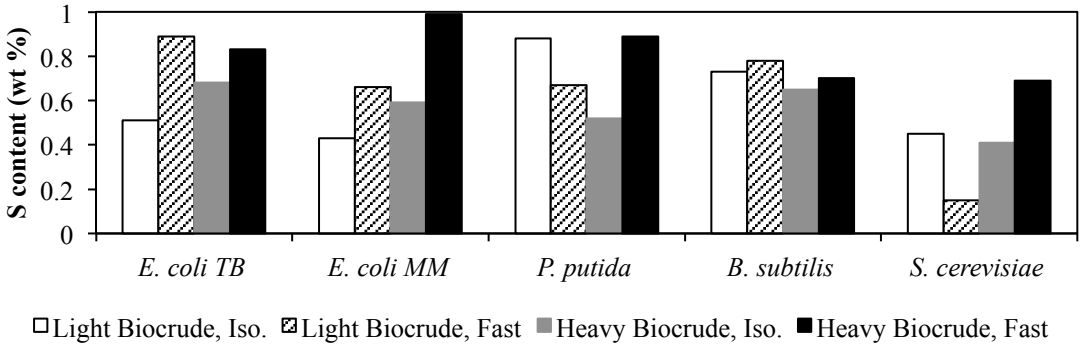

(d)

Figure 8.3. Composition of a) C, b) N, c) O, and d) S in the light and heavy biocrudes

8.4. Ammonia in the Aqueous Phase

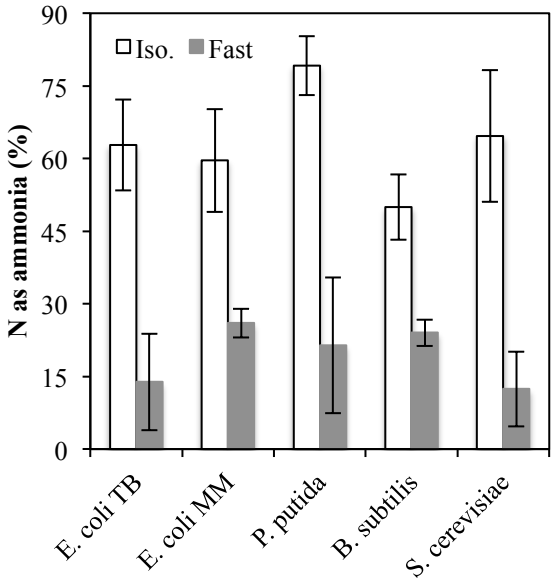

Figure 8.4. Percentage of N as ammonia in the aqueous phase

Figure 8.4 shows the percentage of the total N from the biomass that is present as dissolved ammonia in the aqueous phase. Isothermal HTL of the biomass favors the near complete conversion of water-soluble N products into ammonia. As reaction severity increases more of the N in the biomass is converted into ammonia [16]. Converting N-containing molecules into dissolved ammonia makes the nitrogen more bioavailable for use by most microorganisms. This conversion facilitates the recycling of N in biorefineries, which is an important consideration for environmental sustainability.

8.5. Elemental Distribution

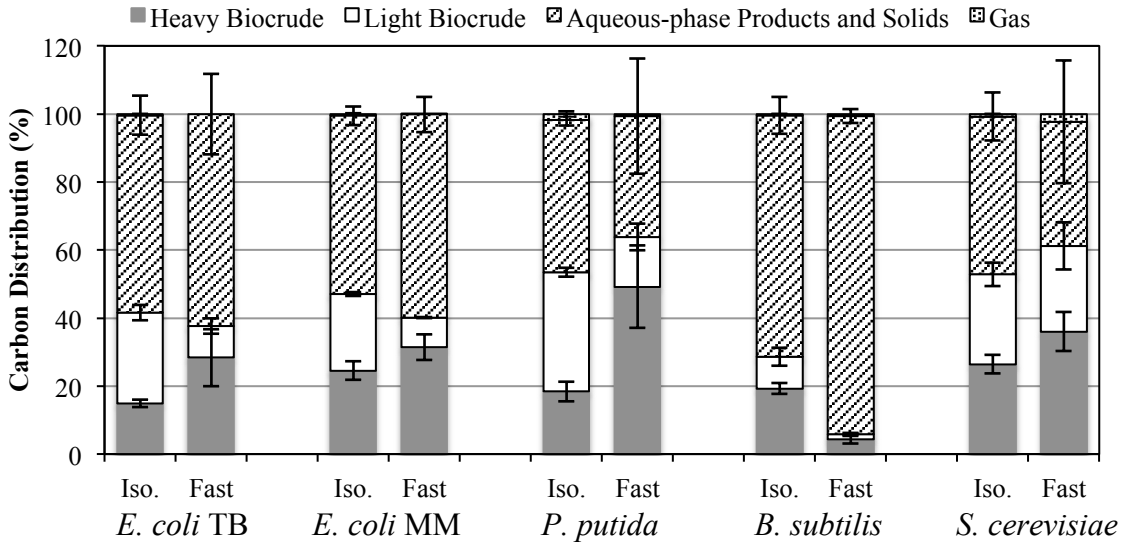

Figure 8.5. Carbon distribution among the product fractions

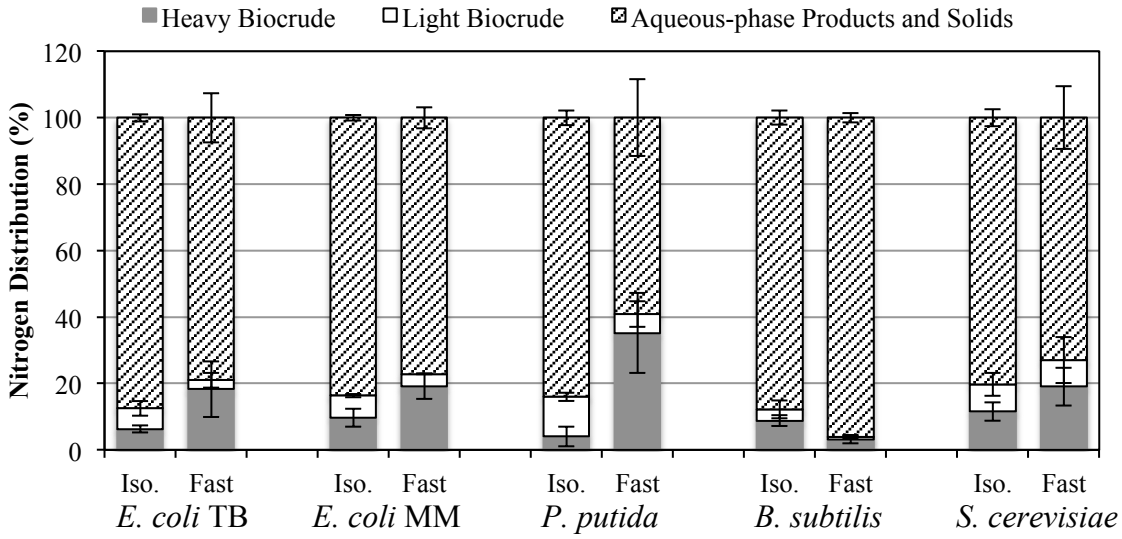

Figure 8.6. Nitrogen distribution among the product fractions

Knowing the gravimetric yields and the elemental composition of each product fraction allows one to calculate how the various elements are distributed among the product fractions.

Carbon and nitrogen are of most interest since the C content strongly influences heating value and N recycling is essential for a sustainable hydrothermal biorefinery. Figure 8.5 shows that at most 64 % of the C in the biomass goes to the biocrude. *B. subtilis* had the lowest C distributed to the biocrude while *P. putida* and *S. cerevisiae* had the highest distribution of C because of their higher yields of biocrude. Similar to the results from the HTL of microalgae, Figure 8.6 shows that the majority of the N (80 % or more for conventional isothermal HTL) resides in the aqueous phase and solids [16]. This outcome is desirable as it facilitates recycling the N-containing compounds as nutrients for cultivation of additional biomass. Less than 41 % of the total N from the biomass is distributed to the biocrude.

8.6. Heating Value and Energy Recovery

Table 8.3 shows the higher heating values of the light and heavy biocrudes and the percentage of the chemical energy in the biomass that is recovered in the biocrude. The heating value of the light biocrude was always higher than that of the heavy biocrude, and biocrudes produced at isothermal HTL conditions had higher heating values than biocrudes produced at fast HTL conditions. These trends are simply a manifestation of the trends in the C and O content of the various biocrude fractions. Regardless of the biomass feedstock processed, the variation in heating value for a given biocrude (light or heavy) fraction from a given HTL approach (isothermal or fast) is always < 2 MJ/kg. It appears that the processing conditions and product fractionation protocol play a larger role in determining heating value than the choice of biomass feedstock [11].

Table 8.3. Higher heating value and energy recovery of the biocrude

Organism	HTL	HHV (MJ/kg)		Energy Recovery in the Biocrude (%)
		Light Biocrude	Heavy Biocrude	
E. coli TB	Iso.	38	33	43 ± 3
	Fast	34	30	38 ± 8
E. coli MM	Iso.	37	34	48 ± 4
	Fast	33	31	40 ± 5
P. putida	Iso.	36	33	52 ± 6
	Fast	34	29	62 ± 10
B. subtilis	Iso.	36	34	29 ± 6
	Fast	33	29	6 ± 2
S. cerevisiae	Iso.	37	35	53 ± 10
	Fast	35	31	60 ± 25

The last column of Table 8.3 shows the total energy recovered in the biocrude from the original biomass. *S. cerevisiae* and *P. putida* had the highest energy recoveries for both hydrothermal treatment conditions. *B. subtilis* had the lowest energy recovery (recall that it gave the lowest yields of biocrude). The energy recoveries in HTL biocrude from bacteria and yeast are not as high as those often observed from HTL of microalgae where values exceeded 70 % at the same processing conditions [6,16]. Of course, microalgae typically have lipid contents an order of magnitude higher than those in the bacteria and yeast used for this study. Higher lipid contents tend to correlate with higher biocrude yields and higher energy recoveries in the biocrude [7]. Nevertheless, Table 8.3 shows that HTL can produce energy-dense biocrudes containing 40 % or more of the chemical energy in the microbial biomass.

8.7. Molecular Composition of the Light Biocrude

We analyzed the light biocrude using GC-MS. Table 8.4 shows the components in the light biocrude for which the GC-MS software gave at least a 50 % match factor with a compound in its library of mass spectra, with their relative abundance quantified by peak area. Not all of the compounds in the biocrude could be identified owing to the large number of low-intensity peaks present in each chromatogram. All chemical identities in Table 8.4 remain tentative, as we used no authentic standards to get positive identities. The peak areas listed in Table 8.4 provide a qualitative representation of the relative abundance of those compounds in the light biocrude.

Table 8.4 shows that the fast-HTL biocrude was less likely to contain heterocycles and aromatics. The nitrogen-containing heterocycles, such as substituted indoles and amines, are possibly derived from the decomposition of porphyrins or proteins that are abundant in the microorganisms [18]. Such nitrogen-containing heterocycles are not uncommon in petroleum crude, but the presence of such compounds in higher concentrations make biocrude more difficult to upgrade to a hydrocarbon fuel. Free fatty acids appear in Table 8.4, and these are also common products in biocrudes from microalgae HTL [8]. For the types of microbial biomass studied here, fatty acids are most likely derived from the cell membrane. The fast HTL biocrudes contain a higher percentage of fatty acids than the biocrudes from isothermal HTL, potentially showing that lipids in the cell hydrolyze faster than the other biomolecules. Fatty acid amides are more common in the isothermal HTL products, suggesting that the higher concentration of NH_3 present in the reactor facilitates replacing the hydroxyl group in the fatty acid. Table 8.4 shows that more diproline, which is likely a decomposition product of proteins, is found in the fast HTL biocrude, suggesting the incomplete decomposition of proteins to amino acids at milder conditions.

Table 8.4. Tentative identities and relative abundance of different compounds in the light biocrude

Name	Structure	% Total Area									
		E. coli TB		*E. coli* MM		*P. putida*		*B. subtilis*		*S. cerevisiae*	
		Iso.	Fast	Iso.	Fast	Iso.	Fast	Iso.	Fast	Iso.	Fast
4-methylphenol	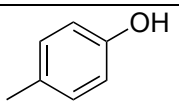	2.43	-[1]	-	-	1.82	-	5.7	-	1.14	-
4-ethylphenol	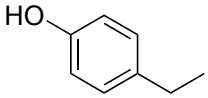	1.88	-	1.4	-	1.41	-	4.09	-	0.58	-
piperidin-2-one	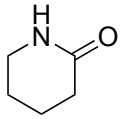	0.8	-	0.44	-	0.79	-	2.72	-	0.29	-
hexahydro-2H-azepin-2-one	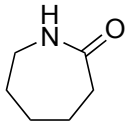	0.81	-	-	-	0.56	-	2.66	-	0.31	-
indole	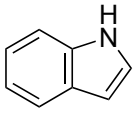	0.75	-	0.49	1.32	0.57	1.04	1.65	1.78	0.12	-
(3,5, or 7)-methylindole	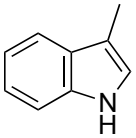	1.46	-	1.1	1.07	1.08	0.55	3.32	1.24	0.56	0.49
N-alkyl-benzamine	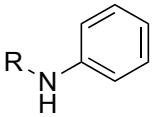	1.67	-	1.68	1.24	1.59	-	3.62	-	0.85	0.67
2,3-dimethylindole	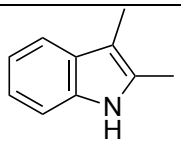	0.57	-	0.57	-	0.44	-	1.21	-	0.51	-
N-(2-phenylethyl)-ethanamide	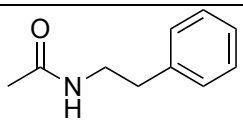	0.42	-	0.48	1.3	-	1.01	2.24	1.61	0.22	0.91
dodecanoic acid	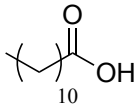	0.58	2.77	0.52	1.07	0.58	3.03	-	-	0.37	0.77
2-(indol-3-yl) acetaldehyde	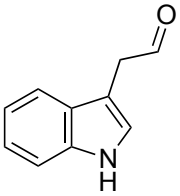	0.64	-	0.67	-	0.61	-	1.6	-	0.43	-

1-(3-methylindol-1-yl)ethanone	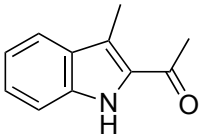	0.57	-	0.69	-	0.53	-	-	-	0.41	-
1-phenylmethyl-2-pyrrolidinone	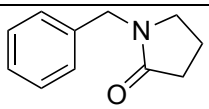	0.3	-	0.36	-	0.28	-	0.96	-	-	-
tetradecanoic acid	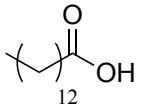	1.39	1.56	2.17	4.86	1.15	3.24	12.41	14.24	1.19	2.2
tetradecanamide	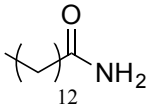	0.52	0.28	0.64	-	0.64	0.53	-	-	-	-
9H-carbazole	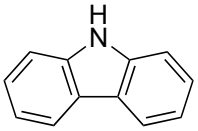	0.56	-	0.58	0.86	0.44	0.96	0.81	-	0.33	1.01
hexadecanenitrile	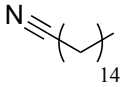	0.81	-	1.41	1.24	0.63	-	-	-	0.84	0.62
cycloheptan indole	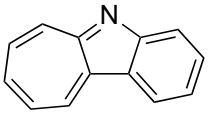	0.58	-	0.7	3.84	0.17	1.01	-	7.49	-	-
9-hexadecenoic acid	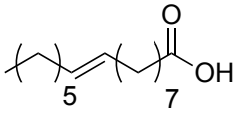		3.63	0.32	-	0.42	1.67	-	-	4.81	21.07
diproline	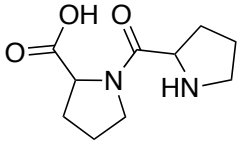	0.64	3.56	0.75	3.18	0.83	2.43	-	-	1.23	7.67
hexadecanoic acid	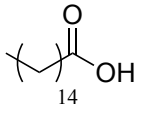	3.97	30.02	3.48	12.32	2.13	7.17	-	3.35	5.19	9.75
9-octadecenoic acid	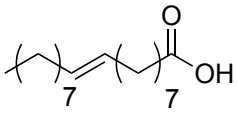	1.85	2.01	1.37	1.83	0.66	-	-	-	0.55	1.4
1-Methyl-9H-beta-carboline	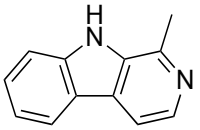	0.6	-	0.27	0.8	0.54	1.04	0.65	-	0.74	-
octadecenamide	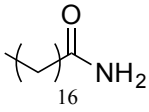	0.24	1.84	0.13	-	0.57	3.05	1.29	1.43	-	-

acridine	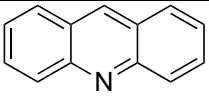	0.26	-	0.41	-	0.3	-	0.79	-	1.87	-
thiazole		-	0.82	-	0.82	-	1.31	-	-	2.38	-
hexadecanamide	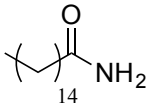	5.46	5.22	7.81	3.72	3.83	2.23	-	-	4.2	1.38
dimethyl hexadecanamide	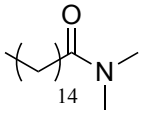	2.47	-	4.01	0.76	2.07	0.59	-	-	1.18	-

[1]Not detected

8.8. Conclusions

We demonstrated the feasibility of using microbial monocultures as a feedstock for HTL to produce biocrude. The high N and O contents of the biocrude, for all organisms and all treatment conditions, necessitate additional treatment of the biocrude before its use as a liquid transportation fuel. The cultivation of bacteria with aqueous-phase byproducts from HTL of microalgae [19] provides an opportunity to improve overall utilization of nutrients and total biocrude output in an algal biorefinery.

The *E. coli* cultivated in the TB (nutrient-rich) medium was higher in ash and lower in lipid content than the *E. coli* cultivated in minimal medium. The growth media used to cultivate the bacterium did not significantly affect the elemental composition of the harvested biomass. The biocrude yields produced at both isothermal and fast HTL conditions were not significantly different for the two different cultivation media. This insensitivity of the HTL outcomes to the growth media suggests that microbial biomass cultivated in aqueous streams that nutrient-depleted or containing substrates that are not easily metabolized [19] may nevertheless be suitable for biocrude production via *E. coli* cultivation.

The Gram-positive organism, *B. subtilis*, provided the lowest yield of biocrude compared to all other microorganisms in this study. Its modestly lower lipid content is probably not fully responsible for the reduced yield, since the *E. coli* TB had a similar lipid content, but significantly higher biocrude yields. The *B. subtilis* biomass did decompose during HTL, however, as the yield of residual solids was only about 4 wt %. The decomposition products were primarily water soluble, which might own in part to the thick peptidoglycan layer in this Gram-positive bacterium's cell envelope.

S. cerevisiae had a higher average yield of biocrude than the bacteria. The higher yield also resulted in a higher average recovery of the energy in the biomass. However, *P. putida* had similar yields, and is capable of growing on the by-product aqueous-phase from the HTL of microalgae [19].

As literature and the presented results indicate, fast HTL can, in many cases, lead to higher total biocrude yields than isothermal HTL [6]. The shorter reaction time necessary for fast HTL would reduce reactor size and capital costs in an industrial process. In exchange for these benefits, fast HTL biocrudes appear to have a less desirable composition. For example, a higher percentage of the total biocrude exists as the heavy fraction. Fast-HTL biocrudes also have higher O, N, and S contents, which are less desirable for biofuels or biofuel precursors in comparison to isothermal HTL biocrudes. More of the N in the isothermal HTL aqueous phase is converted to NH_3, making the N preferable as a nutrient for algae cultivation [20]. Further economic and environmental analysis of these trade-offs is required to determine which of these processes is preferable for the conversion of biomass to biocrude.

References

[1] SU Nwachukwu, *Bioremediation of sterile agricultural soils polluted with crude petroleum by application of the soil bacterium, Pseudomonas putida, with inorganic nutrient supplementations*, Curr Microbiol 42 (2001) 231-236.

[2] LS Gronenberg, RJ Marcheschi, JC Liao, *Next generation biofuel engineering in prokaryotes*, Curr Opin Chem Biol (2013)

[3] K Fagerbakke, M Heldal, S Norland, *Content of carbon, nitrogen, oxygen, sulfur and phosphorus in native aquatice and cultured bacteria*, Aquat Microb Ecol 10 (1996) 15-27.

[4] HC Lange, JJ Heijnen, *Statistical reconceliation of the elemental and molecular biomass composition of Saccharomyces cerevisiae*, Biotechnol Bioeng 75 (2001) 334-344.

[5] EW Becker, *Micro-algae as a source of protein*, Biotechnol Adv 25 (2007) 207-210.

[6] JL Faeth, PJ Valdez, PE Savage, *Fast Hydrothermal Liquefaction of Nannochloropsis sp. To Produce Biocrude*, Energy Fuels 27 (2013) 1391-1398.

[7] P Biller, AB Ross, *Potential yields and properties of oil from the hydrothermal liquefaction of microalgae with different biochemical content*, Bioresour Technol 102 (2011) 215-225.

[8] TM Brown, P Duan, PE Savage, *Hydrothermal Liquefaction and Gasification of Nannochloropsis sp*, Energy Fuels 24 (2010) 3639-3646.

[9] U Jena, KC Das, JR Kastner, *Effect of operating conditions of thermochemical liquefaction on biocrude production from Spirulina platensis*, Bioresour Technol 102 (2011) 6221-6229.

[10] AB Ross, P Biller, ML Kubacki, H Li, A Lea-Langton, JM Jones, *Hydrothermal processing of microalgae using alkali and organic acids*, Fuel 89 (2010) 2234-2243.

[11] PJ Valdez, JG Dickinson, PE Savage, *Characterization of Product Fractions from Hydrothermal Liquefaction of Nannochloropsis sp. and the Influence of Solvents*, Energy Fuels 25 (2011) 3235-3243.

[12] C Torri, L Garcia Alba, C Samori, D Fabbri, DWFW Brilman, *I - Hydrothermal Treatment (HTT) of Microalgae: Detailed Molecular Characterization of HTT Oil in View of HTT Mechanism Elucidation*, Energy Fuels 26 (2012) 658-671.

[13] PJ Valdez, PE Savage, *A Reaction Network for the Hydrothermal Liquefaction of Nannochloropsis sp*, Algal Research (2013) In Press.

[14] H Tao, C Bausch, C Richmond, FR Blattner, T Conway, *Functional Genomics: Expression Analysis of Escherichia coli Growing on Minimal and Rich Media*, J Bacteriol 181 (1999) 6425-6440.

[15] N Sato, AT Quitain, K Kang, H Daimon, K Fujie, *Reaction Kinetics of Amino Acid Decomposition in High-Temperature and High-Pressure Water*, Ind Eng Chem Res 43 (2004) 3217-3222.

[16] PJ Valdez, MC Nelson, HY Wang, XN Lin, PE Savage, *Hydrothermal liquefaction of Nannochloropsis sp.: Systematic study of process variables and analysis of the product fractions*, Biomass Bioenergy 46 (2012) 317-331.

[17] JG Speight, *The Chemistry and Technology of Petroleum*, 3rd ed.; Marcel Dekker, Inc.: New York, NY: 1999; 217-218

[18] MW Sasaki, T. Tanaka, T., K., *Biosynthesis, biotechnological production and applications of 5-aminolevulinic acid*, Appl Microbiol Biotechnol 58 (2002) 23-29.

[19] M Nelson, L Zhu, A Thiel, Y Wu, M Guan, J Minty *et al.*, *Microbial utilization of aqueous co-products from hydrothermal liquefaction of microalgae Nannochloropsis oculata*, Bioresour Technol 136 (2013) 522-528.

[20] L Garcia Alba, C Torri, D Fabbri, SRA Kersten, B (Wim), Derk W.F., *Microalgae growth on the aqueous phase from Hydrothermal Liquefaction of the same microalgae*, Chem Eng J 228 (2013) 214-223.

Chapter 9

Impacts, Conclusions, and Future Work

Chapters 4-8 of this dissertation provide additional details about the hydrothermal liquefaction (HTL) of microalgae, bacteria, and yeast. We thoroughly studied several of the processing conditions that can affect the quantity and quality of the product fractions. By experimenting with different microalgae at various reaction conditions, we developed a reaction network and kinetic model that accurately predicted the yields of the product fractions from the HTL of microalgae.

We increased the knowledge in the field by studying parameters that had not been thoroughly examined before. We demonstrated that increasing the solid concentration of the biomass slurry increased the biocrude yield, but only by increasing the yield of heavy biocrude. We showed that varying the water density at 400 °C between 0.3 - 0.5 g/mL did not significantly affect the yield of the product fractions, but water density may have a more significant effect at concentrations below 0.3 g/mL (section 6.3). Increasing water density at supercritical conditions requires significant increases in operating pressure. Increasing operating pressure will increase the cost of materials and operations to sustain an HTL process at such conditions. Studying the effect of water density at supercritical conditions to determine the ideal condition is a possible direction for future work.

Although we used chlorinated solvents at the laboratory scale for their ease of separation from the biocrude, it is unlikely that large-scale processes would use such solvents in large quantities. We demonstrated the use of decane and hexadecane as solvents to recover the biocrude after liquefaction. These long-chain alkanes represent upgraded biocrude that could possibly be recycled to continuously recover biocrude after HTL.

The complete conversion of the biomass to the product fractions occurs on time scales < 20 min. Future investigations should examine the reactions at shorter time scales on the order of minutes or even tens of seconds. Reducing the time scale would also necessitate incorporating the heating rate into the model as well as investigating how the heating rate can affect hydrothermal liquefaction. Recent results have shown that reducing the batch holding time to < 3 min and increasing the heating rate can significantly improve biocrude yields [1].

After short processing times (< 20 min), more than 70 % of the N in the biomass is recovered in the aqueous phase. Increasing reaction severity increased the recovery of N-containing products in the aqueous-phase and increased the conversion of those products to NH_3. However only a portion of the N is converted to water-soluble products and the remainder is found in the biocrude. Likewise, the high O content in the biocrude reduces its heating value and needs to be reduced to improve fuel quality. Recent research has shown that the biocrude can be upgraded in a hydrothermal environment with [2-4] and without catalysts [5] to reduce the O and N content of the biocrude. Although the content can be dramatically reduced to < 1 wt % in some cases, the crude is not entirely O or N free. The O and N content of the light biocrude can vary with reaction temperature and batch holding time. Increasing reaction severity, both time and temperature, can actually reduce the O content (< 9 wt %) of the light biocrude but the N content of the light biocrude increases and settles between 4 -5 wt%.

We showed that 80% of the phosphorus in the microalgae partitions to the aqueous phase at 250 °C. However, less of the P is partitioned to the aqueous phase at higher temperatures and the fate of the remaining phosphorus is still unknown. Tracking phosphorus partitioning to the solids or the biocrude will be important to know for downstream processing of both product fractions. Since phosphorus is a limited resource that is necessary for algae cultivation it is important for it to be recovered and recycled.

We present the first complete reaction network and kinetic model for the hydrothermal liquefaction of microalgae. The reaction network is comprehensive, including all of the product fractions, not just pathways for producing biocrude. We also incorporated biochemical content into the reaction network and model to broaden its predictive capability to extend to other species of microalgae. More research is needed to investigate how carbohydrates, lipids, and proteins distribute to each of the product phases when treated hydrothermally. Investigations with model compounds and mixtures of these complex macromolecules could provide additional insight into the reactions that take place as biomass cells are decomposed during HTL.

We developed a quantitative kinetic model that provides reasonable correlation of experimental data at different residence times and reaction temperatures. Using the model we found that the total biocrude yield is optimized between 350 - 400 °C at batch holding times of roughly 10 min. The model loses accuracy at temperature > 400 °C, predicting higher gas yields than what has been shown experimentally [6]. Char formation is not included in the reaction networks proposed herein, but it is another possible product during the gasification of biomass [6]. Incorporating this pathway into the network and model may improve the ability of the model to predict yields at reaction conditions that favor gasification instead of liquefaction.

We showed that other microorganisms, such as bacteria and yeast can produce a biocrude that is similar to the biocrude from microalgae, albeit at slightly reduced yields. Results from the study of the hydrothermal liquefaction of bacteria and yeast demonstrated that cellular structure has a more significant effect on liquefaction yields than cellular composition. HTL of other microorganisms with specific structural characteristics could help to fully understand the effect of cell structure during HTL and how to increase the biocrude yield. It may also be of interest to study the HTL of model compounds representing the structure of the cell wall. Compounds such as glycoproteins, lipopolysaccharides, and lipoproteins are possible candidates.

References

[1] JL Faeth, PJ Valdez, PE Savage, *Fast Hydrothermal Liquefaction of Nannochloropsis sp. To Produce Biocrude*, Energy Fuels 27 (2013) 1391-1398.

[2] P Duan, PE Savage, *Catalytic hydrotreatment of crude algal bio-oil in supercritical water*, Appl Catal, B 104 (2011) 136-143.

[3] P Duan, PE Savage, *Catalytic treatment of crude algal bio-oil in supercritical water: optimization studies*, Energy Environ Sci 4 (2011) 1447.

[4] Z Li, PE Savage, *Feedstocks for fuels and chemicals from algae: Treatment of crude bio-oil over HZSM-5*, Algal Res 2 (2013) 154-163.

[5] SG Roussis, R Cranford, N Sytkovetskiy, *Thermal Treatment of Crude Algae Oils Prepared Under Hydrothermal Extraction Conditions*, Energy Fuels 26 (2012) 5294-5299.

[6] Q Guan, PE Savage, C Wei, *Gasification of alga Nannochloropsis sp. in supercritical water*, J Supercrit Fluids 61 (2012) 139-145.

Appendix

Table A.1. Yields (wt %) of product fractions at 400°C and various water densities

Water Density (g/mL)	Time (min)	Gas	Light Biocrude	Heavy Biocrude	Solids	Water-soluble Products
0.3	10	5.1	20.2	20.1	2.4	17.6
	20	5.3	19.5	15.3	1.8	16.9
	30	8.3	18.3	12.7	1.5	14.5
	40	7.2	21.7	13.7	1.7	15.0
0.4	10	5.5	20.4	18.6	3.9	19.7
	20	9.5	20.3	14.5	3.6	17.9
	30	8.0	23.8	12.4	4.3	17.4
	40	6.9	25.5	9.6	4.2	17.4

Table A.2. Ash content of the liquefaction product fractions at 350 °C and 40 min

product fraction	ash content (wt %)
solids	33
aqueous-phase products	0.96 ± 0.01
light biocrude	0.15 ± 0.03
heavy biocrude	0.72 ± 0.07

Table A.3. Optimized values of the rate constants (min^{-1})

Path (Fig. 5.11)	Reaction	Temperature (°C)			
		250	300	350	400
1	Solids → Aqueous-phase Products	0.021	0.084	0.084	0.095
2	Solids → Light Biocrude	0.023	0.044	0.044	0.054
3	Solids → Heavy Biocrude	0.025	0.15	0.16	0.23
4	Aqueous-phase Products → Light Biocrude	0.019	0.029	0.037	0.077
5	Aqueous-phase Products → Heavy Biocrude	0.053	0.060	0.060	0.063
6	Aqueous-phase Products → Gas	0.000019	0.000052	0.000082	0.00075
7	Light Biocrude → Aqueous-phase Products	0.079	0.083	0.086	0.218
8	Light Biocrude → Heavy Biocrude	0.0014	0.0024	0.0026	0.0092
9	Heavy Biocrude → Aqueous-phase Products	0.15	0.15	0.16	0.20
10	Heavy Biocrude → Light Biocrude	0.0055	0.0063	0.0066	0.081
11	Heavy Biocrude → Gas	0.0003	0.0016	0.0044	0.021

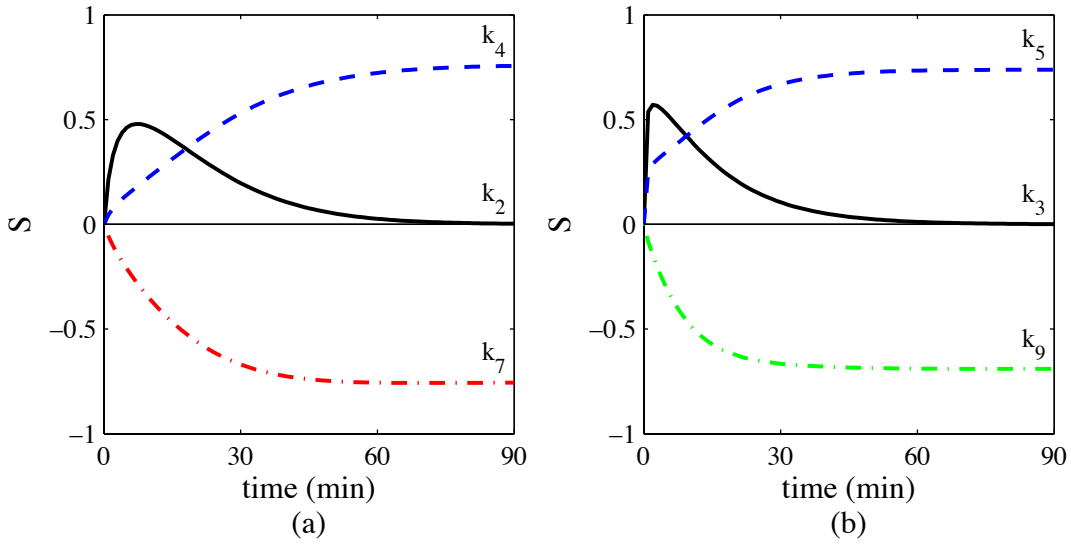

Figure A.1. Sensitivity coefficients (S_{ij}) at 250 °C for a) light biocrude and b) heavy biocrude

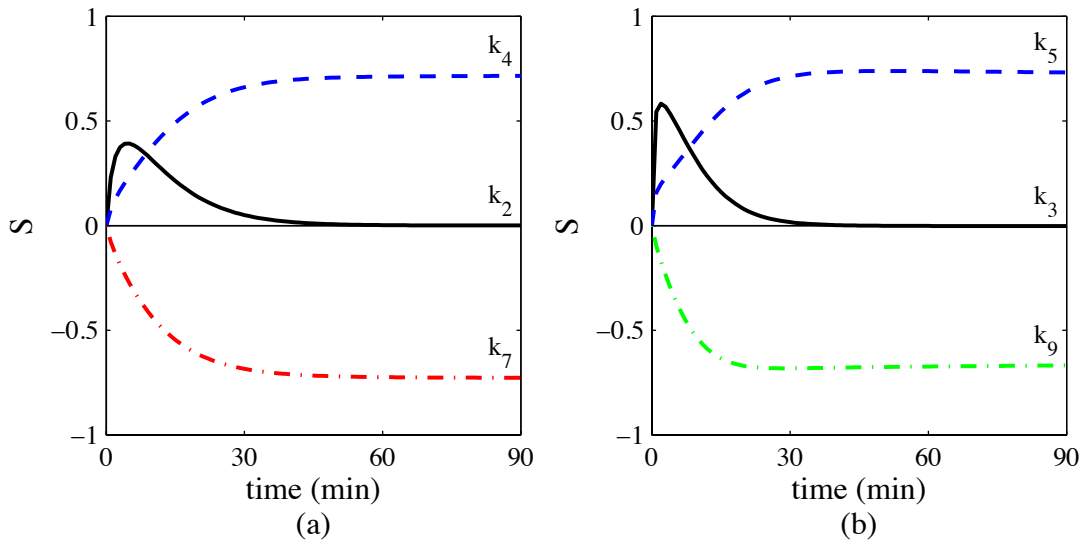

Figure A.2. Sensitivity coefficients (S_{ij}) at 300 °C for a) light biocrude and b) heavy biocrude

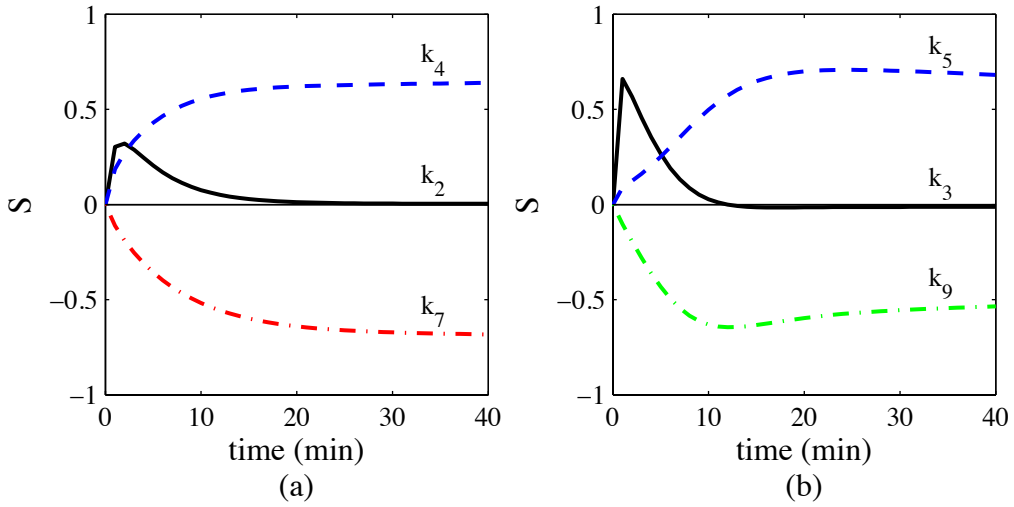

Figure A.3. Sensitivity coefficients (S_{ij}) at 400 °C for a) light biocrude and b) heavy biocrude

Table A.4. Net rates at 350 °C for 5 and 20 minutes

Path (Fig. 5.11)	Reaction	r_j (t) [wt % · min^{-1}] × 10^{-3}	
		5	20
1	Solids → Aqueous-phase Products	15	0.20
2	Solids → Light Biocrude	8.5	0.12
3	Solids → Heavy Biocrude	30	0.40
4,7	Light Biocrude ↔ Aqueous-phase Products	1.6	1.7
8,10	Heavy Biocrude ↔ Light Biocrude	3.4	2.5
5,9	Aqueous-phase Products ↔ Heavy Biocrude	-14	1.3
6	Aqueous-phase Products → Gas	0.068	0.093
11	Heavy Biocrude → Gas	1.3	1.0

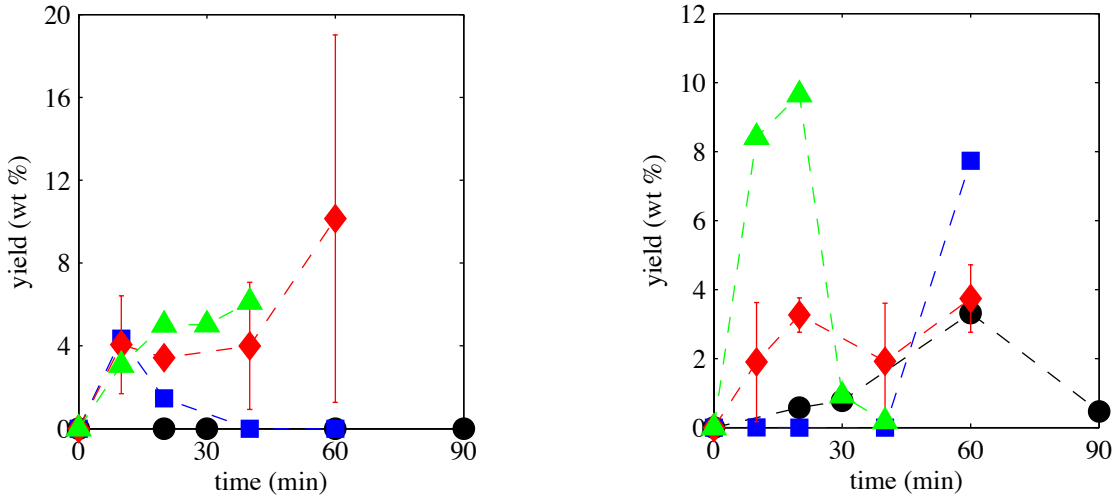

Figure A.4. Yield of gas at 250 °C (●), 300 °C (■), 350 °C (◆), and 400 °C (▲) from a) *C. protothecoides* and b) *Scenedesmus* sp.

Table A.5. Optimized values of the rate constants (min^{-1})

Path (Fig. 7.4)	Reaction	Temperature (°C)		
		250	300	400
1,p	Protein → Aqueous-phase Products	0.065	0.075	0.095
1,c	Carbohydrate → Aqueous-phase Products	0.043	0.12	0.54
1,l	Lipid → Aqueous-phase Products	0.12	0.14	0.18
2,p	Protein → Biocrude	0.059	0.13	0.48
2,c	Carbohydrate → Biocrude	0.071	0.14	0.42
2,l	Lipid → Biocrude	0.0007	0.0012	0.0026
3	Biocrude → Aqueous-phase Products	0.15	0.20	0.33
4	Aqueous-phase Products → Biocrude	0.097	0.15	0.28
5	Aqueous-phase Products → Gas	0.00016	0.00032	0.0010
6	Biocrude → Gas	0.00034	0.00072	0.0024

Table A.6. Yields of light and heavy biocrude product fractions (wt %, dry basis) for each biomass and isothermal (350 °C, 60 min) and fast (600 °C, 1 min) HTL

Organism	HTL	Yield	
		Light Biocrude	Heavy Biocrude
E. coli TB	Iso.	15 ± 2	9.3 ± 1.0
	Fast	5.9 ± 2.1	19 ± 8
E. coli MM	Iso.	14 ± 1	16 ± 3
	Fast	5.8 ± 0.2	22 ± 4
P. putida	Iso.	20 ± 1	11 ± 3
	Fast	8.8 ± 3.5	33 ± 11
B. subtilis	Iso.	4.7 ± 2.4	10 ± 1
	Fast	0.76 ± 0.38	2.6 ± 1.1
S. cerevisiae	Iso.	16 ± 3	16 ± 3
	Fast	19 ± 7	26 ± 5

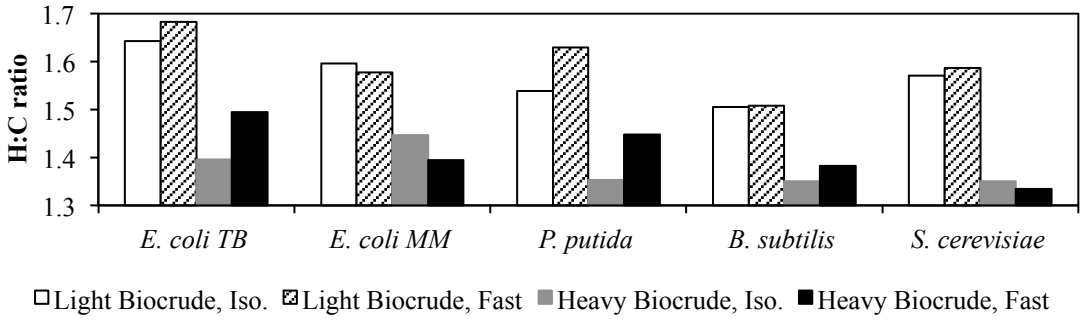

(a)

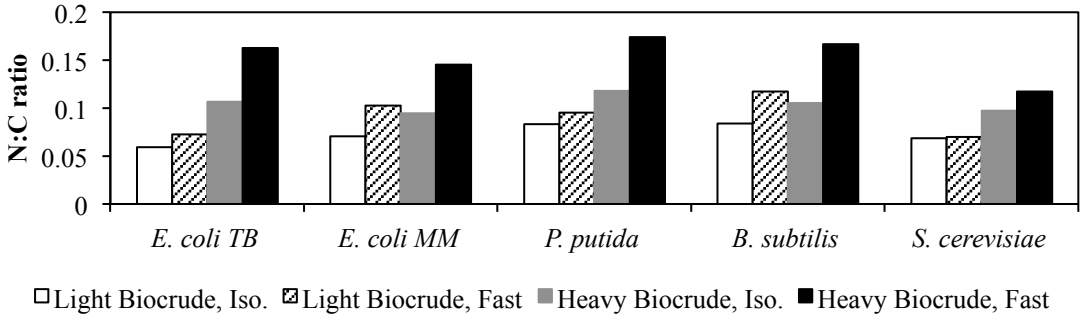

(b)

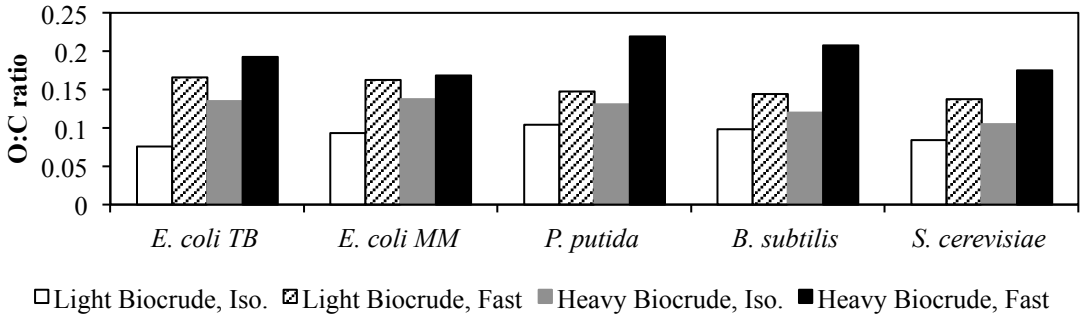

(c)

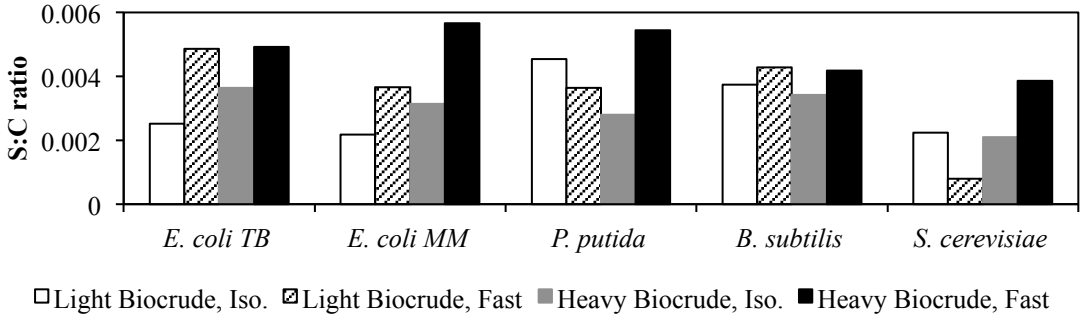

(d)

Figure A.5. a) H:C, b) N:C, c) O:C, and d) S:C atomic ratio in the light and heavy biocrudes for each biomass from isothermal (350 °C, 60 min) and fast (600 °C, 1 min) HTL